TUFTS UNIVERSITY

GRADUATE SCHOOL OF ARTS AND SCIENCES

Dissertation

Mathematical Modeling of the Within-host Dynamics and Evolution of the Human Immunodeficiency Virus

by

REBECCA BATORSKY

Submitted in partial fulfillment of the

requirements for the degree of

Doctor of Philosophy

August, 2012

ABSTRACT

The human immunodeficiency virus (HIV) is one of the fastest evolving entities known. Solving the public health problems it poses necessitates a detailed understanding of the evolutionary processes underlying its spread and persistence. Many of the parameters that govern the course of infection in an individual are not directly measurable in the lab. Mathematical and computational modeling has been successful in estimating many of these parameters by building models that can reproduce the dynamics of various cell types that are observed. Accurate models can be used to aid in the interpretation of data and predict the effect of therapeutic interventions. This thesis focuses on building realistic models of the interaction of HIV with the host immune system. First, we describe HIV adaptation to a host in a chronic infection. The system is simulated by means of a novel Monte-Carlo algorithm including the evolutionary factors of mutation, positive selection with varying strength among sites, random genetic drift, linkage and recombination. By comparing several observables measured in simulation to the same quantities calculated in patient data, we estimate the effective recombination rate and the average selection coefficient to be on the order of 1% per genome per generation and 0.5%, respectively. Next, we simulate virus evolution under dynamical selection pressure from multiple Cytotoxic T Lymphocytes (CTL) in order to quantify the impact of changing CTL levels on the pattern of emergence of immune escapes in CTL epitopes. We conclude that changing CTL levels can give rise to complex, non-nested patterns of intra-epitope variation. In the third chapter, we proposed a model to explain the outcome of vaccination in animals challenged with two viruses, SIVmac251 and SHIV. To explain the mechanism behind the effect of vaccination, we propose a model including two types of CTL regulation, the helper cell-dependent and helper cell-independent response, which control infection in vaccinated and unvaccinated animals, respectively.

Acknowledgments

I would like to thank Dr. Igor Rouzine for introducing me to this exciting new field, and providing guidance and supervision during my research, as well as Drs. Leon Gunther, Peggy Cebe and Krzysztof Sliwa for their invaluable advice over the years. Finally, thanks to my friends and family for giving me support, strength, and more than a few good ideas.

This thesis is dedicated to those who have suffered as a result of the AIDS epidemic.

In der lebendigen Natur geschieht nichts,
was nicht in der Verbindung mit dem Ganzen steht.

Nothing occurs in living nature that is not related to the whole.

– Johann Wolfgang von Goethe

Contents

List of Tables

List of Figures

Chapter 1

Introduction

1.1 Human Immunodeficiency Virus: worldwide, in an individual, in a cell

1.1.1 The epidemic

Acquired Immune Deficiency Syndrome (AIDS) refers to the late clinical stage of infection with the Human Immunodeficiency virus (HIV). To date, it has taken the lives of over 30 million people. Currently, an estimated 40 million people are living with HIV/AIDS, and 2.6 million new infections are formed each year. Though HIV is found throughout the world, the disease is more prevalent in some areas than in others (Fig. 1·1). For example, Sub-Saharan Africa is the most affected part of the world, home to 68% of the world's infected individuals and just 12% of the world's population (UNAIDS 2010 Report on the global AIDS epidemic). The epidemic is expanding most rapidly in Eastern Europe and Asia, where the last decade saw an increase in the percentage of people infected, reaching a prevalence of around 1% in 2010.

Despite three decades of research since the first formal report of the disease, there remains no cure and no effective vaccine. The increasing availability and effectiveness of antiretroviral therapy (ART) has led to a decrease in the number of AIDS related deaths per year as well as a decrease in the rate of new infections. At the same time, the number of people living with HIV has increased due to the increased life expectancy of those living with the disease (Fig. 1·2). Though ART drastically improves the quality of life of infected individuals, it is unable to cure the infection. Treatment is a life-long requirement, and can cause severe side-effects and the evolution of drug-resistance.

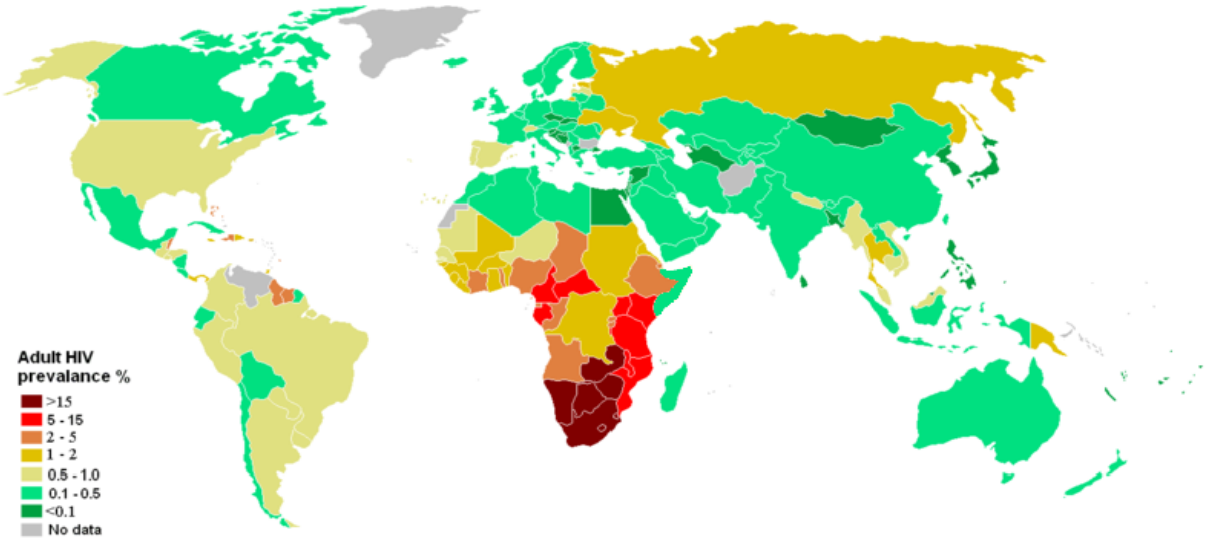

Figure 1·1: Estimate of the prevalence of adults living with HIV in 2010 by country. UNAIDS 2010 Report on the global AIDS epidemic.

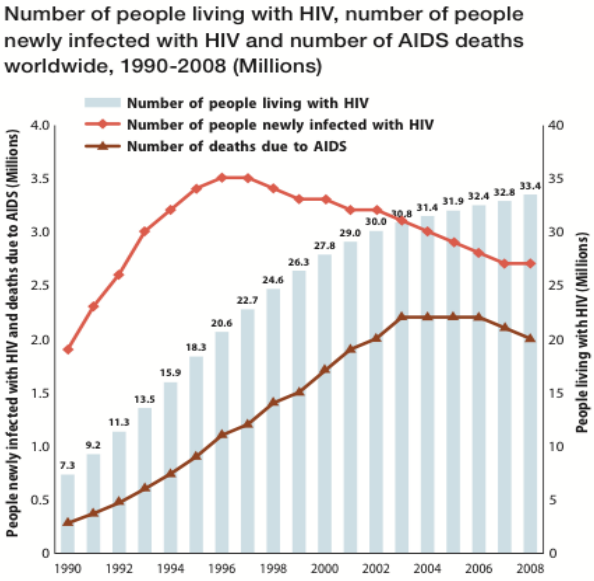

Figure 1·2: Number of people living with HIV worldwide, number of new infections, and number of AIDS related deaths for the period 1990 - 2008. UNAIDS 2010 Report on the global AIDS epidemic

1.1.2 Time course of the infection in an individual

Unlike the majority of viruses that infect humans, HIV is able to establish a lifelong infection in the face of an active immune response. Most viral infections are short-lived; for example, common viruses such as influenza and the virus that causes the common cold are cleared by the immune system in a matter of weeks. More pathogenic viruses, such as Ebola virus, cause death to the host before the infection can be controlled by the immune system. A smaller subset of viruses, such as HIV and Hepatitis C virus, establish chronic infections. It is not currently known what causes a virus to establish an acute or chronic infection. In the case of HIV, the cause of this is likely related to the ability of the virus to mutate in order to evade the host defenses (immune recognition is discussed in section 1.1.4).

The time course of HIV infection consist of three phases: acute infection, chronic infection, and AIDS. A schematic of the time course of infection is shown in Fig. 1·3. During acute infection, the concentration of virus in blood (viral load) rises steeply in time, peaking around one million virus particles per milliliter of blood. The virus infects a subset of white blood cells which express surface protein CD4 (CD4 T lymphocytes), and these cells are rapidly depleted. The depletion of CD4 T cells, around 5-6 weeks after infection, slows the growth of the virus. Expansion of another group of T cells that express surface protein CD8 and can kill infected cells, Cytotoxic T lymphocytes (CTL) causes the viral load to decline around one month post infection. Neutralizing antibodies (nAb), which are capable are binding to virions and preventing infection of new cells, arise several months later. During acute infection the infected individual generally experiences fever and other flu-like symptoms.

Chronic infection ensues, during which time the viral load can remain stable for many years. The magnitude of the viral load in chronic infection varies widely in patient ($10^3 - 10^5$ copies/ml). Strong correlation has been observed between the level of virus infection during chronic infection and the rate of progression to AIDS, though the cause of the large variation in viral loads among hosts is still strongly debated. Chronic infection in untreated individuals lasts anywhere from three

to twenty years, with an average of eight years, and is usually asymptomatic. Upon progression to AIDS, the immune system begins to rapidly deteriorate, viral load climbs, and the individual succumbs to opportunistic infections.

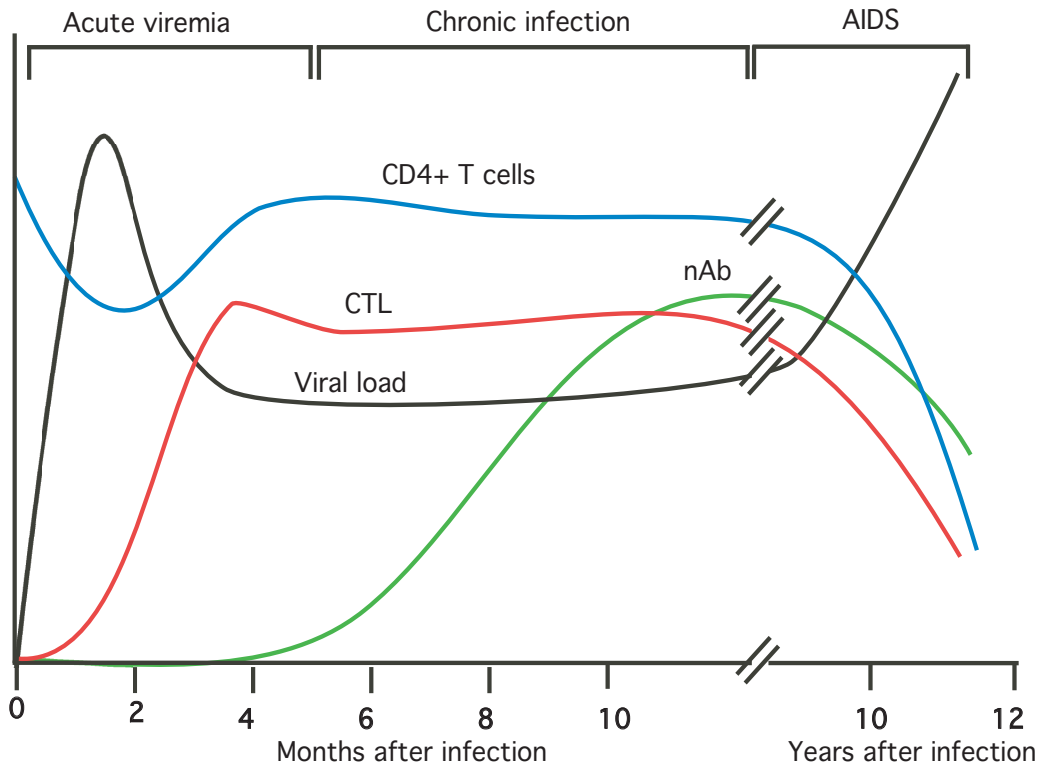

Figure 1·3: The typical time course of untreated HIV infection. The viral load (black) and CD4+ T-lymphocyte population (blue), CD8+ T lymphocyte (red) and neutralizing antibody count (green) change rapidly in acute infection and remain stable in chronic infection. AIDS is characterized by a rapid increase in virus load and a decrease in all components of the immune response. Figure adapted from (Ferrantelli and Ruprecht, 2002).

1.1.3 Viral lifecycle

It was originally thought that the stable nature of the viral load and slow progression to AIDS implied that the virus replicated slowly in chronic infection. It was later determined, with the aid of mathematical modeling, that the entire infected cell population of approximately 1×10^9 cells is killed approximately each day (Perelson, 2002). Since the viral load and number of infected cells

remains roughly constant, the same number of new cells must be infected each day.

Rapid replication, combined with the ability of the virus to mutate its genome, results in a high level of genetic variability in the HIV population in an infected host. A randomly selected pair of HIV genome sequences from a chronically infected individual can have different nucleotides at as many as $3-5\%$ of their 9,700 nucleotide positions (referred to as sites). This is roughly the same level of variation that characterizes an influenza outbreak worldwide (Korber et al., 2001), quite remarkably concentrated in a single host. Several events in the viral lifecycle contribute the the high genetic variablity.

HIV is a retrovirus, which means that it carries two copies of its RNA genome. Entry into a cell is mediated by binding of virion surface proteins to CD4+ proteins present at the cell surface. The binding triggers a conformational change in one of the virus surface proteins, after which the outer membrane of the HIV particle fuses with the host cell and the contents of the virion are deposited into the cell. Once inside, HIV transcribes its genome into DNA via a process called reverse transcription, and integrates it into the host's DNA (the integrated viral genome is referred to as as provirus). Viral RNA is transcribed from the provirus and transported out of the nucleus, where new virions are assembled. New virions bud from the cell. A sketch of the viral lifecycle including the stages of cell entry, reverse transcription, integration, and progeny production is shown in Fig. 1·4.

The majority of mutations in the HIV genome arise due to the error prone reverse transcriptase enzyme. Estimates of the mutation rate range from 2-3 $\times 10^{-5}$ mutations per site per generation. It is therefore expected that each progeny virion differs from its parent by approximately one nucleotide. The ability of HIV to undergo genetic recombination during replication increases the genetic variability in the population by combining mutations present on separate genomes onto a single genome. Recombination occurs when a single cell is infected by two genetically distinct virions, and thus the infected cell genome contains two distinct proviruses (Fig. 2.5.2). During the

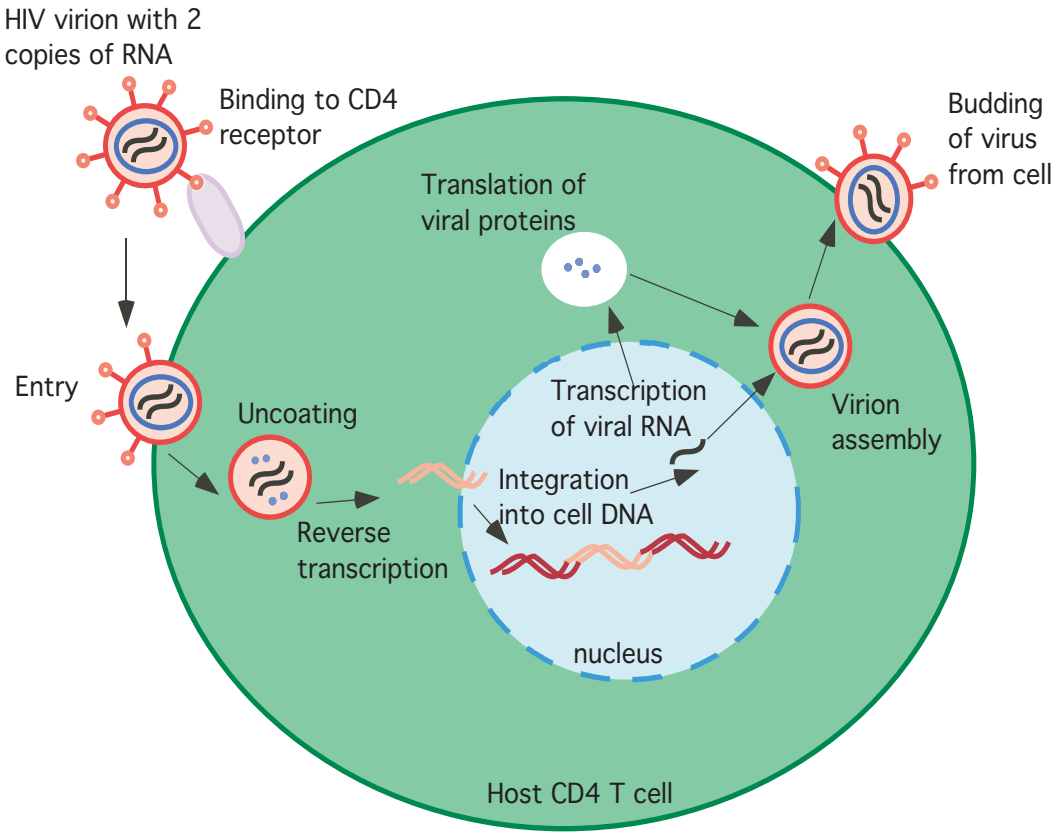

Figure 1·4: HIV life cycle in a host cell. Entry is mediated by binding to the CD4 receptor on the host cell. The virus RNA genome is transcribed into DNA during reverse transcription, after which it is integrated into the host DNA. From the integrated template, new viral RNA is produced and transported out of the nucleus. Viral proteins are translated and new virions are assembled, which subsequently bud from the cell.

assembly of progeny virions, two RNA genomes that originate from distinct parental virions can be included in the same virion. Upon infecting a new cell, the two genomes are combined during reverse transcription to create a single provirus in the new infected cell. If the two parental virions had non-identical genome sequences, the resulting provirus can be a novel variant. In Chapter 2, we study the relative contributions of mutation and recombination to generating the high level of viral diversity that is characteristic of HIV infection.

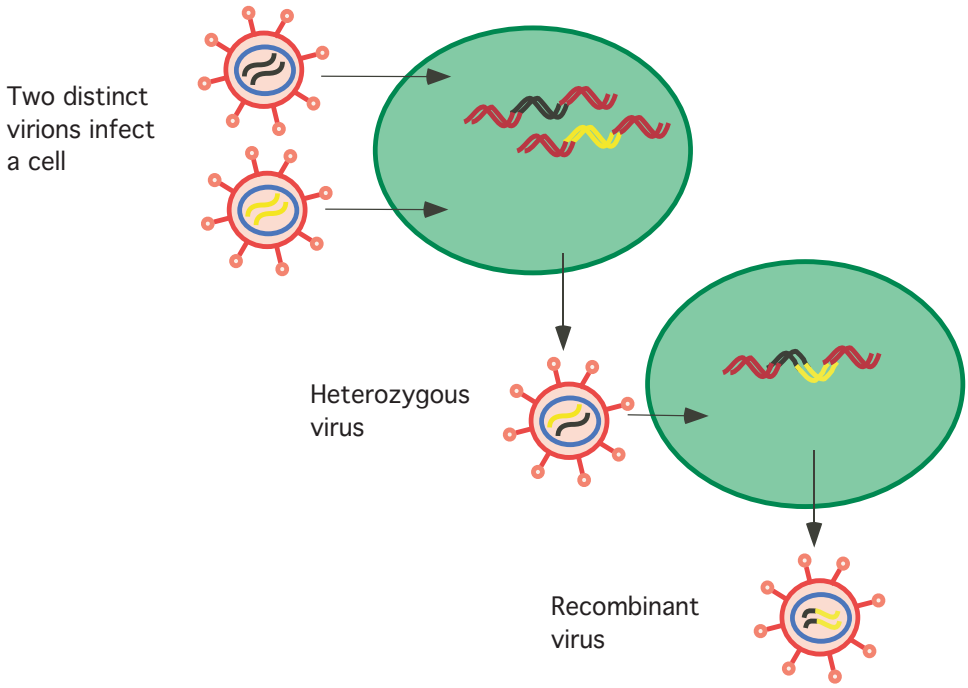

Figure 1·5: When two or more genetically distinct viruses infect a host cell, the progeny virus produced can be heterologous, containing two different RNA genomes. Upon integration into a new host cell, the reverse transcriptase enzyme routinely switches templates, leading to the provirus having genetic material from two genomes. The progeny produced will be a recombinant virus.

1.1.4 CTL recognition of infected cells

When an infected cell begins producing new virions, a portion of viral proteins are processed into small fragments and transported to the surface of the cell. These fragments are displayed on the

cell surface in a complex with a major histocompatibility class I (MHC) molecule. It is through interaction with the MHC-peptide complex that immune cells, such as CTL, are able to recognize and kill infected cells (Fig. 1·6). The viral fragments that are recognized (called epitopes) are 8-10 amino acids in length, and are distributed randomly in the viral genome (Schmid et al., 2009). Recognition takes place through a protein on the CTL surface called the T-cell receptor (TCR), which binds to the MHC-peptide complex. Upon recognition, CTLs begin to proliferate and release various cytotoxic proteins, such as perforin, which induces apoptosis of an infected cell, and interferon-γ, which suppresses viral replication. A schematic of the process is shown in Fig. 1·6. In every individual there exist millions of CTL clones, with distinct TCR that recognize different viral epitopes. Anywhere from $1 \times 10^3 - 1 \times 10^5$ MHC can be present on the surface of an infected cell, but as few as 1% of these will contain an epitope that is recognizable by any given CTL clone. Furthermore, mutations that randomly appear in epitopes can destroy recognition and allow the infected cell to escape being killed by the CTL clone that recognizes that epitope. The process of acquiring mutations in CTL epitopes (immune escape), leads to the rapid diversification of the virus population. Chapter 3 of this thesis will study this process via a mathematical model.

1.2 Modeling the interaction between HIV and the immune response

1.2.1 HIV replication dynamics

The chronic nature of HIV infection raised many questions about the mechanism of persistence of the virus. During the 1990's researchers (Wodarz and Nowak, 2002; Perelson et al., 1996) adapted the framework that had been developed to describe between-host spread of disease to describe the spread of the virus among susceptible cells. The basic model that was developed describes the interaction between uninfected target cells (T), infected cells (P) and free virus (V), as follows:

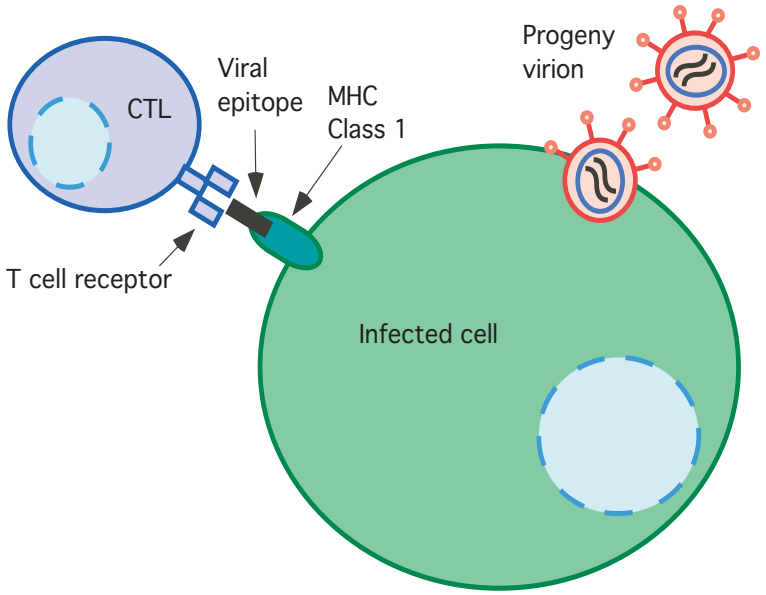

Figure 1·6: CTL recognition of infected cells. Recognition of a viral epitope in conjunction with class I MHC on the surface of an infected cell by a CTL leads to killing of the infected cell.

$$\dot{T} = s - d_T T - \kappa V T \tag{1.1}$$

$$\dot{P} = \kappa V T - d_P P$$

$$\dot{V} = rP - cV$$

Uninfected cells are produced at a homeostatic rate s, die at a rate d_T, and are infected in the presence of free virus at a rate κ. Infected cells are killed by the cytotoxic effects of virus at a rate d_P, and produce virus at a rate r. Free virus (V) is produced by infected cells at a rate c and is cleared at a rate c. The system has two stable, steady states: one infected state and one uninfected

state. The uninfected state is given by:

$$T^0 = \frac{s}{d_T} \tag{1.2}$$
$$P^0 = 0$$
$$V^0 = 0$$

The infected state is given by:

$$T^* = \frac{cd_P}{\kappa r} \tag{1.3}$$
$$P^* = \frac{cd_T}{\kappa r}(\frac{s\kappa r}{cd_P d_T} - 1)$$
$$V^* = \frac{d_T}{\kappa}(\frac{s\kappa r}{cd_P d_T} - 1)$$

The state that is obtained is determined by the basic reproductive ratio, given by $R_0 = s\kappa r/(d_P d_T c)$. The basic reproductive ratio is the number of new infected cells formed by a single infected cell. If $R_0 > 1$, the infected state is obtained, otherwise, the infection is cleared.

One of the first questions that was answered using this approached was to estimate the lifetimes of infected cells. The long asymptomatic period of infection suggested that perhaps the rate of viral replication was very slow, and that infected cells were very long lived. However, in 1995 when the first highly effective ART was available that efficiently prevented virus from forming new infections, it was observed that the viral load in patients dropped 100-fold within the first two weeks of treatment. The fast drop suggested that the infected cell lifespan was short, and using the model of virus dynamics it was possible to estimate the parameters that described the lifetime of free virus and infected cells, c and d_P, respectively (Perelson, 2002).

Blocking all new infections is simulated by setting $\kappa = 0$. If the virus load is initially at level V^*,

after onset of therapy it will decay according to:

$$V(t) = \frac{V^*}{c - d_P}[c\exp(-d_P t) - d_P \exp(-ct)] \tag{1.4}$$

It was known from independent experiments that the half-life of viral particles is much shorter than that of infected cells, $c \ll d_P$. In this limit, the above equation states that after a shoulder phase lasting c^{-1} days, the viral load should decline exponentially at rate at rate d_P. By fitting this function to patient data, it was estimated that the half-life of infected cells was on average 1 day. With these results it became clear that HIV infection is replicating at a high level in the host throughout the chronic phase of infection. The reason for eventual collapse of the immune response and progression to AIDS is still not known.

1.2.2 Immune system dynamics and the steady states

The basic model discussed above was able to fit data for the first 100 days of infection, but was unable to predict the level of steady state viremia in untreated patients. The estimate, given by Eq. 1.4 predicted higher steady state viral load than was observed in patients (Stafford et al., 2000). Thus, researchers set out to determine what controls the steady state level of virus in untreated infection. A clue came from a set of experiments in macaque monkeys infected with simian immunodeficiency virus (SIV). It was shown that when CTL were depleted with anti-CD8 antibodies, the virus load rose by $10 - 10^4$ fold, but resumed the previous steady state level once depletion was ended (Jin et al., 1999a; Schmitz et al., 2005) . This indicated that CTL were responsible for controlling the steady state level of virus, and that the dynamics of CTL must be included in order for the model to make quantitatively correct predictions about the level of virus in chronic infection.

Modeling the immune system is difficult due to the many interacting cell types that can potentially play a role. Furthermore, resolving their rapid kinetics requires a high frequency of sampling which is often not feasible in human subjects. Even so, progress has been made by using animal models and viruses such as SIV. A simple model that includes a CTL response and can reproduce the observation that CTL are responsible for controlling the virus load in chronic infection is:

$$\dot{T} = s - d_T T - \beta PT \tag{1.5}$$
$$\dot{P} = \beta PT - d_P P - kEP$$
$$\dot{E} = \frac{gPE}{h+P} - d_E E$$

CTL (E) capable of killing infected cells are stimulated to expand in the presence of infected cells, with maximum rate c, corresponding to the maximum rate of cell division, and die at rate d_E. Free virus has been eliminated from the model, since it is short lived in comparison with infected cells, and the level of free virus will therefore follow the level of infected cells $V = (r/c)P$. The rate of infection of uninfected cells is now proportional to the number of infected cells, with efficiency $\beta = \kappa r/c$. Infected cells are killed both directly by virus and by CTL with efficiency k (day cell)$^{-1}$. The infected state is given by:

$$T^* = \frac{s}{d_T + \beta P^*} \tag{1.6}$$
$$P^* = \frac{d_E h}{g(1 - d_E/g)}$$
$$E^* = \frac{\beta T^* - d_P}{k}$$

In this model, the level of virus in chronic infection is proportional to the CTL parameter h, which determines the level of infected cells needed for half maximal CTL division rate (h is often referred to the as the inverse avidity, where avidity is the term used to describe the amount of stimulation required to elicit CTL function). The interpretation of the wide variation in HIV levels observed in chronic infection can be explained by postulating wide inter-patient variation in CTL avidity. The reproductive ratio in this model is $R_0 = \beta s/((d_P + kE)d_T)$, where the level of E is changing in time. Thus, if E are able to reach high levels early on in acute infection, they can reduce the reproductive ratio and prevent the establishment of infection. We will consider possibility of elevating the CTL response early on in infection by vaccination in Chapter 4.

Eqs. 1.6 form the basis of more complex models that we will study in Chapter 3 and Chapter 4. The

model selection procedure is similar to that outlined in this section: existing models are extended based on new data that cannot be explained within the current model, and the simplest model is chosen that is able to explain the new data.

1.3 Modeling genetic evolution of HIV

1.3.1 HIV evolution

The simplest model in which all infected cells contain identical virus genomes and all model equations are deterministic cannot accurately describe many aspects of HIV infection. Due to the large mutation rate of HIV, the virus population begins to diversify immediately after infection. In virus genomes that are sequenced from HIV infected patients, the number of sites that are variable at a given times changes drastically over the course of infection. In the weeks following infection, before the CTL response is fully activated, mutations are infrequent in viral sequences. Once CTL populations reach high levels, at several months post-infection, a small number of mutations (average 5 per patient) are present in large fractions of the viral sequences that are collected and the mutations are found to be concentrated in CTL epitopes. Later on, in viral sequences obtained in chronic infection, many hundreds of sites contain mutations that are present at intermediate fractions of the collected sequences. If sequences are collected at multiple time points in chronic infection, it is found that the same sites stay diverse (meaning the site is present in both mutated and non-mutated forms) for many months to years. In the chronic phase of infection, individual genomes sequenced from an individual can differ in certain genes by as much as $3 - 5\%$ of their nucleotide sites (Balfe et al., 1990; Wolfs et al., 1990). Accumulation of mutations in acute infection is of clinical significance, because one of the major obstacles to developing an effective HIV vaccine is the ability of HIV to mutate and avoid the CTL response that is primed by the vaccine. In chronic infection, CTL escapes are generate only a small fraction of the diverse sites. Many of the evolving sites in chronic infection are likely compensatory sites necessary to ameliorate the fitness costs incurred by previous CTL escapes.

Chapter 2 and Chapter 3 describe viral adaptation to the host, which is what we call the process of acquiring beneficial mutations in the majority of sequences in the virus population. The rate

of adaptation depends on the number of simultaneously evolving sites, as well as the evolutionary forces of mutation, selection, recombination, and the overall size of the population of infected cells. The following is a brief introduction to evolutionary population genetics and the models used to calculate the rate of adaptation in evolving population (for more information, see (Ewens, 2004)).

1.3.2 Natural selection

Mutations in the majority of sites are disadvantageous, causing the virus to replicate less efficiently by disrupting a portion of the viral lifecycle. However, some mutations are beneficial for viral replication by enabling the virus to infect new cell types or by enabling the virus to evade immune surveillance. The rate at which beneficial mutations spread through the population of infected cells depends on several factors. One important factor is the size of the advantage that a mutation confers, in terms of increased replication rate. The simplest model of adaptation considers two genetic variants (strains) that replicate at slightly different rates. These strains will be called w, for the wild type strain, and m, for the mutant strain. The change in size of each population over time is replication and death.

$$\begin{aligned} \dot{w} &= (r_w - d)w \\ \dot{m} &= (r_m - d)m \end{aligned} \tag{1.7}$$

Where w, m are the number of wild-type and mutants strains in the population, respectively, and r_w, r_m are the replication rates for the two strains. The death rate, d, is taken to be the same for both strain. The selective advantage, or relative "fitness" of strain m is defined as the ratio of the replication rates, $r_m = r_w(1 + s)$ where $s \ll 1$ is the selection coefficient of the mutant strain. Analytic results can be obtained most easily in limit of small s, and this is expected to be a good assumption for the fitness difference between evolving strains in chronic infection. In Chapter 3 we study the origin of fitness differences in CTL escape mutations, and will relax the this assumption of small fitness gain. When a mutation increases the replication rate of the mutated viral strain relative to the transmitted viral strain, it is said to have a higher fitness.

So far, the two strains are not in competition with each other, because their growth rates are independent. One way to include competition into the model is to require that the total population size is constant, $w+m = N$. The finite population size represents finite resources that are necessary for the replication of both populations. In the last section the resources were modeled as a limiting source of uninfected target cells, which were modeled explicitly, e.g. Eq.1.2. Constant population size means that the sum of the changes in the two populations must equal zero, which, together with the relative replication rate (1+s), can be written as:

$$\dot{w} + \dot{m} = r_w((1+s)m + w) - (m + w) = 0 \tag{1.8}$$

This allows us to rewrite r_w in terms of w and m, using the relative replication rates as defined above:

$$r_w = \frac{m + w}{(1+s)m + w} \tag{1.9}$$

In order to study the dynamics of competition between the two strains, we rewrite the two equations as a single equation in terms of the fraction of the population that is the mutant strain, $f = \frac{m}{N}$ (f is called the frequency of the mutant strain). Using Eq. 1.9, we can replace Eqs. 1.7 with a single equation:

$$\dot{f} = sf(1 - f) \tag{1.10}$$

which has the solution:

$$f(t) = f_0/[f_0 + (1 - f_0)\exp(-st)] \tag{1.11}$$

Where the fraction of m at time zero must be specified, $f(0) = f_0$. If the mutant is generated

at some small frequency, for example, $f = \frac{1}{N}$, the less-fit strain goes extinct and the fitter strain sweeps to fixation in a time $t_{fix} \approx 1/s$ for $s \ll 1, f_0 \ll 1$. A sketch of the process is shown in Fig. 1·7 A.

The dynamic equations can be modified to include continuous mutation between the two strains at rate μ day^{-1}.

$$\dot{w} = ((1-\mu)r_w - d)w + \mu r_m m \tag{1.12}$$
$$\dot{m} = ((1-\mu)r_m - d)m + \mu r_w w$$

The evolution in terms of the frequency of m is now:

$$\dot{f} = sf(1-f) - \mu(2f-1) \tag{1.13}$$

which holds for $\mu \ll s \ll 1$, the regime which will describe HIV. Now, m emerges by mutation and grows to dominate the population:

$$f(t) = (\mu/s)(1-\exp(-st)), f(0) = 0 \tag{1.14}$$

Due to recurrent mutation, w remains at low frequency, given by $1 - f = \mu/s$. This process is shown in Fig. 1·7 B. This model describes the deterministic replacement of one viral strain by a mutant strain with higher fitness. The process of obtaining beneficial mutations that allow HIV to escape detection by CTL is considered in Chapter 3. In this chapter, the difference in growth rate of the variant with a beneficial mutation and the wild type variant is called the rate of escape. For example, in the two variant model considered in Eq. 1.7 the rate of escape is s. In the model considered in Chapter 3 the origin of the difference in replication rate is considered explicitly, and is not constant in time.

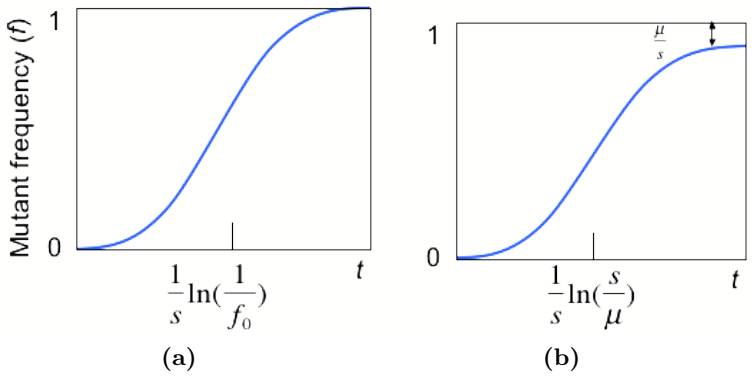

Figure 1·7: Selection mutation balance in a two strain model. (a) Schematic of a selective sweep in the model given by Eq. 1.7, the basic model for competition between two stains with different fitnesses. The fitter strain gradually replaces the less-fit strain. (b) Schematic of a selective sweep in the model given by Eq. 1.13, which extends Eq. 1.7adds mutation between the two strains. As a result the less fit mutant is maintained at a low level.

1.3.3 Genetic drift

The above deterministic treatment predicts that the mutant will grow to dominate the population even if only one mutant is initially present in the population. This does not take into account the stochastic nature of replication, where the replication potential varies within the mutant population. If the mutant strain is only present in a few members of the population, survival is not guaranteed. Random fluctuations in the number of progeny produced by a given genome in a generation could cause the mutant to die out even if it confers a strong advantage in replication rate. The change in the composition of the population over time due to random sampling of individuals is known as genetic drift. Therefore, while the number of individuals containing a beneficial mutation is small, the probability that it survives must also be considered in order to predict the future of the population. The model developed in Chapter 2 considers stochastic replication in a population of evolving viruses.

The most widely known model of genetic drift is the Wright-Fisher model (Wright, 1932). This model considers a population of two strains that replicate in discrete generations, where the population size is held constant. Members of the population in generation t are sampled randomly

to produce the generation $t+1$. At generation t there are m mutants in a population of size N. According to the Wright-Fisher model, the probability that in the next generation there will be a new number of mutated strains, m', is given by the binomial distribution:

$$p_{m,m'} = \binom{N}{m'} (\phi)^{m'} (1-\phi)^{N-m'} \tag{1.15}$$

Where ϕ gives the probability of selecting a mutant variant and depends on the relative fitnesses of the two strains:

$$\phi = \frac{f(1+s)}{f(1+s)+(1-f)} \tag{1.16}$$

Here, $f = m/N$ is the mutant frequency at generation t and $(1+s)$ is the relative replication rate of the mutant variant compared to the wild type variant. Eq. 1.16 can be easily understood in the simple case where the two strain replicate at equal rates ($s = 0$). The probability of selecting the mutant variant is simply given by it's frequency in the population, $\phi = f$. When the two strains replicate at different rates, the probability of selecting a mutant is weighted by it's relative fitness, $1+s$, and divided by the average fitness of the population, $f(1+s)+(1-f)$. This is because relative fitness of the two strains is equal to the expected ratio of the number of progeny of the two strains, and hence the probability of selecting a mutant is proportional to it's fitness relative to the average fitness of the population.

The evolution of the system over time is described as a Markov process.

$$P(m', t+1) = \sum_{m'} P(m,t) p_{m,m'} \tag{1.17}$$

Here, $P(m,t)$ is the probability of having m copies of the mutant strain at time t. In the limit of large $N \to \infty$, small $s \ll 1$, and strong selection pressure $Ns \gg 1$, the process can be described by a continuous-time, continuous-space diffusion process in the probability distribution of the mutant

frequency, f (for derivation see Appendix A).

$$\frac{\partial P(f,t)}{\partial t} = s\frac{\partial[f(1-f)P(f,t)]}{\partial f} + \frac{1}{2N}\frac{\partial^2[f(1-f)P(f,t)]}{\partial f^2} \tag{1.18}$$

The change in $P(f,t)$ is shown graphically in Fig. 1·8 under the separate influences of selection and genetic drift. The first term describes the tendency of genetic drift tends to spread the distribution in time and the second term described the tendency of selection tends to shift the distribution towards higher mutant frequency.

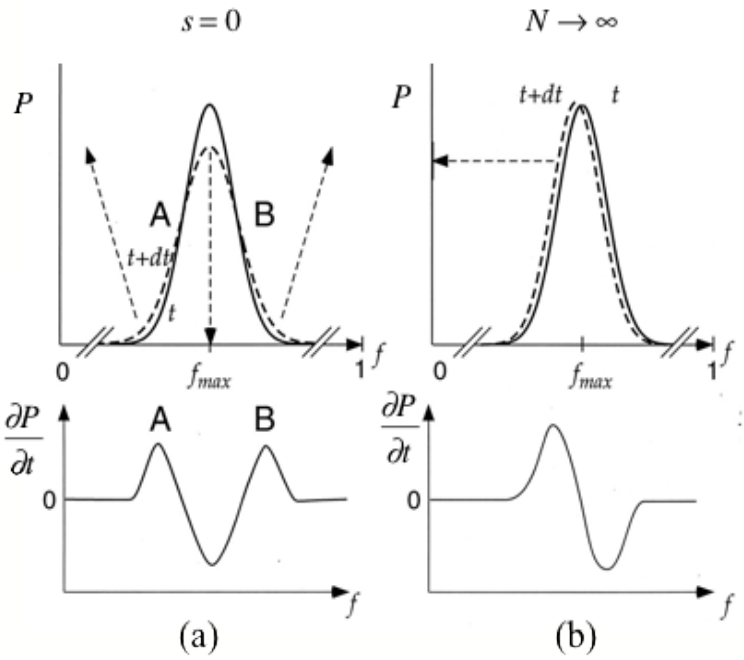

Figure 1·8: Illustration of the evolution equation for the probability distribution of the mutant frequency, $P(f,t)$ (a) When selection is negligible, genetic drift tends to spread the distribution, as shown in the upper panel. (b) When the population size is infinitely large, selection shifts the distribution to higher mutant frequency. The lower panel shows local changes in $P(f,t)$ (according to 1.18) in time for the two cases, $f_{max} = 0.5$. Figure adapted from (Rouzine et al., 2001b).

The probability that a mutation with selection coefficient s, present at one copy in the population eventually grows to dominate population is called the fixation probability, p_{fix}. In the diffusion limit, using 1.18, it can be shown to be:

$$p_{fix} \approx 2s \tag{1.19}$$

The full derivation is given in Appendix A.

Everything thus far has assumed that two strains exist in the population at a given time. This could be because only one site is advantageous to the population at a given time, and the two strains differ by only one site. More realistically, the population could have many sites that are simultaneously advantageous, but a very low mutation rate, such that typically only one site in the entire genome is evolving at any given time (Fig. 1·9 A). In terms of the evolutionary parameters, it takes a site takes $t \sim \frac{1}{s}$ days to sweep through the population (as shown in Fig. 1·7 A), and the rate of new mutations that appear in the population is $N\mu L$, where μ is the mutation rate per site, per individual, per generation, and a genome contains L sites, the condition for having on average one or fewer mutations in the population at any time is $N\mu L \ll 1/s$. The rate at which beneficial mutations are obtained in 100% of the population is then the product of the rate of appearance of a new mutations in the population and the fixation probability of a new mutation:

$$V = 2sN\mu L \tag{1.20}$$

A sketch of the regime where only one site is variable at a time is shown in Fig. 1·9 A.

1.3.4 Evolution with many linked sites

The number of sites at which mutations are present at a given time affects how quickly a given beneficial site can spread to the population. When only a few sites are selected, mutations spread to the population in a series of selective sweeps as described above (Fig. 1·9 A). However, when many

beneficial mutations exist on separate genomes in the population, they cannot grow to fixation simultaneously. They will compete with each other due to finite population size. For example, if two beneficial mutations arise on separate genomes in rapid succession, such that the second begins to sweep deterministically before the first has spread to the entire population, the second mutation may be lost, as illustrated in Fig. 1·9 B. The effect, called clonal interference, results in a slower rate of adaptation than Eq. 1.20, since not all mutations that arise in the population and survive genetic drift will spread to the entire population. Theoretical work has been done to determine the rate of adaptation when clonal interference is an important effect. In this case, the rate of adaptation has a logarithmic dependence on N, the number of individuals in the population, and μL, the rate of appearance of mutations per individual, per generation (Desai and Fisher, 2007b; Rouzine et al., 2008b; Rouzine et al., 2003b).

$$V \approx (2s)\log(Ns)/\log(s/\mu L) \tag{1.21}$$

Recombination can accelerate the rate of adaptation by combining beneficial mutations onto the same genome that might otherwise be in competition. Recently, several studies have shown that even small recombination can dramatically accelerate the rate of adaptation when many sites with small s are simultaneously evolving (Rouzine, 2005b; Gheorghiu-Svirschevski et al., 2006; Neher et al., 2010). These studies were done in the case where all sites have the same selection coefficient. The case where the selective advantage is varies over genome sites is also of interest and is the focus of Chapter 2. Recently, analytic results have been obtained for the rate of adaptation in this case (Good et al., 2012).

1.4 Outline of this thesis

Many of the parameters that determine the dynamics and evolution of HIV in an infected patient are not directly measurable in the lab. Mathematical and computational modeling has been successful in estimating many of these parameters by building models that can reproduce the ob-

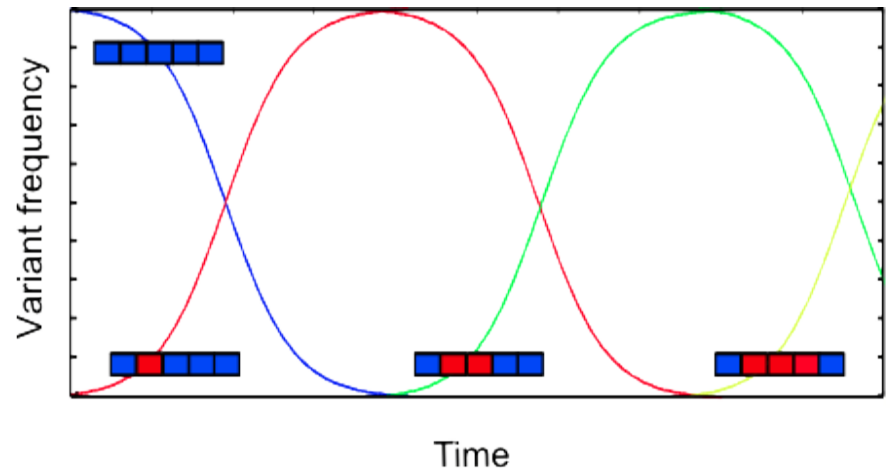

(a)

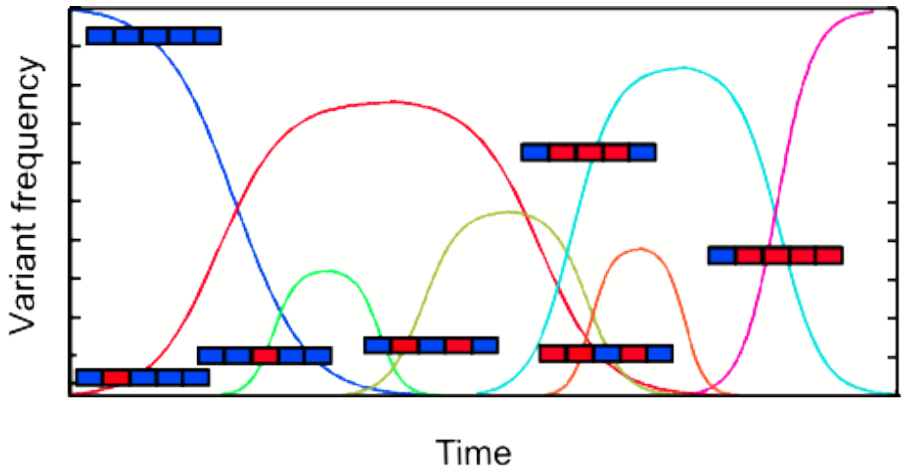

(b)

Figure 1·9: An illustration of successive and multiple mutation regimes. The frequency of a strain (colored curves) is shown over time, where the curves are labeled with a graphical representation of a virus strain with multiple sites. A blue square on these virus strains represents a site of the transmitted variant, a red square indicates a mutation relative to the transmitted variant. (a) Successive regime, in which only one site is diverse at a time. (b) Multiple mutation regime, where many sites are variable at a time and clonal interference is observed.

servable dynamics. The work presented in this thesis uses the models presented above in order to build accurate models that can be used to inform vaccine development and treatment protocols.

It is not possible to directly measure the frequency of viral recombination or the typical size of the selection coefficient of a beneficial mutation in untreated chronic infection. Therefore, in Chapter 2, we develop a method to estimate these quantities by performing stochastic simulations of viral populations undergoing genetic adaptation. Most parameters in our simulation were fixed, such as population size, mutation rate, and fraction of advantageous and deleterious genome positions, while the distribution of selection coefficients and the frequency of recombination were varied over a wide range. At each parameter setting we calculated observables that are sensitive to these parameter choices, and compared the resulting values with the same observables calculated from patient sequences from the HIV *pol* gene. We concluded that a low effective recombination rate of 1% per genome per generation and an average selection coefficient of 0.5% were sufficient to generate the level and pattern of diversity observed in our data (Batorsky et al., 2011a). Our estimates are compatible with those from other computational and experimental studies (Neher and Leitner, 2010b) (Josefsson et al., 2011), but are advantageous since they rely on one-time samples.

Several recent studies have shown the importance of cytotoxic T-lymphocytes (CTL) in controlling viral replication: sites of viral variation early in infection are located overwhelmingly in CTL epitopes (Goonetilleke et al., 2009a), and possession of certain HLA class 1 alleles is correlated with viremic control (reviewed in (Deeks and Walker, 2007)). In Chapter 3, we study the impact on viral evolution of the changing selection pressure due to co-existing CTL clones. We developed a hybrid model in order to describe both viral evolution at multiple epitopes and the dynamics of cognate CTL clones. The selection coefficient of a beneficial mutation is no longer a fixed value, but a combination of increased viral replication rate due to loss of recognition by CTLs, and decreased replication rate due to intrinsic fitness cost (the reduction in replication rate caused by a mutation). We studied a parameter range within which the effective selection coefficient for successive escape mutants decreases in time. This gave insight into the mechanism underlying the experimental observation that the escape rate of mutations in epitopes slows dramatically during the first year of

infection. In addition, this model was able to reproduce many of the complex escape patterns that are observed inside CTL epitopes.

Macaques vaccinated with proteins from the Simian Immunodeficiency Virus (SIV) (Letvin et al., 2006b) did not confer the same degree of protection as those vaccinated with proteins from a chimeric simian-human immunodeficiency virus (S/HIV), a virus combining parts of both the HIV and SIV genomes (Liu et al., 2029) after challenge with the respective viruses. In Chapter 4 we offer an interpretation of these results with a mathematical model of vaccination. We utilized the fact that after infection is established with either virus, there exist subpopulations of infected cells with vastly different lifetimes, and postulated that infection with SIV produces greater numbers of long-lived infected cells than infection with S/HIV. We developed a model including differential lifetimes of infected cells, with long-lived infected cells being formed at different rates for the two viruses. Our simulated experiments were consistent with many experimental observations. For example, unvaccinated animals infected with either virus developed a high viral load, whereas vaccinated animals infected with SIV had a higher viral load than vaccinated animals infected with S/HIV. Thus, we identified an excess of long-lived infected cells as a potential mechanism for the failure of vaccination against SIV to offer the same amount of viral control as vaccination against S/HIV. A comparative overview of our studies, as well as directions for future work are presented in Chapter 5.

Chapter 2

Estimate of effective recombination rate and average selection coefficient for HIV in chronic infection

2.1 Introduction

HIV infection of human hosts is characterized by rapid and impressive accumulation of genetic diversity with time. The main properties of this diversity within an untreated patient change as infection progresses. At the earliest stage, before the adaptive immune response is fully activated, mutations at most variable nucleotide positions are found only once per sequence sample and their accumulation rate is on the order of the spontaneous mutation rate, $\sim (2-3) \times 10^{-5}$ /base/day (Salazar-Gonzalez et al., 2009; Kearney et al., 2009; Keele et al., 2008). At several months postinfection, mutations concentrate in highly diverse sites ($> 5\%$ of minority allele), about 15 sites per genome per patient (Goonetilleke et al., 2009b). Almost all diversity at these sites is nonsynonymous and due to escape from the cytotoxic T lymphocyte (CTL) response. Later, in the chronic stage of HIV infection, the diversity pattern changes (Rouzine and Coffin, 1999a). The number of highly diverse sites increases to 200-300, much greater than the number of predicted CTL epitopes. Many of the mutations at these sites are synonymous. Diverse sites overlap between individual patients: approximately 15% of potentially diverse sites from a large database are observed in an average patient. The high diversity is stable and genetic shift is slow (Achaz, 2004), as most of these sites evolve very slowly, over a period of years. Delayed antigenic escape is observed occasionally (Asquith et al., 2006).

The present work is focused on describing genetic adaptation during the chronic phase of HIV-1 infection in representative untreated patients. Genetic evolution of HIV in infected patients is a

complex dynamic process, which involves many potentially important factors, including mutation, different types of selection, random drift, co-inheritance (linkage) of sites, recombination, and epistasis. Modeling the process of HIV evolution has progressed significantly from deterministic models assuming selection at a single site (Rouzine and Coffin, 1999a) or models assuming selectively neutral evolution (Brown, 1997), to one-site and two-site models including both selection and random genetic drift (Rouzine and Coffin, 1999b; Rouzine et al., 2001a; Frost et al., 2001; Frost et al., 2000), to more advanced models including linkage and recombination among hundreds of genetically diverse sites in an HIV genome.

As has been shown experimentally (Rice, 2002) and theoretically using few-site models (Muller, 1932; Hill and Robertson, 2009; Otto and Barton, 1997; Hadany and Beker, 2003), strong interference between fixation of beneficial mutations at different evolving sites drastically influences the rate and properties of evolution. Adaptation is predicted to be significantly slowed, first, by competition between growing clones containing beneficial mutations (Fisher-Muller and Hill-Robertson effects) and, second, by the background selection effect, which restricts introduction of new alleles into a population to the small fraction of best-fit genomes [see Ref. (Rice, 2002) for review]. Although linkage effects are apparent even in few-site models, their magnitude was argued to increase with the number of evolving sites (Maynard Smith, 1971). More recent analytic studies of asexual populations calculated the magnitude of this negative effect on adaptation of asexual populations (Rouzine et al., 2003a; Rouzine et al., 2008a; Desai and Fisher, 2007a; Brunet et al., 2008). These papers approximated the population as a deterministic traveling wave in fitness space, whose leading front is controlled by finite population size effects (Tsimring et al., 1996; Kessler et al., 1997).

More recent analytic work (Rouzine, 2005a; Gheorghiu-Svirschevski et al., 2006; Rouzine and Coffin, 2007; Rouzine and Coffin, 2010) confirms the previous simulation-based prediction (Iles et al., 2003) that even very infrequent recombination can strongly accelerate adaptation in a broad range of population sizes, provided the number of evolving sites is large. This conclusion is of great practical importance for HIV, since, like other retroviruses, it has an efficient mechanism for recombination. When a cell is co-infected by multiple virus particles, progeny particles can contain

heterologous RNA genomes. During reverse transcription in a newly infected cell, the polymerase enzyme switches templates multiple times, incorporating genetic material from both parents into the DNA provirus. Due to the complex interaction of many evolutionary factors including mutation, recombination and selection, it is not known how large a role recombination plays.

The cited analytic studies assume the same selection pressure for all sites. Taking into account variation of selection coefficient among sites when mutation is frequent and many beneficial mutations segregate in the population at once remains a major analytic challenge. In the present work, for the practical aim of estimating system parameters from HIV sequence data, we use computer simulation based on a model including variation of selection coefficient, linkage, recombination, random drift, and mutation. Using sequence data from untreated patients, we determine the extent to which the effect of linkage on adaptation is decreased by recombination and estimate the effective recombination rate in a typical patient.

2.2 Model

The model, implemented as a Monte-Carlo algorithm, considers a haploid population of N genomes with L evolving nucleotide positions ("sites") and assumes discrete generations (for HIV, 1 day per generation). Each genome represents a provirus inside an infected cell. At each generation step, a genome is replaced with a random number of progeny genomes whose average is equal to its relative fitness, which depends on the number of beneficial alleles, as explained in the next paragraph. We assume the division model, where the progeny number is either 0 or 2. Strictly speaking, the Poisson distribution of progeny number is the appropriate choice for a virus population. However, the two distributions create the same random genetic drift, since the variance of the progeny distribution affects the magnitude of the genetic drift. One can show that the variance of the progeny number is close to 1 for either distribution, provided the difference in fitness between the best-fit genome and the average genome in a population is small.

In the absence of mutation and recombination, progeny genomes are identical to the parental genome. The fitness of a genome with no beneficial mutations is set to be 1. A beneficial mutation

at a site, which occurs with rate $\mu = 3 \times 10^{-5}$ per site, increases its fitness by a factor $\exp(s)$, where s is the selection coefficient at the site. Epistasis is absent, and deleterious mutations are ignored. The selection coefficient s varies randomly among sites according to a distribution. We consider the exponential and power law forms of the distribution, $(1/s_0)\exp(-s/s_0)$ and $as_0{}^a/(s+s_0)^{a+1}$, respectively, where s_0 and a are parameters of the distributions. Our main focus is on the exponential distribution. The initial population is assumed to be uniformly less-fit at all sites, and beneficial alleles are introduced in the course of evolution gradually, by mutation with rate μ per site.

Before progeny sampling, $2rN$ genomes are randomly selected for recombination, representing rN co-infected cells per generation. Each pair of genomes undergoes recombination by crossing over between the two templates at M randomly selected genomic sites, creating two recombinants with complementary sets of segments from alternating templates. One recombinant and one parent are randomly chosen to replace the two parents. This last step represents two assumptions specific for retrovirus populations: first, half of the virions produced by a co-infected cell carry RNA templates from two different proviruses and, second, cell resources do not limit the number of virions produced and, hence, co-infected cells produce twice as many new infections as singly infected cells. The effective recombination rate, r, is thus the probability of producing a recombinant per genome per generation and, at the same time, the cell co-infection frequency. A schematic of the model is shown in Fig. 2·1.

Altogether, for the exponential distribution of s, the model has 6 parameters: N, L, μ, r, M, s_0. The power law distribution has an additional parameter, a, indicating the shape of the distribution. Three parameters are estimated directly from experimental literature: $\mu = 3 \times 10^{-5}$ (Brandin et al., 2006); $M \sim 10$ (Markowitz et al., 2003); $L \sim 2000$ ($\sim 20\%$ of the HIV genome is variable in all patients combined). We simulate effective population sizes up to $N = 10^5$ [cf. earliest estimates based on a 1-site model and a 2-site model in the absence of recombination, $N = 10^5 - 10^6$ (Rouzine and Coffin, 1999b; Frost et al., 2000). Parameters r and s_0 are estimated from single-time sequence data, as explained below.

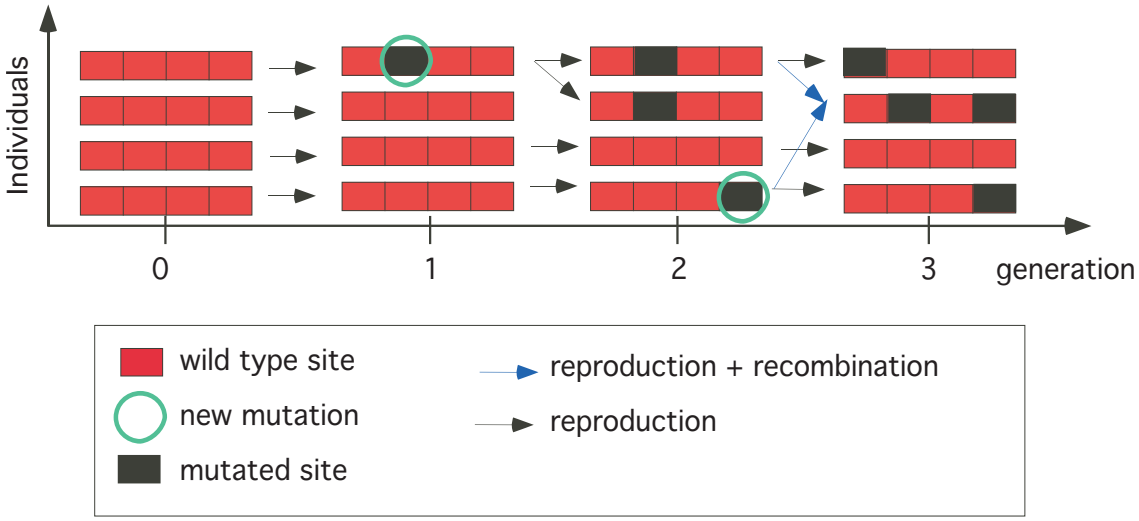

Figure 2·1: A model of evolution including mutation, selection, finite population size and recombination Evolution begins with a population of N identical genomes with all wild type sites. Beneficial mutations are introduced with rate μ per generation per site, and confer an advantage in replication. Genomes with mutations produce on average more progeny than genomes without mutations, which leads to selection for higher replication rate. Each generation, Nr genomes are selected for recombination, which enables mutations present on different genomes to be combined. The population rapidly diversifies and the average fitness of the population increases.

2.3 Results

2.3.1 Simulation of HIV adaptation

The predicted dynamics of several important quantities is shown in Fig. 2·2 for a single choice of parameters r and s_0 estimated in the next subsection to describe patient data. The distribution of genomes in fitness (Fig. 1A) appears as a traveling solitary wave of stable profile moving towards higher fitness values. The average rate of adaptation defined as the rate of log fitness increase is 0.0023/day, which exceeds the asexual rate calculated at $r = 0$ by a factor of 2. At the same time, it is roughly 4-fold below the adaptation rate in the limit of very frequent recombination when sites are almost unlinked, which is equal to $Ls_0^2/\ln(s/\mu)$ (*Materials and Methods*). We observe that a recombination rate of $r = 0.01$ ensures faster adaptation than in the asexual population, but is still too low to annul linkage effects.

The dynamics of beneficial alleles is shown in Fig. 2·2 B for 8 randomly selected sites with a frequency greater than 0.1 at generation 750. If recombination between sites were very frequent (large r and M), linkage effects would disappear and sites would become independent. Beneficial alleles would spread to the entire population in a time inversely proportional to their selection coefficient according to standard deterministic dynamics described by the single-site model. This trajectory is shown by the dashed lines in Fig. 2·2 B. However, at the low r values predicted to describe data for HIV, two different types of behavior are observed. At some sites, a trajectory fluctuates close to the monotonically increasing deterministic trajectory predicted by the single-site model. At other sites, alleles are depleted to low levels within $50 - 200$ generations where they are maintained by new mutation events. All trajectories display a strong random component.

Fig. 2·2 C shows 4 quantities characterizing the average diversity of the population, including (i) the average frequency of beneficial alleles per site $\langle f \rangle$, (ii) the fraction of sites with a frequency of the minority allele greater than 0.04 ("observably diverse" in a sample of 25 sequences), (iii) the fraction of sites with more than 0.25 of the minority allele, and (iv) the genetic diversity $\langle 2f(1-f) \rangle$

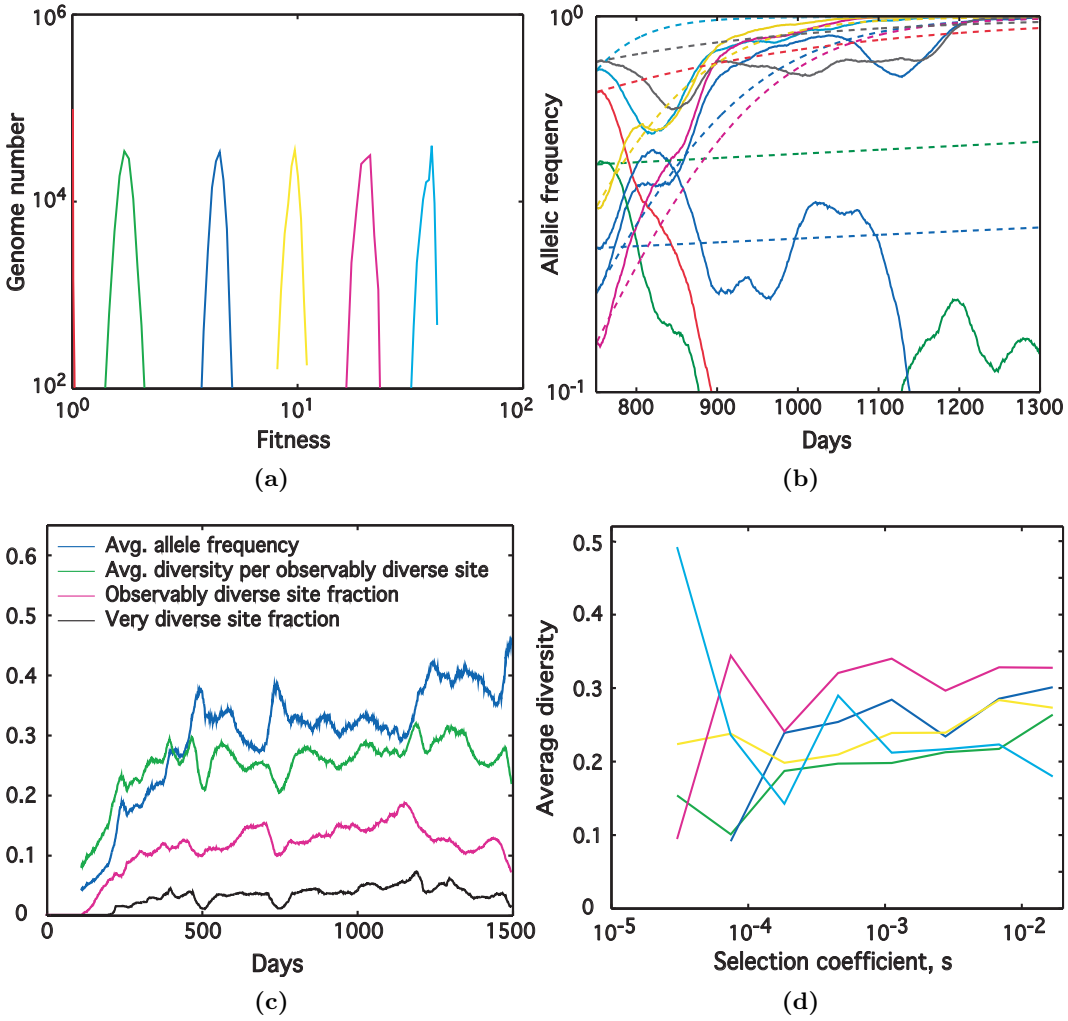

Figure 2·2: Simulation of viral adaptation during chronic HIV infection. Results are shown for the first 1500 days of infection using parameters estimated from pol in a representative patient, $r = 0.01$, $s_0 = 0.005$, $M = 10$, $L = 2000$, $N = 10^5$, $\mu = 3 \times 10^{-5}$. (A) The population distribution in fitness moves as a wave. Distribution is shown at 300 day intervals: day 1 (red), day 300 (green), day 600 (blue), day 900 (yellow), day 1200 (magenta), day 1500 (cyan). (B) Dynamics of beneficial alleles at high frequencies. Trajectories shown for 8 randomly selected sites with frequency of beneficial alleles per site, $f > 0.1$ at day 750: in simulation (solid), 1-site model prediction (dashed). The values of s at the sites shown: 0.02 (cyan), 0.004 (black), 0.004 (red), 4.5×10^{-4} (green), 0.01 (yellow), 3.1×10^{-4} (blue, top), 0.01 (blue, bottom), 0.01 (magenta). (C) Quantities characterizing average diversity of the population. Fraction of observably diverse sites, defined as having more than 0.04 of minority allele (magenta), fraction of very diverse sites, defined as having more than 0.25 of minority allele (black), average frequency of beneficial alleles per site f¿ (blue), genetic diversity $\langle 2f(1-f) \rangle$ averaged over "observably diverse" sites only (green). (D) Average diversity of "observably diverse" sites classified according to their selection coefficient s for 10 equidistant time points at 300-day intervals, as in A.

averaged over "observably diverse" sites only. These quantities reach approximate plateaus after about 500 days, with some fluctuations, indicating arrival at a steady state. The average height of the diversity plateau changes little with variation of model parameters and is similar to the prediction of the single-site model prediction with broadly variable selection coefficients (Rouzine and Coffin, 1999a). Within two decimal orders of the recombination rate ($0.01 < r < 1$), for both the exponential and power law distribution of s (with $a > 1$), the average diversity stays between 0.25 and 0.33, close to the observed value in patients [Ref. (Rouzine and Coffin, 1999a) and the present data set]. In contrast, the fraction of observably diverse sites is sensitive to r and s_0 and can be used to estimate s_0 from sequence data (see below).

Fig. 2·2 D shows the average diversity of "observably diverse" sites classified according to their selection coefficient s for five equidistant time points. Apart from some irregular time fluctuations, all dependences on s are unremarkably flat, showing that sites with large and small s contribute to overall diversity roughly equally at all times. This is indicative of strong linkage effects. Conversely, if sites were independent, the distribution in Fig. 2·2 D would have a sharp maximum at large values of s, which would move in time towards small s, indicating that alleles at sites with large s are amplified first. The flat dependence on s at all times indicates that alleles with small s are joined to alleles with large s within genomes and that selection takes place at the genome level.

2.3.2 Estimation of recombination rate and average selection coefficient.

Quantities shown in Fig 2·2 are instructive in that they reveal the basic properties of the evolutionary process. They cannot be used to estimate the effective recombination rate r, however, because they either are not measurable in real sequences or depend weakly on r.

We introduce two measures of Linkage Disequilibrium (LD) that are sensitive to the value of r. Both measures of LD were calculated in both simulation and in data for pairs of sites, for which the frequency of the minority allele exceeded 0.25 (termed "very diverse" sites, $0.25 < f < 0.75$). The first measure of LD is defined as $1 - \langle f_{AB,LRH}/f_A f_B \rangle$, where $f_{AB,LRH}$ is the frequency of the

least-represented haplotype for a pair of sites A and B, $f_A f_B$ is the product of one-site frequencies or the value of $f_{AB,LRH}$ in the absence of linkage, and $\langle ... \rangle$ denotes averaging over all very diverse pairs. The second measure of LD is defined as the fraction of very diverse pairs for which the frequency of the least-represented haplotype is below 0.04, which corresponds to less than one sequence in an average sample of 25. (This cutoff in simulation serves to approximate the finite size of experimental sequence samples. A more rigorous method would require simulating finite samples. For our aim of estimating r in a typical patient within a factor of 2 or 3, the accuracy is sufficient.).

We have used 9 sets of HIV pol sequences isolated from 4 untreated patients with 2 to 3 time points per patient (Table 1, *Materials and Methods*). LD values calculated from data are compared to those calculated for 11% of the simulated genome for a range of r values (note that we simulate the entire genome, but sample 11%). The first measure of LD obtained calculated in simulation is roughly 20% greater than that obtained when sites in the entire genome are considered (not shown). Some increase is expected, since recombination reduces LD and the probability of recombination between two sites increases with the distance separating two sites. On the other hand, the increase is modest, which validates the use of *pol* gene only.

An example of dependence of the two measures of LD measured in simulation on the recombination rate r, for the best-fitting value of s_0 (below), is shown in Fig. 2·3A and B together with the experimental range calculated from patient data (Table 1). The range of r predicted to describe data is centered at $r \sim 0.01$. Other quantities sensitive to recombination rate and convenient for experimental comparison are the frequencies of "observably diverse" sites and net virus fitness increase (not shown), which confirm the estimate obtained from Fig. 2·3 A and B.

In most cases we assumed $M = 10$ randomly placed crossovers per genome based on estimates from single-cycle experiments (Markowitz et al., 2003). Decreasing that number by a factor of 3, in the values of LD, is roughly equivalent to a decrease of r by a factor of $\sim 2 - 3$ (Fig. 2A, B). In addition, changing the population size from $N = 1 \times 10^5$ to $N = 1 \times 10^4$ shifts the estimate of r by

less than 50% (results not shown).

Table 2.2: Observable quantities calculated from HIV *pol* sequences *

Patient †	Sample size	No. of diverse sites	% in simulation ‡	Observably diverse sites ($f > 25\%$)	% in simulation	Very diverse sites ($f > 0.25\%$)	% in simulation	Avg. LD of v. div. pairs	95% CI over pairs	Fraction of v. div. pairs with 4th hap $< 4\%$
1	20	63	0.28	63	0.28	11	0.05	0.43	0.09	0.09
1	30	72	0.32	28	0.12	14	0.06	0.75	0.05	0.6
1	17	49	0.22	49	0.22	11	0.05	0.8	0.05	0.31
2	30	46	0.2	9	0.04	4	0.02	0.75	0.33	0.33
2	12	21	0.09	21	0.09	5	0.02	0.7	0.28	0.3
3	18	39	0.17	39	0.17	8	0.04	0.55	0.14	0.18
3	43	71	0.31	36	0.16	5	0.02	0.53	0.25	0.2
4	38	76	0.34	44	0.19	13	0.06	0.67	0.09	0.44
4	22	70	0.31	70	0.31	11	0.05	0.37	0.09	0.07
Average ± SD	26	56 ± 19	0.25 ± 0.08	40 ± 19	0.16 ± 0.09	9 ± 4	0.04 ± 0.02	0.62 ± 0.15		0.28 ± 0.17

CI, confidence interval

* Results shown are compared with simulation predictions to estimate model parameters(Fig. 3·2).

† Two to three time points are shown per parient.

‡ For comparison with simulation, where L variable sites in the genome are explicitly modeled, the number of diverse sites observed in data from *pol* is extrapolated to the corresponding percentag of all variable sites that would be observed in the entire genome [i.e., by dividing by the fractino of the entire genome that is considered variable (2,000)].

An upper bound for the best-fit value of s_0 used in Fig. 2A-B has been estimated using the dependence of the net change in virus fitness on s_0 predicted by the model (Fig. 2D). Since fitness gain is not observable for our dataset, we use information from dynamic models specific for HIV infection to estimate the maximum fitness increase during chronic infection. Existing models of HIV dynamics describe a steady state controlled by immune cells (virus specific CD8 or CD4 T cells). These models predict a steady state for the populations of susceptible CD4 T cells, infected cells, and immune cells that control virus. The level of infected cells in these models is fixed by the condition that immune cells stay at a constant level. As a result, the steady state value for uninfected CD4 T cells is inversely proportional to the virus fitness (replication ability) (33-36). This prediction is not completely model-independent, but common for many models in which virus

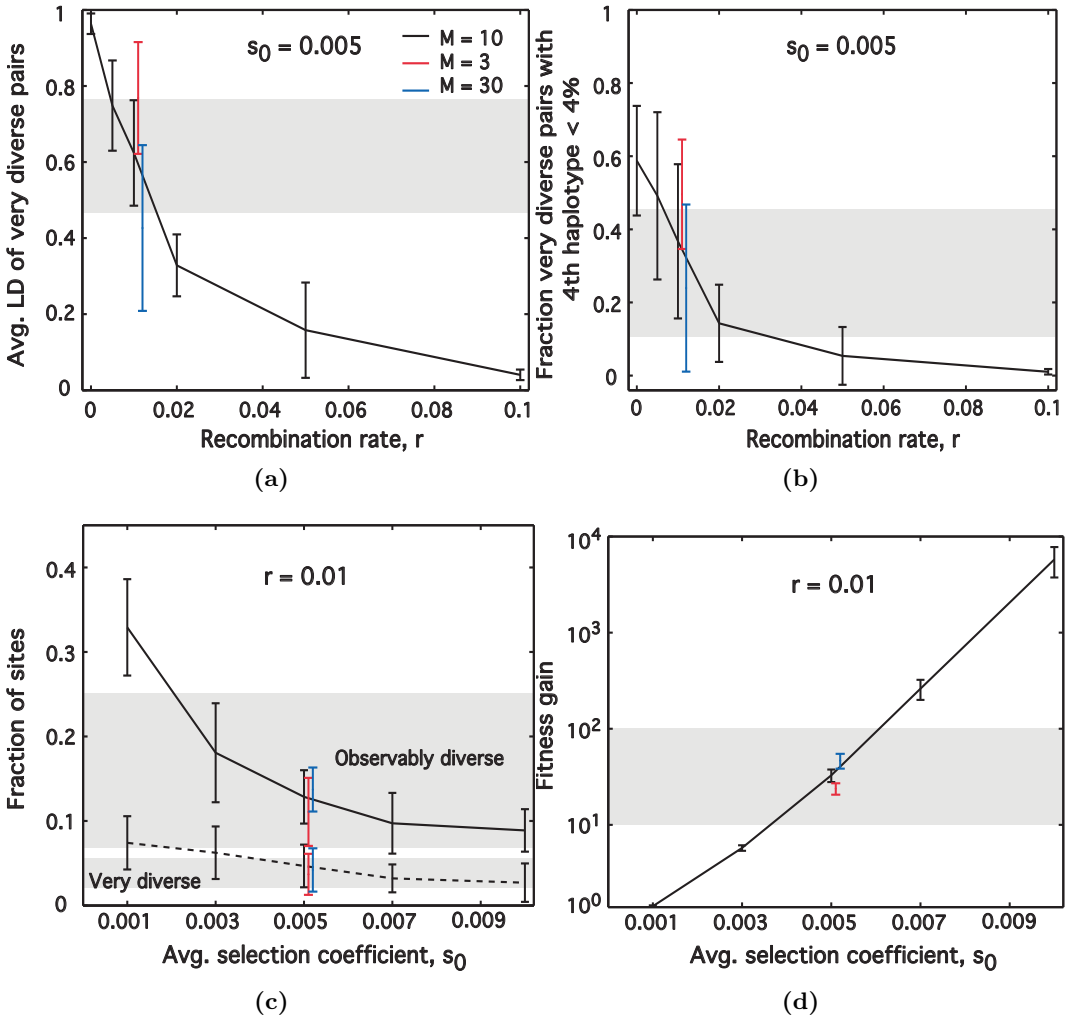

Figure 2·3: Estimation of model parameters for chronic HIV infection. Recombination rate, r, and average selection coefficient, s_0, are estimated by comparing four observable quantities in data with their predicted values in simulation. Grey regions indicate the mean ± one standard deviation of quantities calculated from data from the pol gene in 4 patients (Table 1). In simulation, each quantity is calculated at day 1500 for 11% of the genome. An average over 16 random runs is shown, with error bars showing the standard deviation over runs. Results are shown for a single population size, $N = 10^5$, and 3 values of the crossover number, M: 3 (red), 10 (black), and 30 (blue). Results for different M are shifted slightly horizontally for clarity. (A) Linkage Disequilibrium (LD) of very diverse pairs for $s_0 = 0.005$. LD is defined as $1 - \langle f_{AB,LRH}/f_A f_B \rangle$, where $f_{AB,LRH}$ is the frequency of the least-represented haplotype for a pair of sites A and B, $f_A f_B$ is the product of one-site frequencies or the value of $f_{AB,LRH}$ is in the absence of linkage for $s_0 = 0.005$. (B) Another measure of LD: fraction of very diverse pairs with the frequency of the least represented haplotype below 0.04 for $s_0 = 0.005$. (C) Fraction of sites that are observably diverse (solid) and very diverse (dashed) for $r = 0.01$. (D) Population average fitness for $r = 0.01$. Other fixed parameters are shown in the legend to Fig. 1.

is controlled by the immune response. If virus fitness increases slowly due to adaptation to a host (the process described in the present work), the exact steady state becomes a quasi-steady state, and the CD4 count declines slowly. Furthermore, the increase in virus fitness can be linked to progression to AIDS. Between post-acute phase and fully developed AIDS the CD4 T cell count drops from ~ 500 to $5-50$ cells/μl blood. This decrease in CD4 cell count corresponds to a fitness increase between 10 and 100, which specifies the estimate $s_0 \sim 0.005$ for both the exponential and power law ($a = 2$) distributions. For larger s_0, the fitness gain is too large.

The estimate $s_0 \sim 0.005$ is a reliable upper bound, given that target cells cannot be entirely depleted during chronic infection. However, since depletion could occur by other mechanisms than increasing virus fitness, it is desirable to estimate the lower bound for s_0 by another method. By comparing the predicted levels of observably diverse and very diverse sites in simulation with the respective levels measured in patient data for pol (Fig. 2C), we estimate that s_0 is greater than 0.003. Combining the two methods, we obtain $s_0 = 0.003 - 0.005$.

In the above simulation examples, the initial population is assumed to be uniformly less-fit. We checked that including beneficial alleles at the start of simulation, either at a small frequency at each site or at a frequency determined by the selection coefficient at a site, weakly affects our final estimates of r and s_0 because, at very small $r \sim 0.01$ studied in the present work, preexisting alleles are quickly lost from a population. At larger r, recombination of preexisting alleles can be very important and dominate evolution for a long period of time (Rouzine, 2005a; Gheorghiu-Svirschevski et al., 2006; Rouzine and Coffin, 2007; Rouzine and Coffin, 2010).

We have focused on the exponential distribution, because it is simple and describes data well. Similar results are obtained with the power law distribution $a{s_0}^a/(s+s_0)^{a+1}$, with $a = 2$ or larger. For a less than 1, suitable fitting parameters r and s_0 cannot be found, because too few sites are observably diverse. The likely reason is that too many alleles with large s ("fat tail") push out alleles with small s from the existence before they have chance to be incorporated by recombination. Detailed comparison of various distributions of s based on more recent longitudinal data will be

given elsewhere.

2.4 Discussion

How important is the estimated low incidence of recombination for HIV evolution? On the one hand, it is far to low to fully compensate effects of linkage: The adaptation rate remains smaller than predicted by single-site model by a factor of 4, and significant LD is observed, by either measure (Fig. 2·3 A and B). At the same time, the adaptation rate is higher, and LD is smaller (Fig. 2A and B), than in the case of purely asexual reproduction. We conclude that even a recombination rate of 1%, with 10 crossovers per $200 - 300$ sites observably diverse in small samples, has a significant effect on HIV evolution in vivo.

Linkage effects are predicted to disappear in very large populations. Therefore, the existence of random drift and sampling due to finite population size is also a very important factor. A typical infection comprises $N \sim 1 \times 10^8$ infected cells, and would seemingly suggest that the effect of finite population size is small. However, due to variation in the reproduction rate of infected cells may lead to an "effective population size" that is much lower. That is, a small number of infected cells could be producing the majority of free virus, and hence genetic drift may be an important factor. Early estimates based on few-site models suggested, at least $10^5 - 10^6$ infected cells (Rouzine and Coffin, 1999b; Frost et al., 2000; Frost et al., 2001). Analytic models of multi-site evolution predict that, although a finite population size is important, the adaptation rate depends rather weakly (logarithmically) on it (Rouzine, 2005a; Gheorghiu-Svirschevski et al., 2006; Rouzine and Coffin, 2007; Rouzine and Coffin, 2010; Neher et al., 2010). In our simulation, variation of N between 10^4 and 10^5, leads to only a moderate ($< 50\%$) change in the estimate of r. Obtaining a reliable estimate of N from multi-site model is difficult. Rather, analysis of sites with conspicuously large values of s ($\sim 10\%$ or larger) that can be treated with 1-site models is needed. Possible candidates for such sites include those with primary drug-resistance or antigenic escape mutations.

Our estimate effective cell co-infection rate in a typical untreated patient, $r \sim 0.01$, is much lower than the value of $r \sim 1$ reported previously based on two tissue samples (Jung et al., 2002) and

14 fold lower than obtained in a neutral coalecent-based study (Shriner, 2004). In addition, our experimental studies show that less than 10% of infected cells have a second provirus. The effective co-infection rate can be lower than the census rate due to proximity effects in the tissue and resulting similarity between co-infecting sequences.

Neher and Leitner (Neher and Leitner, 2010a) recently estimated the recombination rate per base per cycle, 1.4×10^{-5}, and the fraction of diverse sites with $s > 0.008$, 15%. Given 10 crossovers per genome and assuming exponential distribution of s, these estimates translate into r 0.014 and s_0 0.05, which is very similar to our results. To estimate the two parameters, these researchers used two different simplified models: The first model, used to estimate r, assumed selectively neutral evolution of partly linked pairs of sites. The value of r was determined from longitudinal samples of sequences by fitting dynamics of the appearance of the fourth haplotype in pairs of sites in which it was initially absent. The second model, used to estimate s_0, assumed deterministic evolution of a site under positive selection unlinked from other sites. In general, both linkage and selection are crucial (Rouzine and Coffin, 2010; Neher et al., 2010). Neher and Leitner justify this simplified approach by applying the two models to sites with either a slow or rapid (top 15%) change in allelic frequency, respectively, interpreted as sites with small s (rather than impeded by clonal interference) and large s (rather than hitchhikers). The lack of synonymous sites among the top 15% sites and estimates are used to support this assumption. It also agrees with our example in Fig. 2·3 B. The validity of this method remains to be tested by simulation.

The advantages of our study are as follows. (i) We estimate both parameters from a relatively realistic model, including mutation, selection, genetic drift, linkage of many sites, and recombination. (ii) Both measures of LD are sensitive to the value of r (rapid decay in Fig. 2·3 A and B), (iii) Our method of estimating r works with single-time samples, thus helping to save experimental labor. (iv) Our sequences were obtained using single genome sequencing much less prone to technical artifact, including PCR-derived mutation and recombination, than that cited by Neher and Leitner (Neher and Leitner, 2010a).

We used two sensitive measures of LD to estimate the effective recombination rate: the average normalized frequency of the least-represented haplotype and the frequency of pairs missing a haplotype in a small sample. Not every measure of LD is suitable for our task. For example, Lewontin's measure, D, which measures the difference in the observed frequency of a haplotype from the expected frequency, is predicted to have a random sign when measured in simulation, and thus to vanish after averaging over pairs of sites separated by the same distance in the genome (Gheorghiu-Svirschevski et al., 2006). This result is specific for a system with a large number of sites, because two-site models predict negative D at a small recombination rate. Also, it is not generally known which nucleotide variant at a site is better fit, information that is required for calculating D. Our observable quantities are designed to be independent of that information. Coalescent-based estimates of r (Shriner, 2004; McVean et al., 2002) are biased by the assumption of neutrality.

The complexity of the model is determined by the aim of the study and the amount of information in the dataset. A rule of thumb is not to use a more complex model when a simpler model provides a good fit to the data. Here, we made a number of simplifications. (i) Epistasis is known to exist for other RNA viruses (Burch et al., 2003; Ayme et al., 2007; Novella, 2004; Weinreich et al., 2005) and has been reported for HIV (Bonhoeffer, 2004; Poon et al., 2010); it may contribute to the average values of LD. We hope that the importance of epistasis for the HIV genome in vivo will become clearer in the future, but we have ignored it here. (ii) Deleterious mutations have similarly been ignored. Although strongly deleterious mutations hardly matter, it is difficult to estimate how many sites have a weak deleterious effect, with a mutation cost of ¡1% or less. They may act through background selection, reducing the effective population size. (iii) We assumed that the pol gene is representative and extrapolated experimental results to the entire genome. (iv) Typical diverse sites have been considered at which there is constant directional selection. Some rare but biologically important sites, such as neutralizing antibody-binding regions or CTL epitopes, may require separate treatment.

By simulating an advanced model of HIV evolution and applying it to sequence data, we have obtained important estimates of the effective recombination rate and the average selection coefficient.

Detailed understanding of system dynamics and interaction between various evolutionary factors will require further development of the existing analytic models.

2.5 Methods

2.5.1 Patient Data

We have used 9 sets of HIV pol sequences isolated from 4 untreated patients with 2 to 3 time points per patient. The number of sequences per sample varied between 12 and 42, with an average of 25. Plasma samples were obtained from adult patients with chronic HIV-1 infection enrolled in studies at the NIH Clinical Center, Bethesda MD. All patients provided written informed consent. Sequences were obtained by single genome sequencing as previously described (46). This method has a very low assay error rate, with essentially no assay-based recombination. Lengths of sequences ranged from 1200 to 1250nt. Sequences were aligned using Clustal X (DNASTAR-MEGALIGN or MEGA). A consensus sequence of length 1100 nucleotides was used to convert each sequence into a binary string, to indicate whether each site in a sequence matches the consensus sequence. Since the measured quantities make no assumption about which allele is beneficial at an observably diverse site, the results are insensitive to the consensus sequence used. Sample sizes for different sequence sets, numbers of diverse sites, and the two measures of linkage disequilibrium (see below) are summarized in Table 1.

2.5.2 Adaptation rate in the limit of frequent recombination.

In the limit of frequent recombination, $r = 1$ and large M, a single-site model applies. The adaptation rate K (defined as the average rate of log fitness increase) depends on the product $N\mu$. At small $N\mu$ below $1/[4\ln(s/\mu)]$, a typical site is uniform most of time. The adaptation rate is limited by generation and establishment of rare alleles. We have $K = N\mu L\langle 2s^2\rangle = 4N\mu L s_0^2$, where $N\mu L$ is the allele generation rate, s is the contribution of an allele to log fitness of a genome, $2s$ is the fixation probability limited by random drift, and we assumed an exponential distribution of s with the average s_0. In the opposite limit $N\mu \gg 1/[4\ln(s/\mu)]$, which is true at $N = 10^5$ assumed

in our simulation, new alleles are always present at each site, and genetic drift is a small correction. The adaptation rate K is now limited by finite time of a selection sweep, $t_{sweep} = (2/s)\ln(s/\mu)$, during which the allele frequency changes from almost 0 to almost 1 (more precisely, from μ/s to $1 - \mu/s$). As a result, we have $K = L\langle s/t_{sweep}\rangle = L\langle s^2/[2\ln(s/\mu)]\rangle = Ls_0^2/\ln(s_0/\mu)$.

Chapter 3

Complex patterns of escape in CTL epitopes

3.1 Introduction

It is widely recognized that CTL contribute to the control of HIV replication. Many CTL clones target the virus simultaneously, each clone recognizing a distinct 8-10 amino acid viral peptide (epitope) presented on the surface of an infected cell by MHC molecules. Escape mutations in CTL epitopes begin to be selected with a month of infection and continue to be selected throughout chronic infection, sometimes causing a decrease in the intrinsic replication rate of the virus (fitness cost) (Leslie, 2005; Friedrich et al., 2004; Troyer et al., 2009). However, despite a sustained CTL response, not all targeted epitopes escape. Moreover, among epitopes that do escape, the rate of escape slows dramatically over the first 100 days post infection (Liu et al., 2011; Ganusov et al., 2011).

During the majority of escapes, the transmitted epitope sequence is not replaced by a single mutated epitope sequence. Rather, between 2-10 mutated epitopes with distinct sequences grow in number to replace the transmitted sequence, and eventually one mutant epitope spreads to the entire population (Cale et al., 2011; Goonetilleke et al., 2009a). Furthermore, the dominant mutated epitope sequence appears to change over time (Goonetilleke et al., 2009a; Liu et al., 2011; Fischer et al., 2010). In (Goonetilleke et al., 2009a) it was observed that the mutated sequence changed over time in the majority of epitope that were followed over time. In a small number of epitopes (3/18) mutations were selected in additional epitope sites without the reversion of the initial mutated site ("nested pattern"). In a larger number of epitopes (7/18) the site in which a mutation was initially selected later reverted, coincident with the selection of a mutation at a different site ("leapfrog" pattern). In the remaining 8/18 epitopes, a single mutation in the transmitted epitope was selected

and the mutation was maintained stably in the population for the duration of the study ("simple" pattern).

Both the timing of escape across many epitopes and the pattern within epitopes can give information about the ease with which a single mutation evades the CTL response and also about the fitness costs of the mutation. In general, an escape mutant does not fully abrogate recognition by a CTL. It has been observed in HIV infected individuals (Liu et al., 2011) and SIV infected animals (Cale et al., 2011) that CTL are capable of recognizing different variants of the epitope with differing efficiencies. Fitness costs of escape mutations can be inferred from the observation of occasional reversion of escape mutations in transmission between MHC mismatched individuals (Leslie, 2005; Friedrich et al., 2004). Reversion in these examples is typically slow, and suggests that the uncompensated fitness cost upon transmission is small. Common escape mutations have been shown to have wide ranging fitness costs using growth competition assays (Troyer et al., 2009). It is of interest to understand the extent to which fitness costs limit the growth of an escape mutant. It would then be possible to create vaccines that prime CTLs that target epitopes with prohibitively high fitness costs.

The interaction between CTL clones and a diverse population of infected cells is a complex and dynamic process. Mathematical models of HIV evolution in the presence of multiple CTL clones have been applied to study the emergence of late escapes (Althaus and Boer, 2008; Mostowy et al., 2011) and the effect of distributed CTL pressure on the rate of escape (Ganusov et al., 2011). We extend the basic model introduced in these works to consider the case where an epitope can escape by mutations multiple epitope sites. Each mutation abrogates a fraction of CTL recognition and thus multiple epitope variants can arise in response to CTL pressure. We analyze the dynamics of escape and conclude that variation in CTL recognition loss among epitope sites is sufficient to reproduce patterns observed in recent data on CTL escapes.

3.2 Model

We model SIV/HIV evolution in the presence of multiple CTL clones, each of which responds to a distinct viral epitope (Fig. 3·1). We consider n epitopes, each consists of m sites, giving a total of 2^{mn} possible strains. Target cells (T) are replenished at a rate λ cells per day and die with a rate d_T and are infected by virus at a rate that depends on the fitness on the infecting strain, with maximum rate β, and the number of productively infected cells in the system (I). An cell infected is labeled by proviral genome j with n epitopes by $g^j = e_1^j, e_2^j, ..., e_n^j$, where each e_i^j has m sites $e_i = a_{1i}^j, a_{2i}^j, ..., a_{mi}^j$, where $a \in 0, 1$; the strains with all 0 is the infecting strain. The fitness of genome j is reduced by mutations, and is given by $f_j = \exp - \sum_{i=1}^{n} \sum_{k=1}^{m} s_{ki} a_{ki}^j$. The fitness of the transmitted strain is defined as 1. Effector cells (E) are replenished with a constant rate σ cells per day, and divide with a rate dependent on the number of infected cells that they recognize, with maximum rate c and die with rate d_E. The recognition ability of the effector to epitope i in strain j is reduced by mutations, given by $\alpha_i^j = \exp - \sum_{k=1}^{m} r_{ki} a_{ki}^j$. Equations for all compartments, are given below, model parameters and estimated range of values are listed in table 3.1.

$$\dot{T} = \lambda - d_T T - \beta T \sum_{j=1}^{2^{mn}} f_j I_j \tag{3.1}$$

$$\dot{I}_j = (\beta f_j T - d_I - \kappa \sum_{i=1}^{n} \alpha_i^j E_i) I_j \tag{3.2}$$

$$\dot{E}_i = \sigma + (\frac{c \sum_{j=1}^{2^{mn}} \alpha_i^j I_j}{h + \sum_{j=1}^{2^{mn}} \alpha_i^j I_j} - d_E) E_i \tag{3.3}$$

Mutations are generated randomly with rate $\mu = 3 \times 10^{-5}$ per site per generation between strains that differ by one site. Only strains that are generated randomly in excess of one infected cell are simulated deterministically according to the above equations. The basic model with one site per epitope ($m = 1$) has been introduced by (Althaus and Boer, 2008). We have introduced several simplifications. In order to focus on the effect of partial recognition and fitness losses in a few, immunodominant CTL, we make the simplification that all CTLs have initially equal avidities. Furthermore, we do not introduce compensatory mutations into the model. In reality, compensatory

mutations outside the epitope do occur, and prevent reversion of costly escape mutations. We focus on the interval of time before compensation occurs. See Discussion for further details of how compensation for fitness losses relates to our results. We also assume that both target cells and CTL are short lived, with average lifetimes of 1 and 10 days, respectively. Finally, we assume that the overall density of epitope-specific CTLs is low during steady state (Haase, 2011), and hence the CTL growth rate does not saturate due to high overall CTL levels.

Table 3.1: Model parameters for a model of escape from the CTL response

Parameter	Realistic Value	
n	1- 8	number of epitopes recognized during first 100 days
m	2 - 10	number of sites per epitope important for recognition
d_T	1 d^{-1}	target cell death rate
λ/d_T	5×10^8 cells	target cell level in absence of infection
d_I	1 d^{-1}	virus-induced infected cell death rate
$\sum_i \kappa E_i^{ss}$	4 d^{-1}	CTL-induced infected cell death rate
β	$1.1 \times 10^{-8}(d \cdot cell)^{-1}$	basic efficiency of infection
$fj = \exp - \sum_{i=1}^{n} \sum_{k=1}^{m} s_{ki} a_{ki}^{j}$	$s_{ki} \in [0, 1]$	fitness of genome j, sum over all epitopes i, sites k.
κ	$1 \times 10^{-9}(d \cdot cell)^{-1}$	killing efficiency
σ/d_E	10^3 cells	small population of naive cells in absence of infection
c	1 d^{-1}	maximum growth rate of effector cells
d_E	0.1 d^{-1}	death rate of effector cells
h	2.5×10^8 cells	number of recognized infected cells for half maximal proliferation of effector i
$\alpha_i^j = \exp - \sum_{k=1}^{m} r_{ki} a_{ki}^{j}$	$r_{ki} \in [0, 1]$	strength of recognition of effector i of strain j.

3.3 Results

In order to study the dynamics of escape in multiple epitopes, we consider a genome with n epitopes and a single site per epitope ($m = 1$). We assume the infection is formed with a single virus strain, called the transmitted strain. The expansion of infected cells in acute infection causes all n CTL clones to expand. The expansion of CTL, in turn, reduces infected cell levels until the expansion of CTL is balanced by their death (steady state). From Eq. 3.1 - 3.3 we obtain the steady state conditions for all cell compartments before escape has occurred.

$$T^{ss} = \frac{\lambda}{d_T + \beta I^{ss}} \tag{3.4}$$

$$I^{ss} = \frac{d_E h}{c}, d_E \ll c \tag{3.5}$$

$$E_i^{ss} = \frac{E_{\text{tot}}}{n}, E_{\text{tot}} \equiv \frac{\beta T^{ss} - d_I}{\kappa} \tag{3.6}$$

Importantly, the level of infected cells in steady state is proportional to the inverse avidity of the CTL clones. For n equal-avidity CTL clones, each clone makes up $1/n$ of the total CTL population, E_{tot}. Once CTL are near their steady state values, escape mutations begin to be selected.

3.3.1 Escape rate is determined by loss of CTL recognition and loss of fitness

Our model provides a way to identify factors that determine the rate escape in CTL epitopes. Though mutations occur randomly in the genome during each replication cycle, they do not confer an advantage to viral replication until CTL reach high levels. Once CTL are near steady state, escape mutations begin to be selected. The escape rate varies among epitopes due to different amounts of recognition and fitness losses caused by a mutation. In the model with one site per epitope, mutations in all epitopes begin to grow simultaneously, albeit with different rates. When the population is uniform in the transmitted variant, a mutated variant with a single mutation in epitope one has the growth rate given by Eq. 3.2:

$$\dot{I}_{100\ldots} = (\beta T e^{-s_1} - d_I - \kappa(\sum_i E_i - E_1(1 - e^{-r_1}))I_{100\ldots} \tag{3.7}$$

The same holds for single mutations in epitopes $1..n$. The selective advantage of this mutant variant relative to the transmitted variant (i.e. the rate of escape) is given by the difference between the mutant and the wild type exponential growth rates. Throughout this work we consider small fitness costs, and therefore neglect changes in target cells. The mutant strain will begin to grow with exponential rate:

$$\epsilon_1 = \kappa E_1^{ss}(1 - e^{-r_1}) - \beta T^{ss}(1 - e^{-s_1}) \tag{3.8}$$

Before escape occurs, all cell compartments are near steady state levels. The initial escape rate can be written in terms of the infected cell death rates kE_{tot} and d_I using Eq. 3.3:

$$\epsilon_1 \approx kE_{\text{tot}}[\frac{1 - e^{-r_1}}{n} - (1 + \frac{d_I}{kE_{tot}})s_1] \tag{3.9}$$

Where in the last step we have made the approximation that all cell compartments are at their steady state values, and that the fitness cost of a mutation is small, $s_1 \ll 1$. The escape rate is thus a balance between the fraction of recognition lost and fitness lost. The first term in Eq. 3.9 reflects the fraction of the total CTL-imposed selection pressure that is focused on that epitope. Since CTL are initially identical, this fraction is initially $1/n$ for all epitopes.

When multiple epitopes are targeted, sequential escape is observed (Fig. 3·3). In a model where recognition is abrogated completely by a single escape mutation (Althaus and Boer, 2008; Ganusov et al., 2011; Mostowy et al., 2011), epitopes targeted by equal avidity CTLs will escape in order of increasing fitness costs. In our model, where recognition loss is allowed to vary over sites, both recognition and fitness losses determine the initial rate of escape. For similar fitness costs at all epitope sites, the initial escape rate of a mutation will be proportional to the amount of recognition lost by the mutation (Fig. 3·3 A).

It data from HIV infected individuals, it is observed that the rate of escape slows dramatically over the first 100 days post infection (Fig. 3·2). Both the absolute escape rates and rate of change over time of escape rates can be reproduced with only minor fitness cost, and variation of recognition loss over multiple epitopes (Fig. 3.8 D).

3.3.2 Steady state is changed by escape

CTL targeting results in the growth of escape mutations, but CTL dynamics are also affected by the escape mutations that they select. Once an escape mutation in an given epitope has spread to the majority of the population, the corresponding CTL clone receives less stimulation from infected cells, and begins to decline in number. We call the level of infected cells that maintains a given CTL clone in steady state the activation threshold for that clone, $I^{th,i}$, for CTL clone i. When an escape mutation in an epitope has spread to the majority of the population, CTL to that epitope recognize infected cells less efficiently. The number of infected cells that would be necessary to maintain the clone in steady state is raised, giving the new thresholds:

$$I^{th,i} = I^{ss} e^{r_i} \tag{3.10}$$

(In an epitope with many sites, the exponent is the sum is over the recognition losses of all sites, k, in epitope i that have escaped, $I^{th,i} = I^{ss} e^{\sum_\kappa r_{ki} a_{ki}}$). CTL thresholds evolve simultaneously with the emergence of escape mutations (Fig. 3·3 B), reaching maximum values given by Eq. 3.10 when escape is complete.

As long as there is at least one CTL clone in the population that targets an epitope of the transmitted variant, and thus maintains it's original low threshold, the steady state level of infected cells will not change. This is because CTL to unescaped epitopes will be able to recognize all infected cells in the population, regardless of sequence, with high avidity.

If escape mutations entail a fitness cause, causing the efficiency of infection of the dominant virus strain to decrease, the number of target cells in steady state will increase. For example, an escape in epitope one will change the target cell level according to:

$$T^{ss} = \frac{\lambda}{d_T + \beta \exp(-s_1) I_0^{ss}} \tag{3.11}$$

Likewise, the total level of CTL in the system, E_{tot}, responds to the replication rate of the virus βT^{ss} (Eq. 3.6). For small fitness costs, we can neglect changes in the total populations of CTL, target cells, and infected cells.

3.3.3 CTL decay in response to decreased recognition ability

Since CTL to partially escaped epitopes receive less stimulus from infected cells due to raised thresholds, their numbers decline. The fraction of the total CTL population made up by an individual CTL clone will change as escape mutants in that epitope emerge.

A schematic of the situation where only one transmitted epitope remains is shown in Figure 3·1 B. CTLs to epitopes in which some sites have escaped receive less stimulus from infected cells, decline in numbers, and hence contribute less to the killing of infected cells. Figure 3·1 C shows the growth rates for the three CTL clones, in the situation where the population is entirely composed of the viral strain shown in Figure 3·1 B. Although recognition losses due to escape are partial ($\exp(-r_i) < 1$), CTL to escaped epitopes decay due to the presence of a more avid CTL clone in the population. Once an escape mutant dominates the population, the corresponding CTL clone will decay according to:

$$E_i(t) = \frac{E_{\text{tot}}}{n} e^{(-d_E(1-e^{-r_i}))t}, \qquad d_E e^{-r_i} \ll 1 \tag{3.12}$$

CTL decay after escape mutations cause a reduction in recognition in ability to recognize infected cells, according to Eq. 3.12 (Fig. 3·3 C). In our model with many CTLs with identical thresholds, escape in an epitope leads to the decay of the corresponding CTL. Intriguingly, this is the case even if the amount of recognition lost is very small, due to the presence of other CTL in the population with lower thresholds.

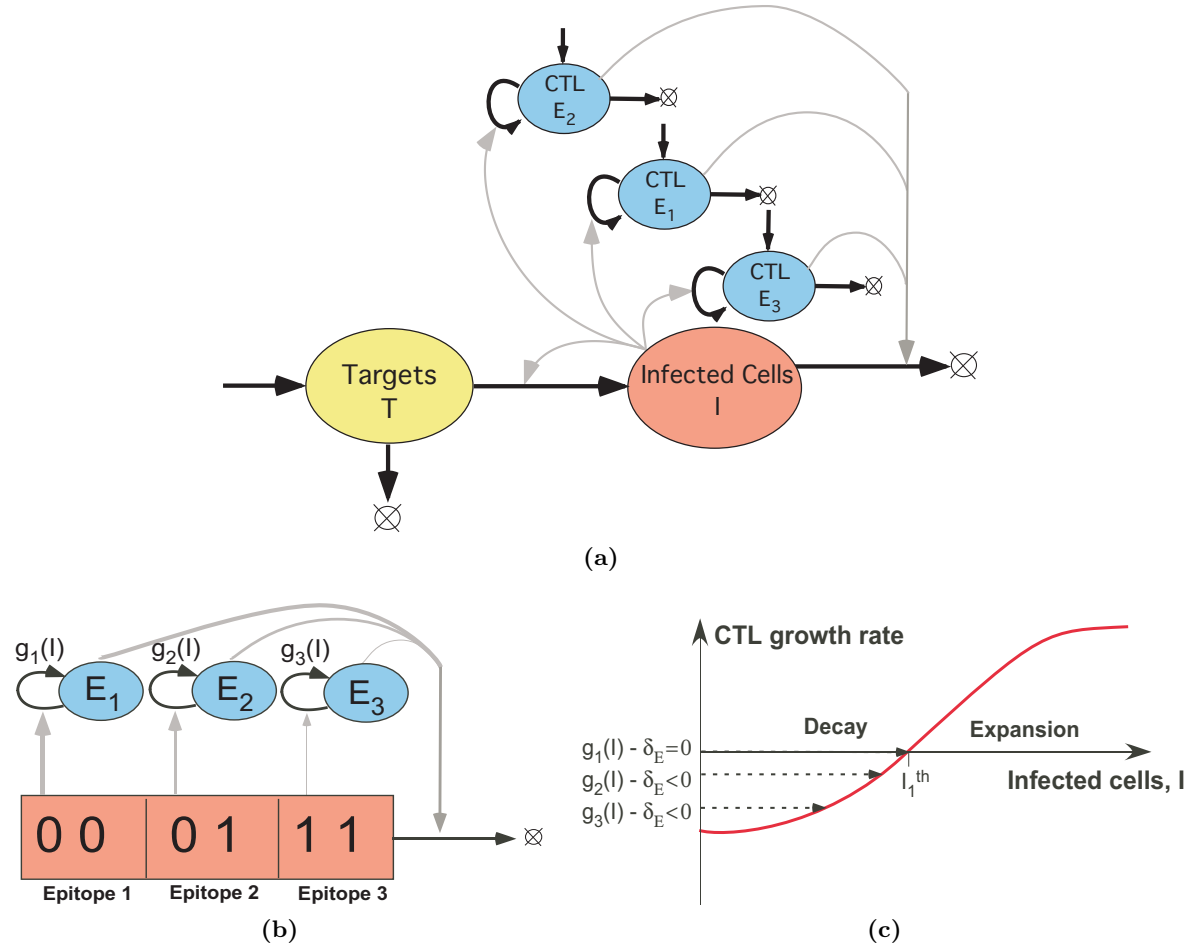

Figure 3·1: A model of the interaction between HIV and the host immune system. (A) The model comprises three interacting cell compartments: target cells (T), productive infected cells (I) and multiple CTL (E_1, E_2, E_3). Black arrows: flux of cells from one compartment to another. Grey arrows: dependence of the rate of flux from one compartment on another compartment. (B) An example with three CTL clones responding to a population dominated by cells infected with the virus strain shown. Each clone is stimulated to divide at a rate proportional to the amount of recognized infected cells in the system. The virus strain has three epitopes, with two sites each. "1" denotes an escape mutation at an epitope site, "0" denotes no escape mutation. The thickness of the grey lines indicates the strength of the interaction. (C) A schematic of the dependence of the effector expansion rate on the number of recognized infected cells for the situation shown in b. When the entirely unmutated epitope reaches steady state, the CTL to mutated epitopes decay.

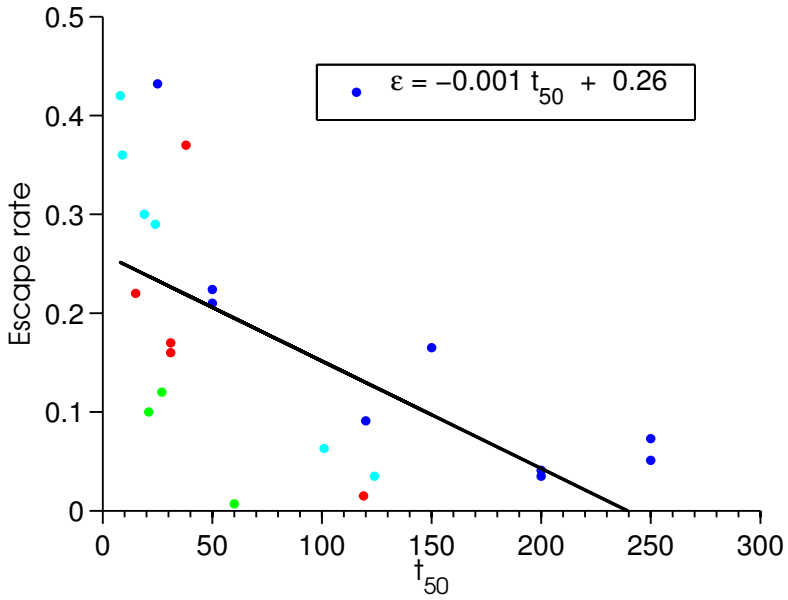

Figure 3·2: Escape rate and t_{50} are negatively correlated in two experimental studies Two experimental studies show slowing of escape rates with time. Parameters ϵ and t_{50} are found that fit the lines in (A) to the curve $f(t) = (1 + \exp(-\epsilon(t - t_{50})))^{-1}$, which describes deterministic selection on a single site with selection coefficient ϵ. Colored dots show data from (Liu et al., 2011), (blue) and (Goonetilleke et al., 2009a) [CH40 (red), CH58 (green), CH77 (cyan)].

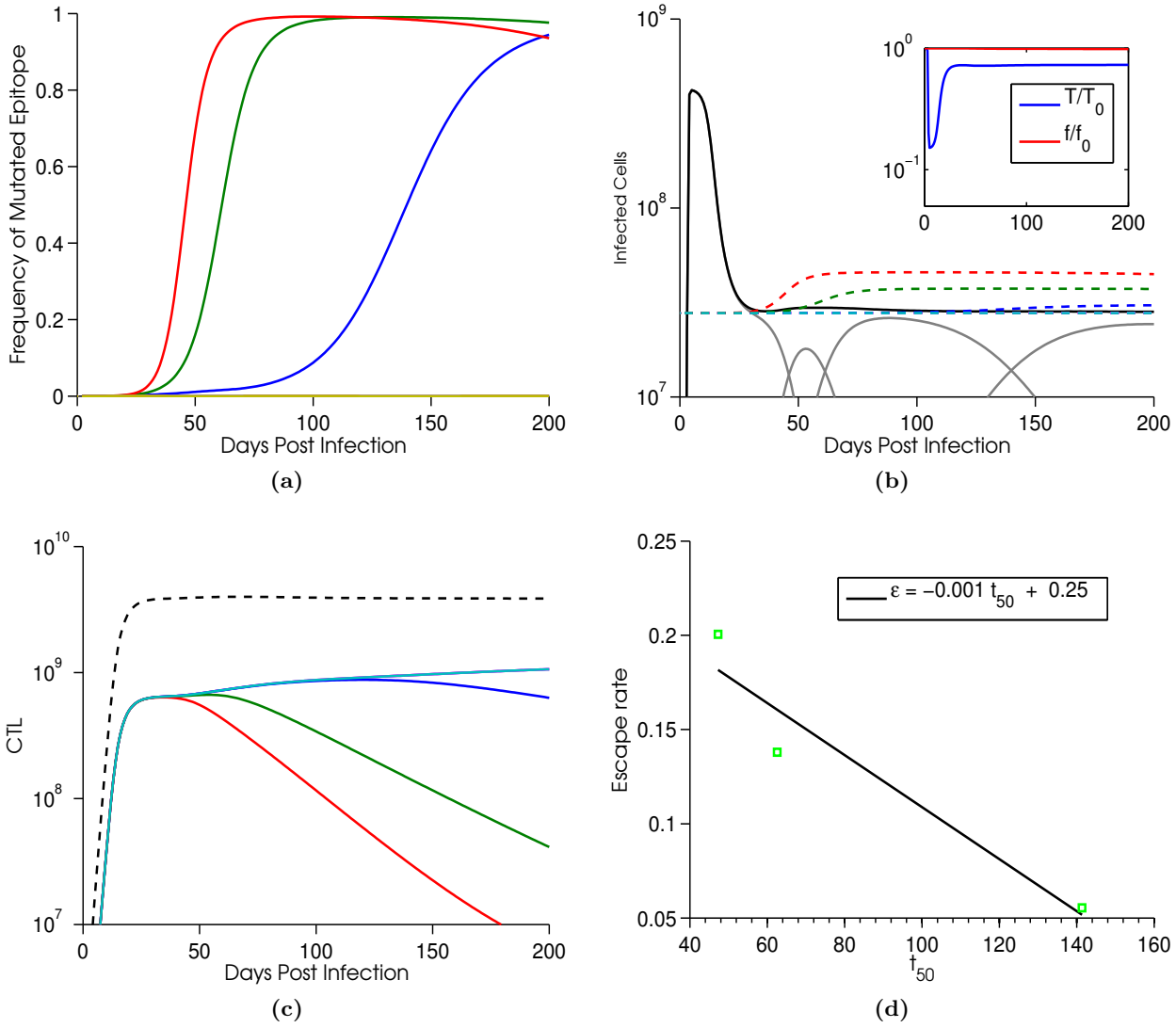

Figure 3·3: Escape in multiple epitopes with one site per epitope (A) Frequency of mutated epitopes (B) Infected cells of wild type (black) are rapidly replaced by mutant strains (grey). CTL thresholds, I^{th}, are initially identical, but change over times as escapes occur (dashed, colors as in (A)). Escapes in impair recognition ability, these thresholds increase in time. Inset: remaining target cells and virus fitness averaged over the population as fractions of their initial values. (C) Individual CTL clones (colors correspond to epitopes as in (A)) respond to the amount of virus infected cells that they recognize, while the total number of all CTL (black dashed) remains constant. (D) Escape rate ϵ and the time to reach 50% for all epitopes. Parameters ϵ and t_{50} are found that fit the lines in (A) to the curve $f(t) = (1 + \exp(-\epsilon(t - t_{50})))^{-1}$, which describes deterministic selection on a single site with selection coefficient ϵ. Model parameters: number of epitopes, $n = 8$; number of sites per epitope,$m = 1$. Epitopes 1-4 have parameters that allow escape $r_i = [0.1, 0.2, 0.3, 0.4], s = 0.01$, epitopes 5-8 have parameters that prohibit escape $s_i = r_i = 0.1$. Other parameters are as listed in Table 3.1. Differences in recognition and fitness losses across many epitopes successfully reproduces many features of escape dynamics.

3.3.4 Patterns of escape in one epitope with two sites

Leapfrog pattern in an epitope

If an epitope has many sites, and the amount of recognition and fitness lost per mutation varies over sites, many possible epitope sequences can emerge in response to CTL pressure. Furthermore, the escape epitope sequence (haplotype) that is dominant can change over time. The leapfrog pattern is characterized by a switch in the dominant single-mutant haplotype in an epitope; For example, in an epitope with two sites, the sequence of haplotypes observed in an epitope is $00 \to 10 \to 01$, rather than the simple escape pattern $00 \to 10$ or the nested pattern $00 \to 10 \to 11$.

The exponential growth rate of any given haplotype depends on the amount of recognition and fitness lost by the mutation(s), as well as level of the CTL to the epitope. The escape rate of a haplotype can be calculated using Eq. 3.8. However, since all sites in an epitope sites are targeted by the same CTL clone, escape in one site of an epitope will change the escape rate of all other sites in that epitope. This is because once a mutation in a single epitope site spreads to the population, the corresponding CTL clone to decay due to decreased recognition.

We consider the simplest model in which leapfrog dynamics can be analyzed and determine the parameter regime in which this pattern of escape can occur. A genome has multiple targeted epitopes, however, only epitope 1 has parameters that allow escape. All site indices in what follows will refer to sites in epitope one. Epitope one has two sites per epitope ($m = 2$) with parameters of fitness and recognition loss s_k, r_k, where $k = 1, 2$ indexes the epitope site. We assume that the amount of recognition and fitness lost by mutating an epitope site varies over sites, and that the escape rate of haplotype 10 in epitope one (ϵ_1) is higher than the escape rate of haplotype 01 (ϵ_2) prior to escape. Comparing initial escape rates when CTL are near steady state using Eq. (3.9):

$$(1 - e^{-r_1})/n - (1 + \frac{d_I}{kE_{tot}})s_1 > (1 - e^{-r_2})/n - (1 + \frac{d_I}{kE_{tot}})s_2 \tag{3.13}$$

If, in addition to having a greater initial escape rate, site one has both a greater fitness $s_1 > s_2$

and recognition loss, $r_1 > r_2$, decreasing E_1 levels can cause the favored haplotype to switch from 10 to 01. In order to observe the leapfrog pattern, r_k and s_k must be correlated in the epitope:

$$r_1 > r_2, s_1 > s_2 \tag{3.14}$$

These conditions are necessary but not sufficient to observe the leapfrog pattern. As CTLs decay, the second haplotype must gain advantage over both the first and the transmitted epitope before the transmitted epitope regains the advantage over the first. Therefore, we must compare the CTL level where 00 gains the advantage over 10, with that where 01 gains the advantage over 10. We assume that haplotype 11 does not reach appreciable frequency before 01 sweeps, and neglect changes in the steady state level of target cells. Both are good approximations as long as the fitness costs are small $s_1, s_2 \ll 1$, which we assume throughout this work. The exponential growth rate of haplotype 01 exceeds that of 10 when $\epsilon_{\text{10-vs-01}} = 0$.

$$\epsilon_{\text{10-vs-01}} = kE_{1,10=01}(e^{-r_2} - e^{-r_1}) - \beta T^{ss}(e^{-s_2} - e^{-s_1}) = 0 \tag{3.15}$$

Which occurs when E_1 decline to level:

$$E_{1,10=01} = \frac{\beta T^{ss}}{k} \frac{e^{-s_2} - e^{-s_1}}{e^{-r_2} - e^{-r_1}} \approx \frac{\beta T^{ss}}{k} \frac{s_1 - s_2}{e^{-r_2} - e^{-r_1}} \tag{3.16}$$

However, the wild type epitope also has a fitness advantage over 10, and will begin to grow once $\epsilon_{10-vs-00} = 0$, at E_1 level:

$$E_{1,10=00} = \frac{\beta T^{ss}}{k} \frac{1 - e^{-s_1}}{1 - e^{-r_1}} \approx \frac{\beta T^{ss}}{k} \frac{s_1}{1 - e^{-r_1}} \tag{3.17}$$

If $E_{1,10=01} > E_{1,10=00}$, then the leapfrog pattern can be observed. This condition can be written as the following inequality:

$$\frac{s_1 - s_2}{e^{-r_2} - e^{-r_1}} > \frac{s_1}{1 - e^{-r_1}} \tag{3.18}$$

As E_1 declines (Fig. 3·4 A), the CTL-induced pressure on epitope 1 declines and fitness losses begin to dominate the escape rate. If the conditions given in Eqs. 3.13, 3.14 and 3.18 are met, at some point the growth rate of haplotype 01 surpasses that of 10 and a switch in the dominant haplotype is observed (Fig. 3·4 B). We next consider the dynamics of the two single-mutant haplotypes in order to compare the time intervals during which a given haplotype is observed at high frequencies.

Lifetimes of single mutant haplotypes

The length of the time interval for which a given haplotype dominates the population will depend on parameters of loss and recognition at epitope site, s_k, r_k. In (Goonetilleke et al., 2009a), the 7/18 epitopes that display the leapfrog pattern show that the first haplotype is short lived compared to the second, and the transmitted epitope remains at low frequencies after it initially declines. In order to estimate the parameter range in which leapfrog escapes , we estimate the lifetimes of the two haplotypes (t_{10}, t_{01}). We define the lifetime of a particular haplotype, as the time interval during which a haplotype is dominant ($f > 0.5$) in the population.

The lifetimes of the two haplotypes for the two epitope example are shown schematically in Fig. 3·4. The lifetime of 10 the lifetime is comprised of two intervals: t_{g1}, the time interval from the moment 10 reaches 50% of the population to the moment that the second haplotype, 01 begins to grow, and t_{d1}, the time for 01 to grow to 50% of the population. Likewise, the lifetime of haplotype is composed of two intervals: t_{g2}, the time interval from the moment 01 reaches 50% of the population until 00 begins to grow, and t_{d2}, the time for 00 to grow to 50% of the population. The details of these calculations are given in Appendix B and the results in Table 3.2.

Table 3.2: Lifetimes of the two haplotypes in the leapfrog pattern

phase	haplotype 10	haplotype 01
growth	$t_{g1} = \frac{1}{\delta_1}\log(\frac{e^{-r_2}-e^{-r_1}}{n(1-\frac{d_I}{\beta T^{ss}})(s_1-s_2)})$	$t_{g2} = \frac{1}{\delta_2}(\log[\frac{E_{10\to 01}}{E_{01\to 00}}] - \delta_1 t_{d1}]$
decay	$\exp(-\delta_1 t_{d1}) = \frac{\delta_1}{\gamma_1}\log(N) + 1 - \delta_1 t_{d1}$	$\exp(-\delta_2 t_{d2}) = \frac{\delta_2}{\gamma_2}\log(N) + 1 - \delta_2 t_{d2}$

Where $\delta_1 \equiv d_E(1-\exp(-r_1))$, $\delta_2 \equiv d_E(1-\exp(-r_2))$, $\gamma_1 \equiv \beta T^{ss}(s_1 - s_2)$, $\gamma_2 \equiv \beta T^{ss} s_2$.

From table 3.2 we can find the lifetimes of the two single-mutant haplotypes:

$$t_{10} = t_{g1} + t_{d1} \tag{3.19}$$

$$t_{01} = t_{g2} + t_{d2} \tag{3.20}$$

In order for haplotype 10 to be short-lived relative to haplotype 01, the parameters must satisfy:

$$t_{10} < t_{01} \tag{3.21}$$

We hypothesize that model parameters that obey inequalities given in Eqs. 3.21, 3.14, 3.13 and 3.18 give a pattern of escape within an epitope that matches the qualitative features of data.

Parameter ranges for simple and leapfrog escape patterns

Using the above conditions on parameters r_k, s_k, we can determine the parameter space that corresponds to either the simple or leapfrog pattern for a given escape rate. By fixing the number of epitopes, n, the escape rate for the first haplotype ($\epsilon_{10\text{vs}00}$) and the ratio of the two fitness costs (s_1/s_2), the regions where simple and leapfrog escape pattern will be observed can be determined in terms of the fraction of recognition lost by a single escape mutation in either site, $(1-\exp(-r_1)), (1-\exp(-r_2))$. Fig. 3·5 shows the regions of simple and leapfrog escape patterns

for values of $s_1/s_2 = 5 - 20$ and $\epsilon_{10\text{vs}00} = 0.05 - 0.5$ for $n = 4$ and $m = 2$. These values are chosen to be representative of the range of escape rates escapes observed in data in the first 100 days after infection. For large escape rates, large values of r_1 are required, allowing a broad range of r_2 that can produce the leapfrog pattern (Fig. 3·5 A, C). Smaller values of r_1 produce smaller escape rates, and leapfrog is observed in a very narrow range of small r_2 (Fig. 3·5 B,D). Furthermore, in the majority of the leapfrog region Eq. 3.21 is fulfilled.

The absolute lifetime of the second haplotype is also of interest. In our simplified model with two sites per epitope, t_{01} represents the amount of time before full reversion, when the transmitted epitope variant begins to dominate the population. If the epitope had many sites in which s_k and r_k are correlated, this time until full reversion could be lengthened by repeatedly switching to lower and fitness cost sites. Reversion would be avoided entirely if there exists a site in the epitope which confers recognition loss but no fitness cost. If indeed the second haplotype does entail a fitness cost, t_{01} can be thought of in terms of the amount of time during which the compensatory mutations are obtained that ameliorate this cost. Fig. 3·5 also plots the absolute lifetime of the second haplotype, determined by the right hand side of Eq. (3.21). For small ratio of $s_1/s_2 = 10$ (Fig. 3·5 A, B), the lifetime of the second haplotype becomes short for large values of r_1, by reducing t_{g2}. For large ratio of $s_1/s_2 = 10$ (Fig. 3·5 C, D), the second haplotype is always long lived.

Our analysis shows that correlated recognition and fitness losses can produce complex patterns of intra-epitope escape, such as the leapfrog pattern. By choosing a simple model, we are able to show explicitly which parameters determine the escape rate of a given epitope site, and calculate the regions in parameter space that match the qualitative features of data.

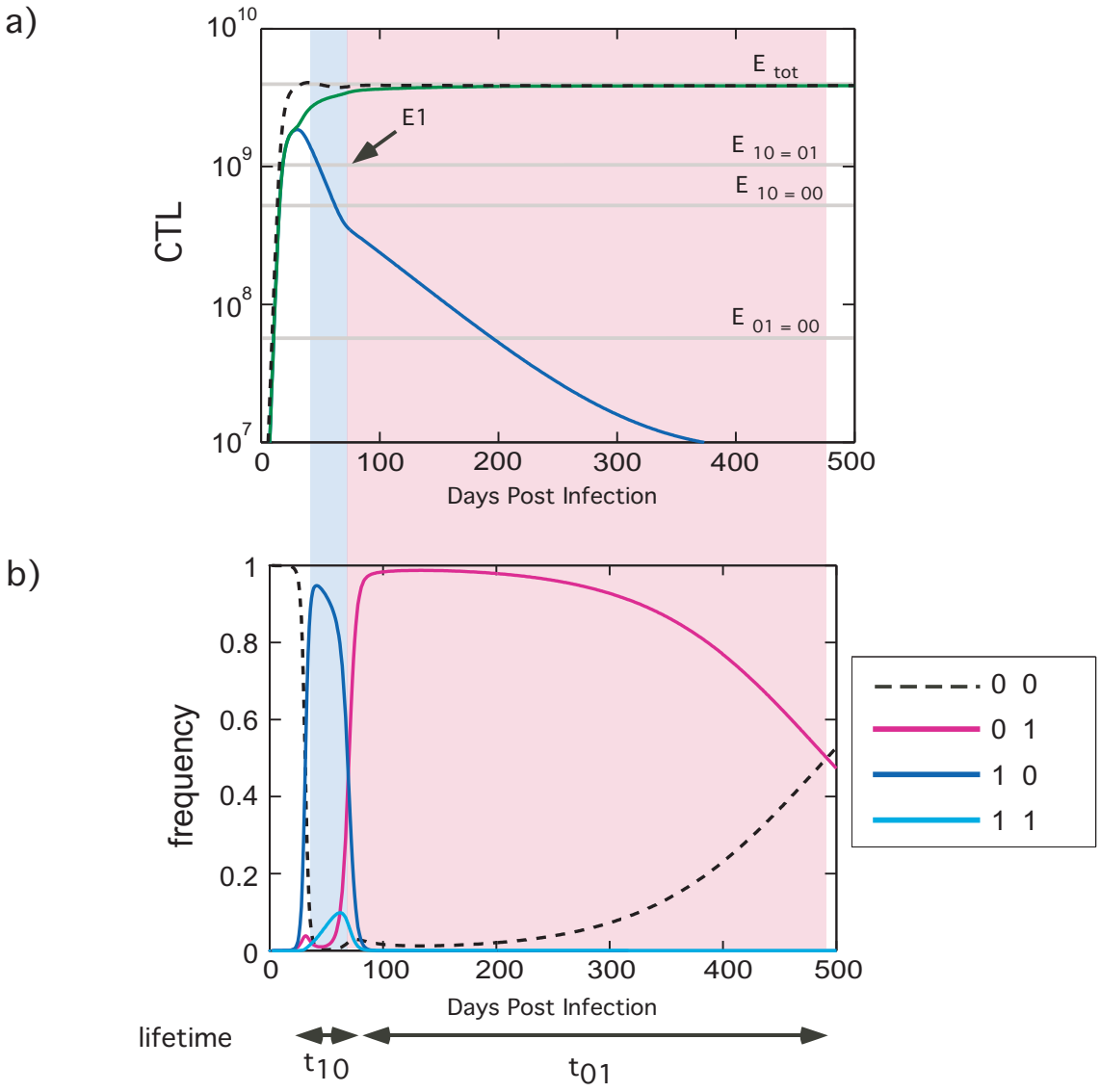

Figure 3·4: Leapfrog escape in an epitope: two epitopes with two sites per epitope. The leapfrog pattern of escape results from partial recognition loss per escape mutation and declining selection pressure from CTL. a) Individual CTL clones (solid lines) and total CTL (black dashed). E_1 induces escape and subsequently declines (blue). Grey horizontal lines: Critical points in E_1 that cause the haplotype with the greatest growth rate to change (Eq. 3.16 - 3.17). b) Frequency of all haplotype in epitope one. Shaded regions that span all plots show the lifetimes of haplotypes 10 (blue region) and 01 (pink region). The lifetime of a haplotype is defined as the time interval where a given haplotype dominates the population. Parameters are chosen that result in leapfrog in one epitope. $r_k = [1, 0.20], s_k = [0.1, 0.003], n = 2, m = 2$ other parameters given in Table 3.1)).

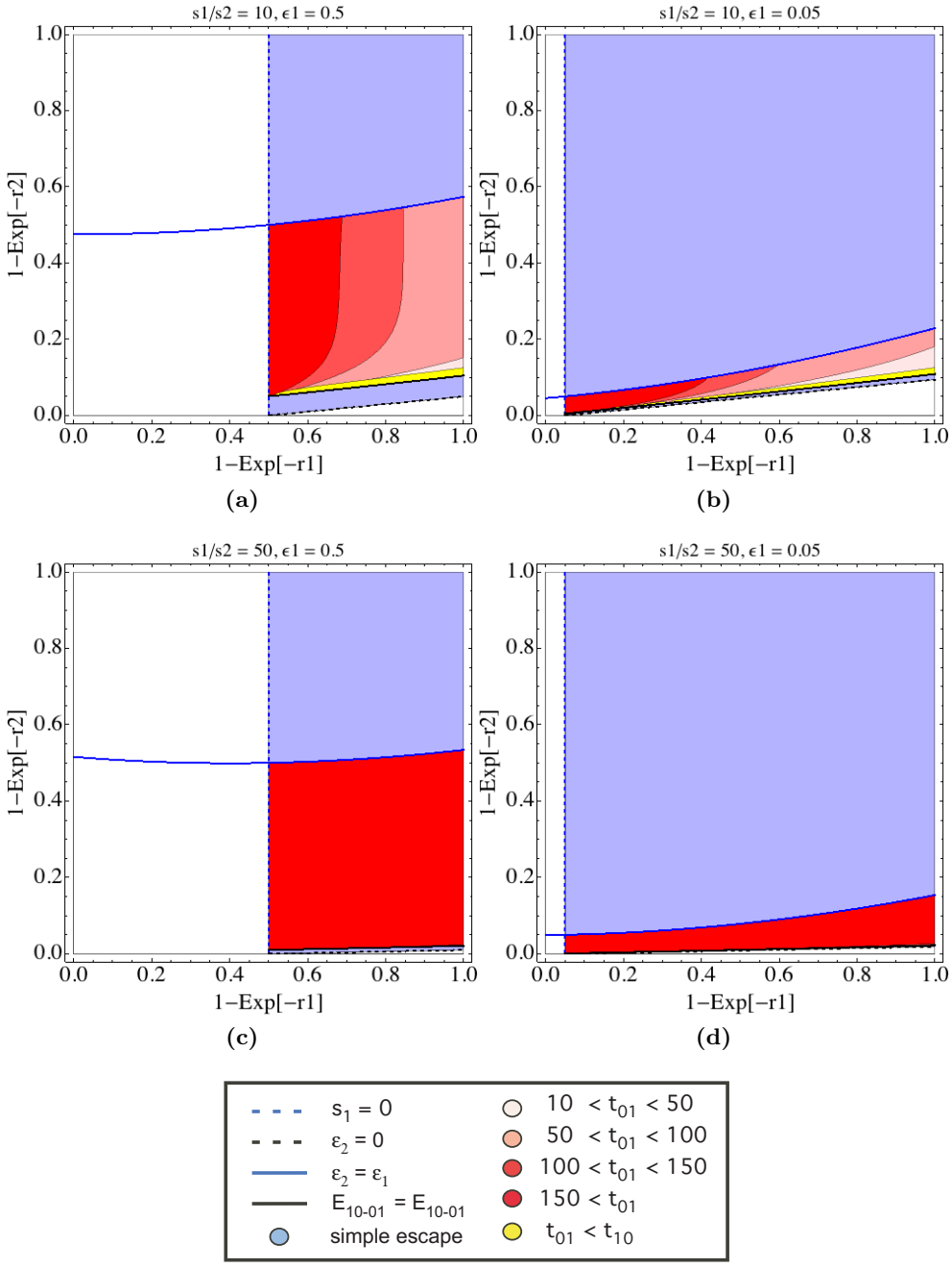

Figure 3·5: Dependence of intra-epitope escape pattern on the amount of recognition lost for a single epitope with two sites. (A-f) Equations (3.13),3.14, (3.18), and (3.21) determine the allowed parameter ranges for simple and leapfrog escape patterns in terms of r_k, s_k for $k = 1, 2$ with $n = 4$ and $m = 2$. Each panel uses a fixed value of $\epsilon_{10\text{vs}00}$ (here called ϵ_1) equal to 0.5 in (A, C) or 0.05 (B, D)and s_1/s_2 equal to 10 in (A,B) or 50 in (C,D). Regions are: leapfrog with long lived 01 compared to 10 (red), leapfrog with short lived 01 compared with 10 (yellow), simple escape (light blue), not allowed by definition, since we require $s_1 > 0, \epsilon_2 > 0$ (white). Shaded red regions indicate lifetimes of different lengths for the second haplotype (t_{01}). Which pattern of escape is observed in an epitope is determined by the distribution of fitness and recognition losses among epitope sites.

3.4 Discussion

The availability of time resolved, deep sequencing data has illuminated the complex interaction between CTL clones and the diverse population of infected cells that they recognize. Using a model of the interaction of HIV with multiple CTL clones with equal avidity, we have shown that partial recognition and fitness losses associated with an escape mutation, together with the breadth of the CTL response, determine the rate of escape. Furthermore, changing selection pressure on an epitope due to declining CTL following escape can cause the dominant haplotype in an epitope to change over time a non-nested fashion.

As in (Althaus and Boer, 2008; Mostowy et al., 2011), we assume a large population of infected cells in acute infection and steady state, such that single escape mutants pre-exist in the population before the rise of CTL. This is supported by estimates of the population size of HIV (Rouzine and Coffin, 1999b; Kouyos et al., 2006). We can also infer from the early emergence of single drug-resistant mutations under mono-therapy (e.g. (Richman et al., 1994)), that single CTL escape mutants always exist at low levels in the population. Before the onset of selection pressure, imposed by the rise in CTL for an escape mutation or the introduction of drug for a drug resistance site, the site in question will be disadvantageous to viral replication. Since there are more escape mutaions per epitope than drug resistance sites per replication inhibitor, we can infer that, on average, an escape mutation will be less disadvantageous than a drug resistance mutation. In other words, if the number of possible sites that can be mutated is large, a low fitness cost mutation can be more easily found. As a result of mutation selection balance, mutations in epitopes will be at higher initial levels than drug resistant mutations. Therefore, we rule out the possibility that late escapes are the result of late appearance of an escape mutation that is not initially present in the population as has been suggested (Liu et al., 2006). The possibility remains that late escapes are caused by the delay to obtain an escape mutation and one or more compensatory mutations on the same genome. This pattern depends sensitively on the strength of the epistatic interaction, and the number of compensatory sites required for the escape mutation to grow.

We have not included compensation for fitness losses incurred by escape mutations. While compensation for fitness losses has been documented for drug resistance mutations (E.g. (Quiñones-Mateu and Arts, 2002; Bonhoeffer, 2004; Hinkley et al., 2011)) and for immune escapes (Troyer et al., 2009; Crawford et al., 2011; Kelleher et al., 2001), the dynamics of compensation remain poorly understood. Compensation is implied in our analysis of reversion times for an escape mutation. Epitopes that have escaped are seldom observed to revert to the transmitted variant in the host in which they were initially selected. In our model without compensation, we study the time until reversion is predicted to occur, which is the same interval in which where compensation would be able to occur. In escapes that follow the leapfrog pattern in data, typically the first variant is relatively short lived compared to the second, and the transmitted variant is not observed after the initial escape. It is possible that the first variant does not have time to be compensated before the second variant gains the advantage, and that the second variant either has a very small fitness cost or is compensated gradually during its lifetime. Our estimates of the lifetimes of different escape variants in an epitope is a first step towards understanding the time during which a given fitness costs must be compensation before the transmitted epitope begins to dominate the population.

It has been hypothesized that the majority of sites that are avolving in chronic HIV infection are compensatory in nature for early escape mutations (Rouzine and Coffin, 1999a). Several recent works have developed models where the evolutionary dynamics of many simultaneously evolving sites can be analyzed (Batorsky et al., 2011b; Rouzine and Coffin, 2010; Neher et al., 2010). It remains a challenge to describe early dynamics of immune escape with the late phase of compensatory evolution.

In our model CTL have initially identical avidities. In reality, this is not the case. Typically, a few CTL to immunodominant epitopes rise initially, coincident with the decline from peak viremia. Escape in these epitopes during the resolution of acute viremia is followed by a wave of many CTL (Turnbull et al., 2009) at a few months post infection. We focus on this phase, and make the approximation that the CTL that appear at this time have identical avidities. The early wave of CTL clones can be included in our model by adding a small number of clones with higher avidity.

If parameters of recognition and fitness loss are independent of CTL avidity, it can be assumed that the initial wave of CTLs will escape more quickly due to the smaller number of clones.

If the group of CTL that rise several months post-infection have closely spaced, but not equal, avidities, escape in the most avid CTL clone will cause the infected cell level to rise to the threshold of the CTL with the next highest avidity. If the process continues, the virus load is predicted to climb over time. Kadolsky and Asquith (Kadolsky and Asquith, 2010) use a mathematical model to estimate that a single CTL escape leads to a viral load increase of of 0.11 log copies/ ml. This small increase, which we interpret to be the average difference avidity spacing between CTL clones, justifies our assumption that the avidities of controlling CTL avidities are very closely spaced. As a consequence of this close spacing, recognition and fitness losses govern the order and timing of escapes, rather than variation in CTL avidity.

Previous studies have modeled the sequence of escape mutations in the presence of multiple CTL clones (Althaus and Boer, 2008; Ganusov et al., 2011; Mostowy et al., 2011). We have extended this basic model to describe escape in an epitope with many sites. Whereas these studies were focused on explaining the appearance of late escapes, we focus on a narrower time interval in the first year after infection. To this end, we have made a number of simplifying assumptions: i) We assume that stimulation of CTL clones saturates as a function of infected cell number, but not as a function of total CTL level This assumption is justified by SIV tissues studies in the peak of infection show that most CTL are not bound to targets, and that the overall effector/target ratio is less than two (Haase, 2011). In the original model (Althaus and Boer, 2008), the authors postulate that the total number of CTL limit the growth of individual CTL clones, which enables the co-existence of multiple CTL clones with different avidities. We believe that further study is needed to determine the possible origin of the interclonal interaction. ii) We assume that CTL are short lived in the absence of antigen, with an average lifetime of 10 days as is consistent with early studies of CTL dynamics in SIV (Ogg, 1998; Kuroda et al., 1999) and mathematical modeling of this data (Sergeev et al., 2010c). iii) We ignore recombination, which has been shown to increase the emergence of escapes among many targeted epitopes (Mostowy et al., 2011). For the intra-epitope dynamics of

escape, recombination between neighboring sites will be a small correction.

In this work, we have shown that partial recognition losses, in addition to fitness costs and the breadth of the CTL response, influence the rate of escapes. In the case where CTL avidities are similar and fitness costs are small, recognition loss is the most important determinant of the order and rate of escape among epitopes. The pattern of escape that is observed in an epitope with many sites indicates the flexibility of the epitope. The leapfrog pattern, which is observed often in data, implies that recognition losses and fitness losses correlate positively within an epitope. Our work emphasizes the importance of studying the effect of compensatory mutations on the maintenance of escape mutations in CTL epitopes.

Chapter 4

Predicted Confounding Effect of Weakly Immunogenic Long-Lived Infected Cells on Vaccination against Simian Immunodeficiency Virus

4.1 Intro

Developing a prophylactic HIV vaccine is vital to controlling and reversing the AIDS pandemic. Viral genes and delivery methods are continuously under investigation to determine which are most efficacious in terms of immunogenicity and protection. Due to the early formation of latently infected cells (Chun et al., 1997a; Chun et al., 1997b), achieving sterilizing immunity through vaccination may be very difficult. However, a number of vaccine studies in Simian Immunodeficiency Virus (SIV) show that it may be possible to achieve a lower steady-state viral load upon challenge in vaccinated individuals, thus postponing the onset of AIDS symptoms and decreasing transmission risk. Rhesus macaques vaccinated with DNA vaccines expressing SIVmac239 Gag and HIV-1 89.6P Env and then challenged with a SIV/HIV recombinant, SHIV, developed a much lower level of persistent virus ($<$ 300 Plasma RNA copy/ml in vaccinated animals versus $10^5 - 10^6$ Plasma RNA copy/ml in non-vaccinated), a higher CTL and a much higher CD4 helper cell frequency in the steady state, compared with controls (Barouch, 2000) (Fig 4·1A). Although this low-virus state proved to be unstable in the long-term due to antigenic escape occurring during the three-year follow-up period, the success was promising. A similar vaccine regimen utilizing SIVmac239 proteins, however, was unable to achieve even transient establishment of the low-virus state upon challenge with SIVmac251 (Letvin et al., 2006a). Despite increased helper cell and CTL frequencies comparable to that observed in SHIV challenged macaques, viral loads remained relatively high, re-

duced, on average, by a factor of 30 relative to controls ($10^2 - 10^5$ RNA copy/ml blood) (Fig 4·1 B).

Mathematical models have been used to address the effect of vaccination on acute infection (De Boer, 2007; Sergeev et al., 2010a). However, the present work is the first to focus specifically on the questions pertaining chronic infection. The mechanisms underlying the effect of vaccination on the level of virus in chronic infection, as well as the failure of vaccines to enable the same degree of control of virus replication after SIV challenge as after SHIV challenge, remain unclear. The dynamic interaction of the virus with the immune response must be understood in order to address these issues.

To explain the effect of vaccination in animals challenged with SHIV, we propose a model (Model 1) that specifies interaction between cells uninfected cells susceptible to infection, infected cells, helper CD4+ cells, and CTL. It is our interpretation of the cited data that there exist two steady states in an host infected with SHIV, which may or may not be achieved based on host parameters, vaccination status, and virus strain (Rouzine et al., 2006; Sergeev et al., 2010a). The two steady states exist because CTL can be stimulated to divide by two mechanisms: directly by infected cells or indirectly through CD4+ helper cells. Which state is achieved is dependent on vaccination status. Infection in unvaccinated animals results in the high-virus steady state controlled by helper-independent CTL, while infection of vaccinated animals with sufficient initial memory cells results in the low-virus steady state, in which the virus level is predicted to be near the antigen sensitivity threshold for helper cells. To illustrate the process of model selection, we consider predictions of several other models of similar complexity and show that our model is the simplest model consistent with data.

We extend Model 1 to explain the divergent outcomes of vaccination between the two infecting strains, SHIV and SIVmac251. In the context of Model 1, observed higher steady-state viral loads in vaccinated animals challenged with SIV imply that the antigen sensitivity threshold for helper cells is higher by several orders of magnitude relative to SHIV infected animals (Sergeev et al., 2010a; Sergeev et al., 2010b). Although the infecting virus strains differ virologically in coreceptor specificity (tropism for memory CCR5 and nave CXCR4 CD4 T cells, respectively), the reason for

such strong immunological differences is unclear. Different immunodominant epitopes can account for variation in sensitivity of the immune response within an order of magnitude, as can be seen from studies in unvaccinated macaques expressing different MHC subtypes (Newberg et al., 2006). Such variation, however, is not sufficient to account for a 1000-fold difference in immunological parameters between the animal groups challenged with SHIV and SIV.

Our second model (Model 2) focuses on the results of vaccination after challenge with SIV postulates that the dominant infected cell type in vaccinated, SIV challenged macaques produce virus at a lower rate than those in vaccinated, SHIV challenged macaques. The biphasic viral decay after the onset of anti-retroviral therapy (ART) in SIV infected animals (Dinoso et al., 2009; Perelson et al., 1997) and studies of HIV RNA content per infected cell in the lymphoid tissue of unvaccinated patients before and after ART (Cavert, 1997; Zhang et al., 1999) strongly imply the existence of two types of infected cells with very different levels of virus production. We postulate that as a results of the low level of virus production, these cells are not recognized efficiently by helper cells and, hence, are relatively long-lived. The reduced ability of helper cells to detect virus results in higher virus levels than if the dominant infected cell type were producing virus at a high rate (as in SHIV).

4.2 Models

4.2.1 Model 1: Animals infected with SHIV: Two types of CTL regulation

To describe the two possible steady states in vaccinated macaques infected with SHIV, we introduce a model with two types of CTLs responding to signals from infected cells and helper cells, respectively. The model comprises three blocks that determine dynamics of infected cells and cells permissive for virus replication, direct CTLs, and helper cells and helper-dependent CTLs, respectively (diagrams in Fig. 4·2 A to C).

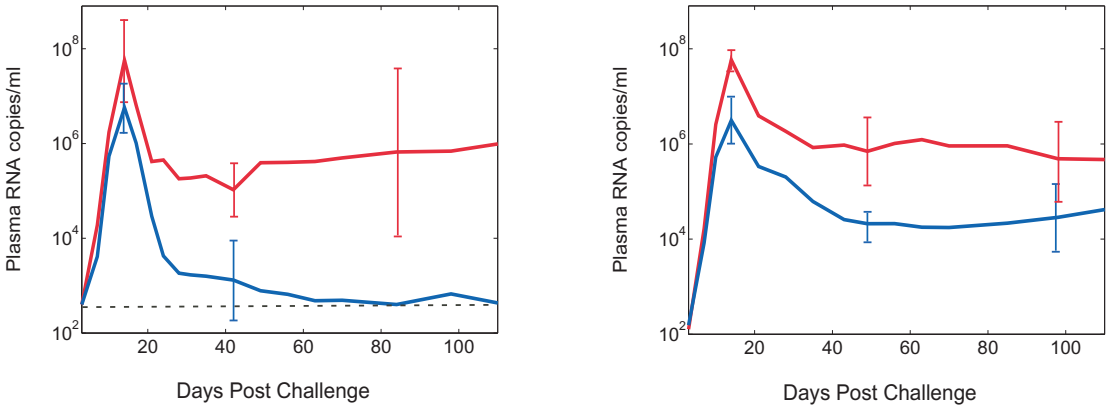

(a) **(b)**

Figure 4·1: The effect of vaccination on virus dynamics in macaques infected with two strains of SIV. (A) SHIV-89.6P infected rhesus macaques (Barouch, 2000). The average plasma viral load (log10) is shown for 5 of the 6 control animals (red) and 4 animals vaccinated with SIV mac239 Gag and HIV-1 Env 89.6P DNA (blue). Control animal 780, observed in the low-steady state, was removed. Dotted line shows detection threshold. (B) SIVmac251 infected rhesus macaques (Letvin et al., 2006a). The average plasma viral load (log10) is shown for 6 control animals (Red) and 6 animals vaccinated by with plasmid encoding SIV gag/pol/nef (prime) and rAd-SIVmac239 gag/pol (boost) (Blue). Bars show 95% confidence intervals.

Block A: Permissive and infected cells

A single type of uninfected target cells (R) is replenished at the average linear rate s and dies at the average exponential rate d_T. The average rate of infection is proportional to virus-producing cell number and the infectivity, p_R. Upon infection, these cells enter the eclipse phase (I) with the average length d_I^{-1}. After the eclipse phase, these cells enter the productive phase of infection (P) and produce virions until they die due to virus cytopathicity at the average rate d_P or are killed by CTL effector cells. Free virus is not included in the model as a separate compartment because it is very short-lived [half-life 30-100 min in plasma (Ramratnam et al., 1999)] and, therefore, should remain proportional to the virus-producing cell number, P, as it varies in time. Equations for the block (Fig. 4·2A) are given by

$$\dot{R} = s - (d_R + p_R P)R \tag{4.1}$$

$$\dot{I} = p_R RP - d_I I \tag{4.2}$$

$$\dot{P} = d_I I - [d_P + k(E + E_D)]P \tag{4.3}$$

Equations for CTLs E and E_D are given in the next subsection. Although Equation 4.3 and all models presented in this work implicitly assume lytic killing of virus-producing cells by CTL, none of our conclusions are dependent on this assumption. Recent studies have cast doubt on the extent to which CTL limit the lifetime of productively infected cells (Klatt et al., 2010; Wong et al., 2010) (see *Discussion*).

Block B: Helper cell-independent CTL response

When helper-independent CTL ("direct CTL", denoted E_D) , encounter virus-producing cells, they proliferate at a rate dependent on the virus-producing cell number, P, at maximum rate c. The dynamics for their population (Fig. 4·2B) is described by the equation

$$\dot{E}_D = [\beta c - (1-\beta)d]E_D \tag{4.4}$$

Here $\beta = 1 - \exp(-P/P_0)$ is the fraction of direct CTL that detects virus-producing cells with activation threshold P_0 in the number of infected cells (see *Control Functions* below).

Block C: Helper cell-dependent CTL response

Helper cell expansion depends similarly on the productive cell number. In the presence of virus, the maximum rate of expansion is limited by value c_H. The infectivity for activated helper cells, p_A, is assumed to be higher than that of non-virus-specific target cells, since activated cells are rapidly dividing and more susceptible to infection. In the absence of virus-producing cells, helper cells die out slowly at rate d_H. The resulting dynamics for the population of helper cells (H) (Fig. 4·2C) is given by the equation

$$\dot{H} = [\alpha c_H - (1-\alpha)d_H - \alpha p_A P]H \tag{4.5}$$

where $\alpha = 1 - \exp(-P/P_{H0})$ is the fraction of helper cells that detects virus, secretes cytokines, and divides (see *Control Functions* below). The characteristic activation threshold in the number of infected cells, P_{H0}, is assumed to be lower than the threshold for direct effector cells, P_0.

When helper cell-dependent effector CTLs ("indirect CTLs", denoted E) receive signals from helper cells detecting virus, they proliferate with a rate dependent on the level of helper cells, up to a maximum rate c. When CTL no longer receive signals, they retire at rate d, becoming memory cells without significant cytotoxic function. The dynamics for the population of indirect CTLs (Fig. 4·2C) obeys the equation

$$\dot{E} = [\sigma c - (1-\sigma)d]E \tag{4.6}$$

where $\sigma = 1 - \exp(-\alpha H/H_0)$ is the fraction of indirect CTL receiving a cytokine signal from helper cells, where H_0 is the activation threshold in number of helper cells. The entire model is given by the system of Equations 4.3 - 4.6 or represented by three connected blocks in the diagram in Fig. 4·3A.

4.2.2 Model 2: Animals infected with SIVmac251: Including infected cells with low levels of virus production

To describe the steady state in vaccinated animals infected with SIV, the block of infected and permissive cells (Block A) is expanded to include long-lived infected cells with low levels of virus production. Now, after a short eclipse phase, an infected cell can follow either a short-lived pathway with a high rate of virus production, I $\rightarrow$ P, or a long-lived pathway with a low rate of virus production, $I \rightarrow I_L \rightarrow P_L$ (Fig. 4·3B). Equations for infected and permissive CD4+ T cells, which replace Equations 4.3, now include two more compartments, I_L and P_L:

$$\dot{R} = s - (d_R + p_R P_V)R \tag{4.7}$$

$$\dot{I} = p_R R P_V - d_I I \tag{4.8}$$

$$\dot{I}_L = \gamma d_I I - d_{IL} I_L \tag{4.9}$$

$$\dot{P} = (1-\gamma)d_I I - [d_P + k(E+E_D)]P \tag{4.10}$$

$$\dot{P}_L = d_{IL} I_L - [d_{PL} + k_L(E+E_D)]P_L \tag{4.11}$$

Here the duration of the eclipse phase and of the productive phase in the absence of an immune response for long-lived cells are given by d_{IL} and d_{PL}, respectively. Due to their low rate of virus production, long-lived infected cells are killed by CTLs much less efficiently than short-lived in-

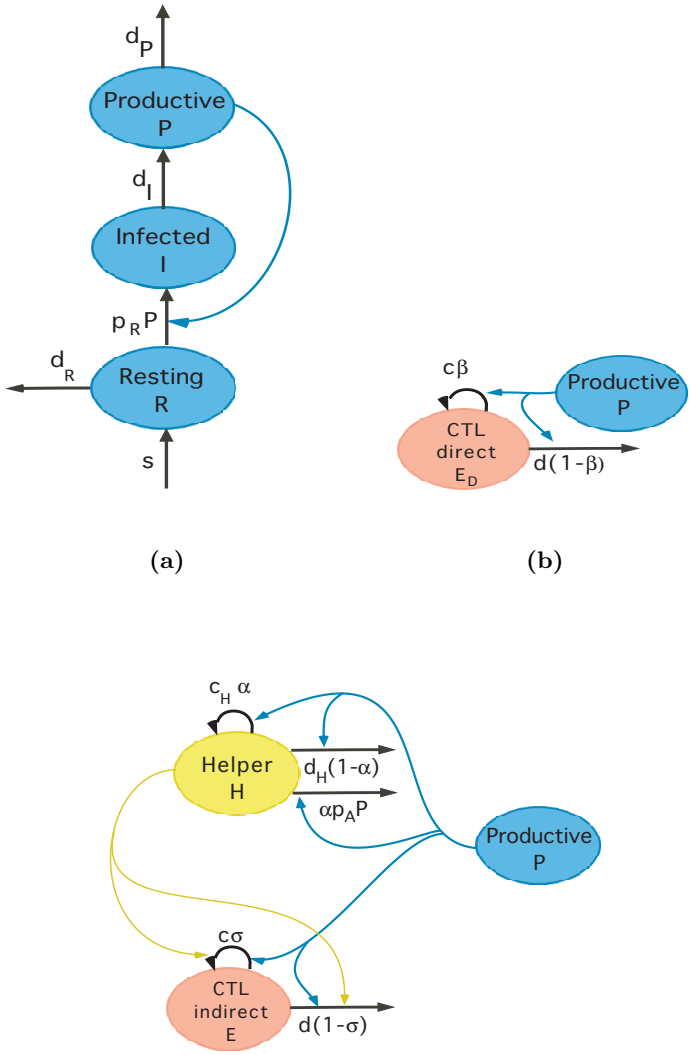

Figure 4·2: Model building blocks (A) Permissive and infected cells (blue), (B) Direct CTL response, comprising virus-specific effector CD8 T cells (red), (C) Indirect CTL response, comprising effector CD8 T cells (red) and virus-specific helper CD4 T cells (yellow). Color oval: Cell compartment measured as percentage of total CD4 or CD8 cells in an average uninfected animal. Thick black arrow: Flux of cells from one compartment to another, from a source to a compartment, cell death, or cell proliferation. Thin color arrow: Control of flow from one compartment to another by a third compartment. Control functions: $\beta = 1 - \exp(-P/P_0)$, $\sigma = 1 - \exp(-\alpha H/H_0)$, $\alpha = 1 - \exp(-P/P_{H0})$, where P_0, H_0, and P_{H0} are characteristic activation thresholds in units of cells in the respective signal-sending cell compartment.

fected cells ($k_L \ll k$). New notation in Equations 4.11 is, as follows. $P_V = P + xP_L$ is the effective number of virus-producing cells reflecting their contribution to production of free virus, and x ($x < 1$) is the ratio of the rate of virus production of long-lived infected cells to that of short-lived infected cells. Control function $\gamma = \gamma_0 \exp(-P_V/P_{single})$ represents the fraction of cells that follow the long-lived pathway after the short eclipse phase. At viral loads above P_{single}, the fraction of newly infected cells following the long-lived pathway decreases rapidly.

The immune responses and their control by virus and helper cells (Blocks B and C) remain as in Model 1 (Fig. 4·3A). However, the control functions for helper cells and direct effector CTLs, α and β, now contain linear combinations of the two infected cell types, as they contribute to stimulation of the corresponding component of the immune response. The control function of helper cells, $\alpha = 1 - \exp(-P_H/P_{H0})$, now depends on the effective number of virus-producing cells $P_H = P + x^3 P_L$ (see *Control functions* below). The control function for direct CTLs becomes $\beta = 1 - \exp\{-[P + (k/k_L)P_L]/P_0\}$.

Control Functions dictate interactions between cell types

In all models presented, interaction of the three virus-specific cell compartments shown in Figs. 4·2 and 4·3 (H, E_D and E) and their regulation by virus-producing cells are formally described by control functions α, β and σ. These control functions reflect different types of interaction between various cell types. Each control function represents the fraction of a type of controlled cell that receives a signal from controlling cells. For helper cells and direct CTL, signal-sending cells are virus-producing cells (P and P_L). Indirect CTL receive signals from helper cells that detect virus. The control function contains an activation threshold in the concentration of the signal-sending cells, above which the receiving cell type quickly approaches the maximal expansion rate.

The control function for helper cells (α) is illustrated in Fig. 4·4A showing the distribution of relevant cells types around a virus-producing cell in tissue. The infected cell releases soluble virus products (soluble antigen), which diffuse outward from the cell. APC can internalize soluble antigen

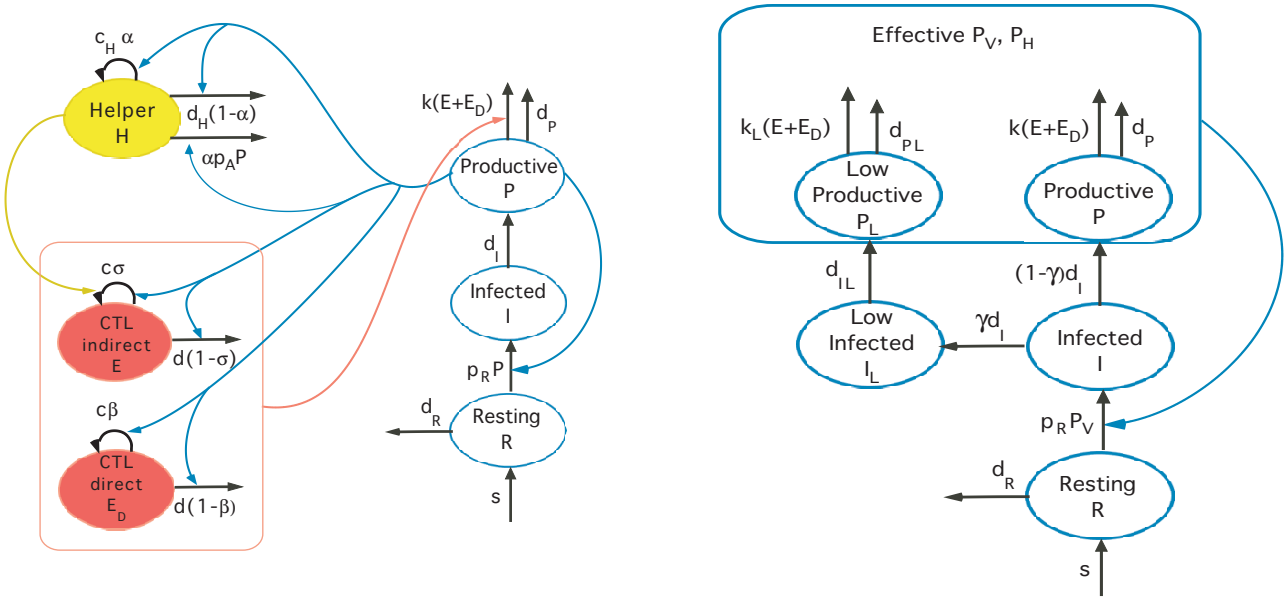

(a) **(b)**

Figure 4·3: Two main models (A) Basic model with two CTL types (Model 1). Three model blocks A, B and C from Fig. 2 are combined: Permissive and infected cells (blue), virus-specific CD8 T cells (red), virus-specific CD4 T cells (yellow). Shaded oval: Cell compartment measured as percentage of total CD4 or CD8 cells in average uninfected animal. Pink frame: the sum of the two CTL compartments ED+E. Other notation as defined in the caption to Fig. 2. (B) The updated block of infected and permissive cells including low-producing, long-lived infected cells (Model 2). Blue frame: effective numbers of virus-producing cells: PV=P+xPL (for production of free virus), or PH=P+x3PL (for activation of helper cells). Revised control functions: $\beta = 1 - exp[-P + (k_L/k)P_L]/P_0$, $\sigma = 1 - \exp(-\alpha H/H_0)$, $\alpha = 1 - \exp(-P_H/P_{H0})$. Probability of following the weakly producing pathway: $\gamma = \gamma_0 \exp(-P_V/P_{single})$.

and present it on their surface in MHC-II context to helper cells, activating them upon contact. Only those APC that pass sufficiently close to an infected cell (the inner region in Fig. 4·4) pick up sufficient amount of antigen to be able to activate a helper cell. The radius of the region rich in antigen depends on the antigen sensitivity of helper cells and the efficiency of internalization and presentation. Based on the standard diffusion law, which states that the local concentration of soluble antigen in the tissue is inversely proportional to the distance from the source, the radius of the region is also proportional to the rate of antigen release by an infected cell. Furthermore, helper cells are activated by APC for a short time. Once activated, a helper cell divides, secretes cytokines (IL-2), and then returns to the resting state unless it encounters another APC within this period of time. Antigen-presenting APC travel outward from the critical antigen-rich region, so that their concentration decreases with the distance. Helper cells that pass within a region where the frequency of well-presenting APC is still high (the grey circular area in Fig. 4·4A) will encounter APC frequently enough to stay activated. The ratio of the radii of the two regions depends on the travel (diffusion) speed of helper cells and the average time allotted for their activated state. If the antigen production rate per infected cell increases (due to a different virus strain or infected cell type), the radii of both regions will increase proportionally to the antigen production rate. Assuming random distribution of infected cells in tissue, the probability of a helper cell being within at least one APC-rich region, and, hence, the fraction of the tissue occupied by the APC-rich regions is given by the Poisson distribution, $\alpha = 1 - \exp(-P/P_{H0})$, where P is the concentration of infected cells in tissue, and P_{H0} is the inverse volume of the APC-rich sphere. The value of P_{H0} is inversely proportional to the cube of the outer radius in Fig. 4·4A and, hence, to the cube of virus production rate per infected cell. In Model 2, we take into account the existence of two types of APC-rich regions around two types of infected cells with different rates of virus production, as shown in Fig. 4·4B. In this case, control function is $\alpha = 1 - \exp(-P_H/P_{H0})$, where $P_H = P + x^3 P_L$ is the effective number of virus producing cells as pertains to helper cells. The choice of the cubic dependence of P_H on x is not arbitrary and follows from the standard diffusion law in uniform tissue. Using a model of non-uniform diffusion, based, for example, on the existence of preferntial channels of APC transport, would simply lead to raising x to a higher power.

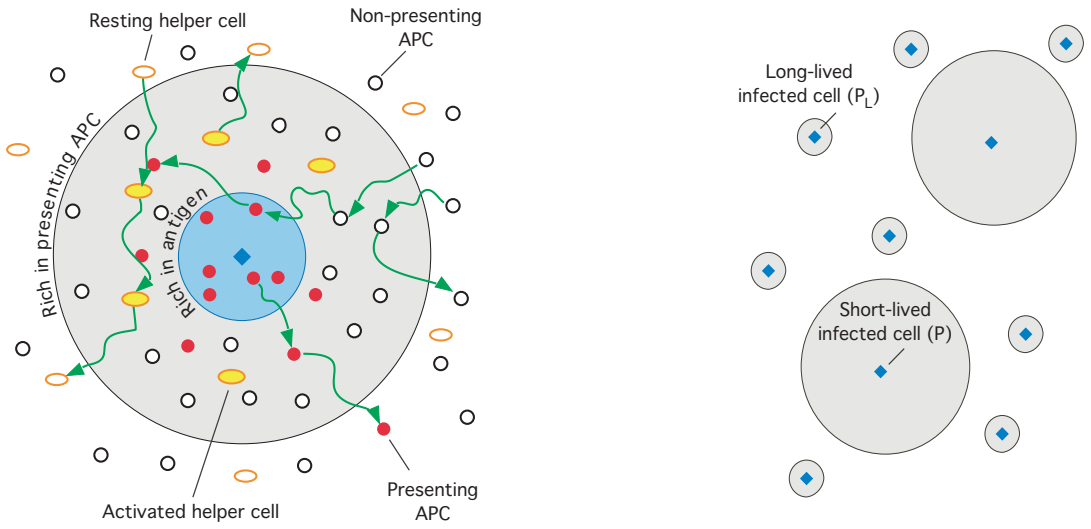

(a) **(b)**

Figure 4·4: Illustration of the control of helper cells by virus infected cells (A) Blue diamond: A virus-producing cell. Blue circle: Region rich in soluble antigen. White circles: APC. Red circles: APC presenting antigen in sufficient amount to activate a helper cell. White ovals: Resting helper cells. Yellow ovals: Activated helper cells. Grey circle: Region where antigen loaded APC are frequent enough to keep helper cells activated. (B) Grey circles show regions rich in antigen-loaded APC where helper cells are activated around long-lived infected cells (P_L) and short-lived infected cells (P). In the low steady state predicted for macaques vaccinated and challenged with SIV, P_L are the dominant type of infected cells. The fraction of the tissue occupied by all grey regions is the fraction of helper cells detecting antigen, i.e., control function $\alpha = 1 - \exp[-(P + x^3 P_L)/P_{H0}]$.

Direct CTL recognize antigen upon direct contact with infected cells. In Model 1, the fraction of activated CTL can be approximated, by analogy with helper cells, as $\beta = 1 - \exp(-P/P_0)$. Here the characteristic number of virus-producing cells, P_0, required for activation of direct CTL is treated as a model parameter. It depends on the CTL diffusion speed, the attachment time to infected cells, and the probability of recognition.

The respective activation thresholds in the number of virus-producing cells, P_0 and P_{H0}, are expected to differ strongly between direct CTL and helper cells: The ability of APC to pick up soluble

antigen at a distance from an infected cell and travel further can greatly expand the virus-detecting volume. The expectation is confirmed by very low viremia and high helper cell response in vaccinated macaques challenged with SHIV (Barouch, 2000). In Model 2, the control function for direct CTL becomes $\beta = 1 - \exp[-(P + (k_L/k)P_L)/P_0]$, where the ratio of the killing efficiencies of long-lived to short-lived infected cells represents a lower sensitivity of CTL to long-lived infected cells. Finally, indirect CTL are activated and divide when they receive cytokine signals from activated helper cells (αH), which interact with antigen-presenting APC. Considering cytokine concentration around an activated helper cell, analogous to antigen concentration around an infected cell in Fig. 4·4A, the activated fraction of CTL is $\sigma = 1 - \exp(\alpha H/H_0)$, where characteristic helper cell number H_0 depends on the effective radius of cytokine action. The form of σ is the same in Models 1 and 2.

4.3 Results

4.3.1 Model 1: Animals infected with SHIV: Two types of CTL regulation

Model 1 postulates two pathways of CTL differentiation, Fig. 4·3A. For the purpose of addressing the steady state, whether they are distinct cell subtypes or a single type with two mechanisms of activation is not important; the two CTL subtypes appear separated for clarity of presentation. In the high-virus steady state, the CTL response is dominated by direct CTLs. These cells keep virus replication in check maintaining the number of infected cells at a steady state level similar to the activation threshold for direct CTLs (P_0), so that CTLs neither expand nor decay. Helper cells, on the other hand, are infected at a higher rate than they proliferate, so that their number is small, and helper-dependent CTL response is absent. By contrast, the low-virus steady state is controlled by the helper-dependent CTL response. Based on data from vaccinated macaques infected with SHIV (Barouch, 2000), this value is lower by 3-4 orders of magnitude than viral loads in unvaccinated animals. In this state, the number of infected cells (P^{LSS}) is too low to maintain the direct CTL response.

Both steady states, once obtained, can be stable in the same parameter range. Properties of each

steady state depend only on model parameters in an individual. Which of the two steady states takes place, depends also on initial conditions determined by the vaccination status (Sergeev et al., 2010a). The dependence has a threshold: at small numbers of initial CTLs, the system ends up in the high-virus steady state. At sufficiently high initial CTL and helper cell numbers, virus replication is checked early, depletion of helper cells is decreased, and the low-virus steady state ensues.

The sizes of measurable cell compartments (shown as percentage of the total CD4 or CD8 cell count in an average uninfected animal) in the two steady states, as well as CTL and viral loads from experiment (Barouch, 2000) are shown in Fig. 4·5. The model parameters have been estimated previously (Sergeev et al., 2010b) (Fig. 4·5 legend and Table 1 in Appendix C). Analytic expressions for all compartments in steady state are given in Table 3 in Appendix C. More detailed discussion of the mechanics behind steady states is presented below in subsection Alternative models.

4.3.2 Model 2: Animals infected with SIVmac251: Including infected cells with low levels of virus production

Model 1 cannot explain why viral loads in vaccinated animals challenged with SIVmac251, which are identified in the model with the antigen threshold of helper cells, are much higher than after challenge with SHIV-89.6P. A possible explanation for the puzzlingly high viral loads needed to maintain the helper response is that viral loads are dominated by a second infected cell type which produces virus at a lower rate and is thus less immunogenic. The central idea of the present work is expressed in Model 2, which has a more complex block of permissive and infected cells.

Evidence for long-lived infected cells with a low rate of virus production.

Experiments under potent ART in HIV infected humans (Perelson et al., 1997) and SIV infected macaques (Dinoso et al., 2009) show the existence of two types of infected cells with different properties. First, the observed biphasic viral decay indicates the presence of infected cells with different lifetimes. Long-lived and short-lived pathways of infected cell differentiation are respectively identified with the first and the second phase of decay. An additional assumption is that these long-lived cells produce virus at a rate lower by a factor of x than their short-lived counterparts,

which dominate virus production in untreated infection. Studies of SIV/HIV RNA hybridization in vivo (Cavert, 1997; Zhang et al., 1999) show a decrease in virus RNA copy per cell by a factor of 5 after two days of treatment, suggesting $x \sim 0.2$. On the other hand, by combining observations from the two cited experiments, the decrease in the effective virus production per cell is estimated to be somewhat larger than the decrease in the RNA production: $x \sim 0.07 - 0.1$. All parameters for long-lived infected cells used in calculating steady-state values of cell types are given in the legend to Fig. 4·5, with detailed estimates provided in Table 2 in Appendix C.

Impact of long-lived infected cells on the immune response

Two effective virus-producing cell compartments, P_V and P_H, are introduced to account for the unequal contributions of long and short-lived infected cells to virus production and stimulation of the helper cell response, respectively. The effective number of virus producing cells as they contribute to free virus is simply $P_V = xP_L + P$. The effective productive cell number for soluble antigen as detected by helper cells, denoted P_H, is less obvious. Assuming diffusion of antigen and cells in uniform tissue, we show that it is $P_H = x^3 P_L + P$ (section Methods, Interaction between cell types). The predicted cubic dependence of P_H on x is a central feature of this work and gives rise to the observed properties of the low steady state in vaccinated animals challenged with SIV.

The strong (cubic) effect of the virus production rate on immugenicity with respect to helpr cells can be visualized for long-lived and short-lived virus-producing cell types (Fig. 4·4). Each productive cell has an effective radius within which the density of antigen-loaded APC is above the threshold necessary for activation of helper cells. Due to lower rate of virus production, the radius of this APC-rich region is smaller for long-lived virus producing cells. While the contribution to virus production decreases linearly with x, the impact of long-lived cells on stimulation of helper cells (through control function α) decreases much more quickly, requiring relatively high viral loads to maintain the helper cell-dependent response in equilibrium.

Differentiation of infected cells

An additional consideration is necessary in order to account for the dominance of long-lived infected cells when viral loads are low, as in vaccinated animals, but not when viral loads remain high, as in control animals. Hence, it is postulated that the chance (denoted γ) of a newly infected cell in the eclipse phase following the long-lived pathway decreases with the virus load. Indeed, were the probability constant, the model would predict that a single infection pathway, either short-lived or long-lived, will always dominate regardless of vaccination status and resulting viral load. A sharp dependence is required, such that the short-lived pathway is favored at viral loads characteristic of the high-virus steady state. The form $\gamma = \gamma_0 \exp(-P_V/P_{single})$ is assumed, where constant $\gamma = \gamma_0$ at very low virus loads, and P_{single} is the characteristic viral load above which γ decreases sharply. Possible biological explanations for this dependence and further interpretation of parameters γ_0 and P_{single} are given in Discussion.

Low-virus steady state in the presence of low-producing cells. Predicted steady-state levels for all cell compartments, as well as the experimental levels of CTL, helper cells, and viral load (Letvin et al., 2006a; Sun et al., 2006), are shown in Fig. 4·5. Analytic expressions for these values and the method of their calculation are specified in Table 4 in Appendix C. Estimates of model parameters are given in the legend for Fig. 4·5 and Table 2 in Appendix C.

In the high-virus steady state (predicted by the model for unvaccinated animals), short-lived infected cells dominate both the viral load and the soluble antigen detected by helper cells by the same mechanism as in Model 1. The effective producing cell numbers are approximately equal, $P_V \approx P_H \approx P$. The role played by long-lived infected cells is minor; they produce roughly 1% of the free virus and have a negligible effect on helper cells.

In contrast, in the low-virus steady state, inequality of the effective productive cell numbers gives rise to the intermediate properties characteristic of the low steady state observed in vaccinated macaques challenged with SIV. In this state, long-lived infected cells dominate production of free

virus, while short-lived infected cells dominate stimulation of the immune response. The low production rate of long-lived infected cells and strong dependence of immunogenicity on production rate make their contribution to activation of helper cells minor; the effective virus-producing cell number for helper cells is $P_H \approx P$. As in Model 1, the indirect CTL response is established, and the number of short-lived infected cells is at the low activation threshold for helper cells, $P\ P_{H0} \log(1 + d_H/c_H)$. At the same time, because CTL kill long-lived infected cells much less efficiently than short-lived cells, long-lived infected cells are maintained at higher steady-state levels and dominate the total free virus (effective producing cell number for free virus is $P_V \approx xP_L$). The predicted CTL level is higher than predicted by Model 1, again, because of the low killing efficiency of long-lived infected cells. Individual variation in the ratio k/k_L, as well as in production ratio x and γ, through parameters γ_0 and P_{single} , could account for the broad variation of steady state viral loads observed in vaccinated macaques (Fig. 4·1A).

Some alternative simple models

Using the three building blocks described in Methods (A, B, and C in Fig. 4·2), we construct several simple models alternative to Model 1 above (Fig. 4·3A) and show that they fail to predict correct steady state properties for vaccinated and control macaques challenged with SHIV (Barouch, 2000). Some explanations of SIV infection in vaccinated macaques alternative to Model 2 are addressed in Discussion.

- Block A alone: No immune response. The model consisting only of permissive and infected cells (Fig. 4·2A) predicts two steady states: An uninfected host and an infected host. In the absence of infection, $I = P = 0$ and the homeostatic level of target cells is given by, $R(0) = s/d_R$. Below, we do not discuss a steady state without infection. Upon infection, assuming an initial reproductive ratio greater than 1, the model predicts establishment of infection at a level limited by the rate of target cell replenishment, $P^{SS} = \frac{s}{d_P} - \frac{d_R}{p_R}$.

- Blocks A and B: Single helper-independent CTL subset. The simplest model with an immune response includes a direct CTL response against a single epitope (E_D), which is stimulated

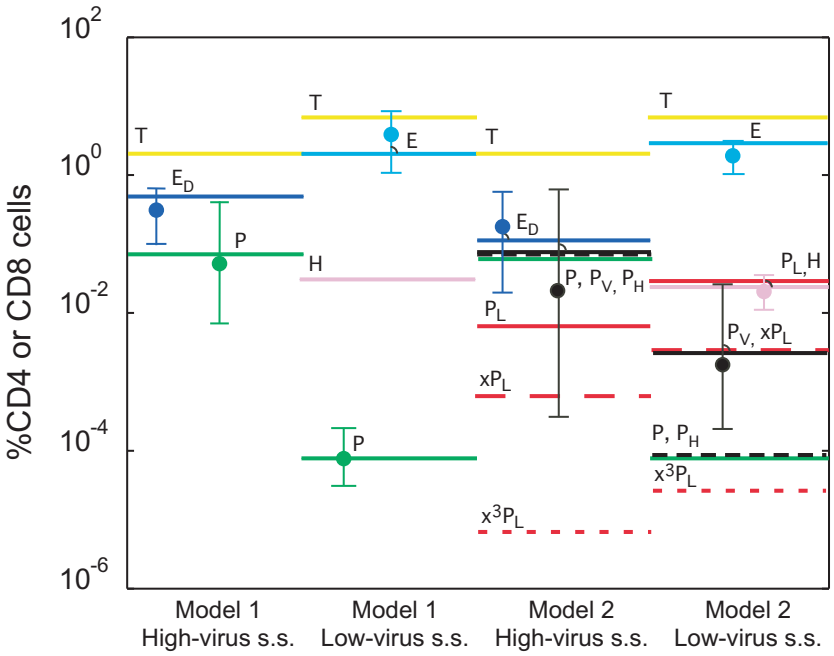

Figure 4·5: Estimates of cell compartment sizes in steady states predicted by Models 1 and 2. The two models with and without low-producing infected cells (Fig. 3) are used to interpret vaccination experiments with SIV and SHIV challenge, respectively (Fig. 1). Horizontal solid bars: Steady state values of cell compartments shown in Fig. 4·4 Dashed and dotted bars: Effective virus-producing cell numbers, $P_V = P + xP_L$ (for free virus) and $P_H = P + x^3P_L$ (for soluble antigen), as well as the contributions from low-producing cells. The steady state values, obtained from Equations 1 to 5 in Methods (see Tables 3 and 4 in Appendix C in Supplement for the full list) are shown as percentage of the total CD4 or CD8 T cell count in an average uninfected individual (%CD4 or %CD8). Circles and bars: Average values with 95% confidence intervals for the two experiments (Fig. 4·1). Data for Model 1 from Ref. (Barouch, 2000): Plasma viral load (green) converted to %CD4 cell using 1e7 RNA copies/% CD4 cell; p11c specific CD8 T cells detected by tetramer assay on day 49 postinfection for control (blue) and vaccinated (cyan) animals (legend to Fig. 4·1). Data for Model 2 from Refs. (Letvin et al., 2006a; Sun et al., 2006): Plasma viral load for vaccinated and control groups (legend to Fig. 4·1) (black) and Gag-specific CD4 T helper cells (magenta) measured by IL-2 intracellular cytokine staining on day 205 (Letvin et al., 2006a) and Gag-specific CD8 T cell measured by IFN-γ intracellular cytokine staining on day 203 for all 6 control animals (blue) and 24 vaccinated animals (cyan) (Sun et al., 2006). Helper and CTL measurements were reported in Refs. (Letvin et al., 2006a; Sun et al., 2006) only for these days. Model parameters: Estimated previously [Ref.citeSergeev:2009km and Table 3 in Appendix C]: $p_R = 0.5$/(day %CD4), $p_A = 125$/(day %CD4), $s = 0.07$ %CD4 /day, $d_T = 0.01$/day , $d_I = 1.0$/day, $c = 1$/day, $d = 0.4$/day, $c_H = 1.0$/day, $d_H = 0.04$/day, $P_0 = 0.2$%CD4, $P_{H0} = 2.10\text{-}3$ % CD4. Estimated in the present work (Table 4 in Appendix C): $H_0 = 3 \times 10^{-3}$ %CD4, $x = 0.1$, $k = 2$/(day %CD8) for Model 1 and $k = 9$/(day %CD8) for Model 2, $\gamma_0 = 0.8$, $P_{single} = 1.4 \times 10^{-2}$ %CD4, $d_{IL} = 0.1$/day, $d_{PL} = 0.05$/day, $k_L/k = 1 \times 10^{-2}$.

to expand by virus and kills infected cells (P). A combination of blocks A and B (Fig. 4·2A and B) predicts a single steady state controlled by direct CTLs. The corresponding level of virus-producing cells, P^{SS}, is determined by the equilibrium condition for direct CTLs (such that their proliferation rate is equal to their death rate, $\dot{E}_D = 0$, and is on the order of the activation threshold for indirect CTLs ($P^{SS} \sim P_0$). In turn, the steady-state level of CTLs is determined from the equilibrium condition for infected cells. Since CTLs will always expand while levels of infected cells are above the activation threshold for CTLs, the target cell-limited steady state described for the previous model (Block A alone) is unstable.

- Blocks A and C: Helper-dependent CTL response. Since it is well established that SIV and SHIV preferentially infect CD4+ T cells, several published models assume a helper cell-dependent CTL response that is impaired by high viral loads (Altes et al., 2003; Rouzine et al., 2005; Rouzine et al., 2006; Wodarz, 2001; Wodarz et al., 1998). In these models helper cells play the dual role of being a part of the immune response as well as targets for infection by virus and subsequent elimination by CTL. The simplest model utilizing the helper cell-dependent CTL response is a combination of blocks A and C (Fig 4·2A and 4·2C). The smeared-threshold control of CTLs by helper cells takes into account the existence of a maximum expansion rate for eukaryotic cells and also the death of CTLs at low levels of activated helper cells. CTLs begin to expand only when helper cells reach a critical level. The model predicts two steady states, one with a high virus load and without an active immune response, and another with a low virus load and with an active immune response. At high virus loads, helper cells are infected at a higher rate than they expand. Once their levels fall below the activation threshold for CTL, the CTL response turns off, and the virus remains in a steady state limited by availability of target cells. If helper cells or CTLs are at high initial levels (e.g., boosted by vaccine), or virus infectivity parameters, p_R and p_A, are decreased (e.g. by therapeutic intervention), the virus can be stabilized at a lower level determined by the condition of helper cell equilibrium ($\dot{H} = 0$). The virus load is maintained near the low activation threshold for helper cells [$P^{LSS} \sim P_{H0} \log(1 + d_H/c_H)$]. The helper cell level adjusts to maintain the indirect CTL response in equilibrium; the helper cells level in steady state is on the order of the activation threshold for indirect CTL ($H^{SS} \sim H_0$). Finally, the

steady state CTL level (E^{SS}) is determined by the equilibrium condition for infected cells (P).

Although two steady states are possible in this model, the prediction that in the high-virus steady state CTLs are absent and, thus, that the virus load is determined by target cell availability contradicts evidence of the importance of CTLs in untreated, infected individuals (Jin et al., 1999b; Schmitz, 1999). Furthermore, since helper cells are usually undetectable in the high steady state (Kalams et al., 1999; Kalams et al., 1999), a model with only a helper-dependent response is fundamentally incomplete.

- Blocks A, B, and B: two helper-independent CTL subsets. A model containing two direct CTL responses to two epitope, assuming a distinct activation threshold for each CTL subset, is unable to produce two stable steady states in an infected individual. Due to competitive exclusion, two subsets that compete for target cells cannot coexist. The more sensitive subset will always expand while viral loads are above its activation threshold. Once the more sensitive subset has expanded sufficiently to decrease the virus-producing cell level to its activation threshold, the resulting level of virus-producing cells will be too low to maintain the less sensitive CTL subset.

  Coexistence of different CTL subsets can be obtained formally by postulating that CTL responses are self-limiting, i.e., the CTL lifetime is not constant, as assumed above, but decreases as the CTL level increases. One clone is more efficiently stimulated, and thus remains at a higher steady state level than that of the less sensitive clone. However, in addition to the difficulty in justifying the saturation of CTL expansion at the low observed steady state levels levels ($< 1\%$ of total CD8 cells), the model still has only one steady state.

- Blocks A, C, and C: CTL response with two helper cell subsets. Introducing two helper subsets differing in activation threshold but having the same maximum expansion rate and the same constant death rate would suffer competitive exclusion, as in the case of direct CTL clones. The more sensitive helper and CTL subset will persist, and the other will

die out, resulting in only one possible steady state. In principle, two steady states can be obtained by assuming a higher maximum expansion rate for the less sensitive subset. The difference between parameters of the two subsets has to be extremely large to explain the 3-4 log difference in the steady state viral loads observed between vaccinated and control macaques challenged with SHIV. In addition to the difficulties with justifying vastly different parameters for two dominant clones, such a model does not explain why similar viral loads are observed for unvaccinated animals if there exists such a wide range of clone behaviors. A modified model containing two helper subsets with self-limiting expansion (e.g., with the death term quadratic in the helper cell number) is another method to predict multiple steady states with coexistence of helper-dependent CTL clones (Altes et al., 2003). This model is considered in Discussion in the context of SIV vaccination experiments.

- Blocks A, B, and C: Helper-dependent and helper-independent CTL response. This is Model 1, which predicts two immune-controlled steady states in a single host with drastically different viral loads and properties correct for the SHIV system (Fig. 4·3A).

4.4 Discussion

Two models are presented to interpret steady-state levels of virus-producing cells, CTLs and helper cells observed in control and vaccinated macaques challenged with SHIV (Barouch, 2000) and SIV (Letvin et al., 2006a), which are achieved by 100 days post-infection (Fig. 4·1). The differences between infections in vaccinated and unvaccinated animals challenged with SHIV can be interpreted, in a simple way, using a model with both a helper-independent and a helper-dependent CTL response, as in Model 1.

Model 1 is similar to an existing model featuring both a direct and an indirect CTL response, which control the virus in a high and low steady-state, respectively (Wodarz, 2001). In contrast to the cited work, here we have separated the small fraction of virus specific helper (Th1) CD4 cells from the total population of CD4 cells in order to study specifically the steady state regulatory mechanism of virus-producing cells by the helper dependant CTL response. Another important

difference is the smeared-threshold control of helper cells by virus and of CTLs by both virus and helper cells, as opposed to the linear dependencies postulated in the cited work. The change takes into account the existence of a maximum proliferation rate of the controlled cells.

Developing a relatively simple, biologically plausible and mathematically consistent model to explain the observed effect of vaccination against SIVmac251 on virus load in chronic infection is not trivial. Apparently convincing, yet insufficient, ideas have been proposed. For example, that steady state in vaccinated, SIV-infected animals is not distinct from the steady state in unvaccinated animals, because the distributions of viremia in the two groups of animals overlap, without showing a pronounced gap. However, the statistical difference in observable parameters between vaccinated and unvaccinated animals is a fingerprint of two steady states. The overlap of the distributions of viremia levels between the high and low steady states may result from individual variation of model parameters and is not relevant to the issue of the existence of two steady states. Another commonly held idea is that the variation of viremia resulting from different vaccination status and virus strain may be due to variation of the killing potential of CD8 T cells (or their non-lytic function). However, most immune-controlled models predict that, in a steady state, viremia is determined by the avidity of relevant immune cells (helper cells or CTLs). Due to interaction between virus and the immune response, the infected cell number is automatically adjusted to keep either CTLs (for the high-virus state) or helper cells (low-virus state) at a nearly constant level; variation in the CTL killing potential would affect only the CTL number.

In this work, it is assumed that CTLs control virus replication by killing infected cells. Two recent studies demonstrate that the first phase viral decay slope under ART does not change significantly in the absence of CTL (Klatt et al., 2010; Wong et al., 2010), with the conclusion that the mechanism of control of virus by CTL is likely to be non-lytic. In Models 1 and 2 above, the first phase decay rate is associated with the inverse duration of longest Poisson-distributed interval downstream from the latest point in the viral life cycle at which the drug acts. In animals with active CTL response, this is assumed to be the eclipse phase. In this context, the cited studies show conclusively that the productive phase of infection, even in the absence of CTL response, is not

longer than the eclipse phase, 1 day. The mechanism of CTL action remains under investigation; however, it does not impact the conclusions we draw for the steady state.

Alternative explanations for the different effects of vaccination in the two systems have not been proposed. Models which predict the coexistence of multiple helper cell subsets and multiple helper cell-dependent states with a range of virus loads (Korthals Altes et al., 2003) could potentially be applied to this problem. The general conclusion of the cited work is that the steady-state viral load is determined by the number of helper-dependent clones co-existing in a steady state is intriguing. However, to predict the coexistence of helper clones at a steady state, one needs to assume that expansion of helper cells is self-limiting and saturates at low characteristic densities ($< 1\%$ of the total CD4 T cell count). In addition, as explained above, it is difficult to explain why the sensitivity to dominant helper cell epitopes would differ so strongly (by a factor of 1000) between the vaccinated macaques challenged with SHIV and those challenged with SIV. Hence, we focus on the virological differences between the infecting strains and invoke the long-lived productive infected cells known to exist for the CCR5-tropic HIV and SIV.

One could also consider an alternative scenario to reduce the appearance of long-lived infected cells in the high steady state, by postulating that co-infection of a long-lived cell occurs at the virus-producing phase and returns the cell to the short-lived phenotype. However, reinfection at this late stage predicts a transient increase in viremia in the second phase of ART instead of the observed decay (results not shown). In addition, virus entry during the productive phase is less likely due to downmodulation of CD4 receptors mediated by viral protein Nef (Benson et al., 1993; Wildum et al., 2006).

The proposed explanation of the steady state observed in vaccinated macaques challenged with SIV requires further experimental investigation. One way to test the prediction that long-lived infected cells dominate virus production in these animals is by analyzing viremia decay after administration of potent ART during steady state infection in a vaccinated animal. Due to the dominance of long-lived cells, the decay is predicted to be monophasic and 10-30 times slower than the first-phase

decay in unvaccinated animals. In order to estimate parameter x directly, it would be useful to quantify the long-lived subset of infected cells after several weeks of ART in both unvaccinated animals and untreated vaccinated animals several months after challenge. Model 2 predicts that long-lived infected cells that produce little virus dominate infected cells in both situations.

Chapter 5

Conclusion and Outlook

5.1 An incremental approach to model building

For decades, mathematical modeling has been an important tool in understanding the spread and control of infectious diseases in a population of hosts. The increasing availability of sequence data, paired with detailed immunological studies, has enabled the same techniques to be applied in a single host. In this thesis we have presented several approaches to modeling HIV infection. All of our investigations have the common goal of building a realistic model of HIV dynamics and evolution in a host. As our understanding progresses, the complexity of the system becomes apparent. At the same time, we would like to build models that are simple to understand and capture the parts of the system that are relevant to the features of the data that are being modeled. Therefore, in each investigation we have chosen the simplest model that can reproduce interesting, or counter-intuitive, features of the data. In order to summarize the results of this thesis, some remarks on what is included in some models and not others.

In Chapter 2 and Chapter 3 we presented models of evolution of HIV in chronic and acute infection, respectively. We have developed different methods for these two phases, because the origin of selection pressure and the resulting pattern of diversity are different. In acute infection, selection is mainly due to CTL pressure, few sites are diverse, and a typical site stays diverse for only a few months. Thus, in Chapter 3 we developed a model that includes the dynamics of multiple CTL clones. We have analyzed the effects of changing CTL pressure that are observable in sequence data. With this model, we demonstrated that the site which is favored in an epitope can change over time, leading to "complex" intra-epitope escape patterns. Thus, in early infection, it is necessary

to model the CTL clones in order to accurately portray the magnitude of the selection pressure on each epitope.

In Chapter 2 we study evolution in the chronic phase of infection, during which there are many more diverse sites than predicted CTL epitopes, and a typical site will stay diverse for many years. Since escape from the immune response is observed much more rarely in chronic infection than in acute infection, we do not include CTL dynamics in this model. Instead, we assumed a distribution of selection coefficients over genome sites, which are constant in time. The origin of the selection pressure is thus not explicitly specified in the model. We hypothesize that it may be compensation for immune escapes that occurred earlier in infection. We used a Monte Carlo method, which can accurately capture the role of genetic drift in the evolution of many sites with low selection coefficient. Recombination is another important factor when many sites are simultaneously diverse and interference is strong. The focus of our study was to develop a method to estimate the frequency of recombination from single time-point data obtained from chronically infected patients. In order to estimate the parameters of recombination and selection that describe data, we consider several observables that are sensitive to these parameters and compare the resulting measures in real and simulated data. Out method predicts a low incidence of recombination, around 1%. Yet, despite this low value, linkage disequilibrium is lower, and the rate of adaptation higher, than it would be for purely asexual evolution. We thus conclude that recombination is indeed important for HIV evolution in chronic infection, when many sites are evolving at once.

In both Chapter 2 and Chapter 3, we considered a highly simplified model of the immune response. The relevant features of data could be explained by assuming selection pressure on a site, either static or dynamic. In order to model the effects of prior vaccination on the outcome of SIV infection in macaques, it is necessary to consider the immune response in more detail, as we have done in Chapter 4. Vaccination can result in the preservation of a cell type, CD4+ helper cells, which in untreated chronic infection is severely depleted. Helper cells can be infected by virus but also can increase the sensitivity of CTL to infected cells. We showed that these cell types are crucial to understanding the effect of vaccination against SIV infection in macaques. Relative to the previous

works, we made the simplification that all infected cell types are identical in order to focus on the immune system dynamics.

In this work, we proposed a model to explain the different outcome of vaccination in animals challenged with two viruses, SIVmac251 and SHIV. The steady state infected cell level is lower, and helper cells higher, in vaccinated animals infected with SHIV than in vaccinated animals infected with SIVmac251. In the model, the sensitivity of CTL and helper cells to virus is inversely proportional to the steady state level of infected cells. In addition, the sensitivity is proportional to the rate of virus production of infected cells. We postulate that Helper cells are responsible for controlling the steady-state level of infected cells in vaccinated animals. The difference in outcomes for the two experiments then indicates that the sensitivity of helper cells to antigen is lower in SIVmac251 infected animals relative to SHIV infected animal. We show that a possible mechanism behind this observation is that the dominant virus producing cell in SIVmac251 infected animals produces virus at a low rate, thus reducing the sensitivity of Helper cells to infected cells.

5.2 Future work

Little is known about the impact of compensatory mutations on the dynamics of CTL escapes. The compensatory effects that have been reported may represent extreme examples, where the fitness cost of the escape mutation is too high for escape to occur without the compensatory site present on the same genome. Thus they are always observed together and the escape mutation can be verified by experiment to have a high fitness costs. However, evidence also exists for low fitness costs for escape mutations. For example, when a virus containing an escape mutation in a CTL epitope is transmitted from a donor who contains the HLA that presents the epitope to a recipient that does not contain the HLA, the escape mutation is observed to slowly revert over many hundreds of days. This argues for a low fitness cost, on the order of 1%. In our work, we have assumed that the process of obtaining compensatory mutations is slow, as would be the case if many sites with small fitness gain per site are needed to compensate the fitness of an escape mutation. We have thus modeled the dynamics of escape before the compensation phase begins. It is not clear which of these

examples is representative, and how much fitness costs is incurred on average by an escape mutation.

It is not feasible to test each combination of sites for an epistatic effect experimentally, due to the large number of possible combinations of mutations. A more practical computational approach has been developed recently (Carlson et al., 2008). This approach detects correlations between presence of a particular HLA allele and presence of a mutation in the viral genome from a population of infected hosts. From the strength of the correlation, selection by the CTL response in a host is inferred. Compensatory interactions between mutations in the viral genome can also be detected. This method has been successful in expanding the knowledge about compensatory interactions, and has the potential to provide enough information to include these interactions in a model of viral evolution.

The cause of the wide variation in viral load between hosts during chronic infection remains illusive. It is of great clinical importance to determine which factors are responsible for the viral load in an infected host. For example, the ability to lower viral loads in infected patients would have the consequences of lowering transmission and mortality risks. One of our central hypotheses is that the sensitivity of CTL to infected cells determines the level of infected cells in steady state. We assume a CTL activation function for which CTL proliferation is proportional to recognized infected cells and saturates at some maximum level. As a result of the assumed form of the activation function, multiple CTL with different sensitivities cannot co-exist in steady state. In data, however, typically multiple clones appear at nearly constant levels for many years. This indicates that either the sensitivities of active CTL clones are nearly identical, as proposed in Chapter 3, or that another factor is contributing to the steady state viral load. Other factors could potentially influence CTL recognition of an infected cell, such as unequal presentation of epitopes on the surface of infected cells, or changing levels of virus production in a cell over time. We plan to investigate alternative models that predict co-existance of many CTL clones in steady state, and which leave intact our existing understanding of the importance of CTL to controlling infected cells.

Appendix A

Diffusion Approximation

When a population is composed of two variants with slightly different replication rates, as outlined in Chapter 1, the probability distribution for the mutant frequency can be studied using a diffusion approximation. The treatment is found in many textbooks on population genetics and closely follows the treatment given in (Sethupathy and Hannenhalli, 2008). According to the Wright-Fisher model, the probability that in the next generation there will be a new number of mutated strains, m', is given by the binomial distribution:

$$p_{m,m'} = \binom{N}{m'} (\phi)^{m'} (1-\phi)^{N-m'} \tag{A.1}$$

Where ϕ gives the probability of selecting a mutant variant and depends on the relative fitnesses of the two strains, $(1+s)$, as follows:

$$\phi = \frac{f(1+s)}{f(1+s)+(1-f)} \tag{A.2}$$

Where $f = m/N$ is the mutant frequency at generation t and $(1+s)$ is the relative replication rate of the mutant variant compared to the wild type variant.

The evolution of the system over time is described as a Markov process.

$$P(m', t+1) = \sum_{m'} P(m,t) p_{m,m'} \tag{A.3}$$

Where $P(m,t)$ is the probability of having n copies of the mutant variant at time t. We change

notation in order to include explicitly the initial mutant number at $t = 0$, m_0:

$$\rho(m', m_0.t + 1) = \sum_{m'} \rho(m, m_0, t) p_{m,m'} \tag{A.4}$$

In the limit of infinite population size, $N \to \infty$, small $s \ll 1$, and strong selection pressure $Ns \gg 1$, the process can be described by a continuous-time, continuous-space diffusion process.

$$\rho(f + \Delta f, f_0, t + \Delta t) = \int \rho(g, f_0, t) \rho(f + \Delta f, g, \Delta t) dg \tag{A.5}$$

Where now we have used f, g to denote the mutant frequency, and $\rho(f, f_0, t)$ is the probability distribution of f at time t, given that the mutant frequency was f_0 at time 0, and Δf is the change in mutant frequency in time Δt.

By expanding both sides to first order in Δt and second order in Δx we arrive at the Kolmogorov forward equation:

$$\frac{\partial \rho(f, f_0, t)}{\partial t} = \frac{\partial [a(f) \rho(f, f_0, t)]}{\partial f} + \frac{\partial^2 [b(f) \rho(f, f_0, t)]}{\partial f^2} \tag{A.6}$$

where:

$$\begin{aligned} a(f) dt &\approx E(\Delta f) \\ b(f) dt &\approx Var(\Delta f) \end{aligned} \tag{A.7}$$

Plugging in the expected increase in mutant frequency per unit time $a(f) = sf(1 - f)$ and the variance of the expected increase per unit time $b(f) = \frac{f(1-f)}{2N}$, we obtain the Kolgomorov Forward Equation, as given in Chapter 1:

$$\frac{\partial P(f,t)}{\partial t} = s\frac{\partial[f(1-f)P(f,t)]}{\partial f} + \frac{1}{2N}\frac{\partial^2[f(1-f)P(f,t)]}{\partial f^2} \tag{A.8}$$

For the purpose of calculating the probability that a mutant will grow to fixation given that it was initially present at one copy in the population, it is easier to consider a related equation, the Kolgomorov Backward Equation.

Instead of times $(0, t, t+\delta t)$, we consider the times $(0, \Delta t, t+\Delta t)$ where the mutant frequency is given by $(f_0, f_0+\Delta, f)$. The evolution of the distribution is given by:

$$\rho(f, f_0, t+\Delta t) = \int \rho(f+f_0, f_0, \Delta t)\rho(f, f+\Delta f, t)d(\Delta f) \tag{A.9}$$

By expanding, as before, we arrive at the Kolgomorov backward equation.

$$\frac{\partial \rho(f, f_0, t)}{\partial t} = a(f_0)\frac{\partial[\rho(f, f_0, t)]}{\partial f} + b(f_0)\frac{\partial^2[\rho(f, f_0, t)]}{\partial f^2} \tag{A.10}$$

We are interested in calculating the probability of a single mutation to fix. We define $F(k,t)$ as the probability of having frequency k or more mutants at time t, given frequency $1/N$ at $t=0$:

$$F(k,t) = \int_k^1 df\rho(f, f_0, t) \tag{A.11}$$

Integrating A.10 we get:

$$\frac{\partial F(f_0,t)}{\partial t} = a(f_0)\frac{\partial[F(f_0,t)]}{\partial f} + b(f_0)\frac{\partial^2[F(f,t)]}{\partial f^2} \tag{A.12}$$

We are interested in the case when $f=1$, at which point the population is uniform in the mutant

for all future times. In the $t \to \infty$ limit, the left hand side of Eq. A.12 is equal to zero. Call $F(1, \infty) = p_{fix}$, the fixation probability. By integrating twice and using the boundary conditions, $p_{fix}(0) = 0$ and $p_{fix}(1) = 1$, we find:

$$p_{fix} = \frac{\int_0^{1/N} \psi(y)dy}{\int_0^1 \psi(y)dy} \tag{A.13}$$

Where:

$$\psi(y) = \exp[-2 \int^{y} \frac{a(z)}{b(z)}dz] \tag{A.14}$$

Where $a(f) = sf(1-f)$ and $b(f) = f(1-f)/2N$, as above. Plugging these in, we can solve for p_{fix} given initial frequency $1/N$:

$$p_{fix} = \frac{1 - \exp[-2s]}{1 - \exp[-2Ns]} \approx 2s \tag{A.15}$$

For $Ns \gg 1$ and $s \ll 1$. The probability of fixation of a mutation that is present at the level of one copy in the population is proportional to the selective advantage it confers.

Appendix B

Lifetime of the two haplotypes in the leapfrog pattern

When escape in an epitope follows the leapfrog pattern in an experimental data, the second haplotype is long lived compared to the first. In order to calculate the parameter range in our model that can describe this qualitative observation, we compare the lifetimes of haplotypes 10 and 01, the two haplotypes that arise in succession during escape in a single epitope with two sites. The lifetime of a haplotype is defined as the time when a haplotype is dominant ($f > 0.5$) in the population. We determine the lifetimes of haplotypes 10 and 01. Let $t = 0$ be the time when 10 reaches $f = 0.5$. E_1 begins in steady state:

$$E_1(0) = \frac{\beta T^{ss} - d_I}{nk} \equiv \frac{E_{tot}}{n} \tag{B.1}$$

We make the approximation that E_1 remains at this level until haplotype 10 reaches $f = 0.5$. Furthermore, we neglect changes in target cells and total E levels during escape in epitope 1, since fitness costs are small.

B.1 Lifetime of the first haplotype

For haplotype 10 the lifetime is comprised of two intervals.

1. t_{g1}: The time interval from the moment 10 reaches $f = 0.5$ until the moment when 01 begins to grow.

2. t_{d1}: The time from the moment 01 begins to grow, to the moment it reaches $f = 0.5$.

Growth of the first haplotype

Once haplotype 10 is the dominant haplotype, the inverse avidity of E_1 is increases to $h\exp(r_1)$, and the rate of change of E_1 is:

$$\dot{E}_1 = (\frac{cP^{ss}}{h\exp(r_1) + P^{ss}} - d_E)E_1 \tag{B.2}$$

Where P_{ss} is determined by the equilibrium condition for E_1, found by solving for $\dot{E}_1 = 0$ with $r_1 = 0$ in Eq. B.2. E_1 starts in steady state at E_{tot}/n and decays according to:

$$E_1(t) = \frac{E_{tot}}{n}e^{-\delta_1 t}, \qquad \frac{d_E}{c}e^{-r_1} \ll 1 \tag{B.3}$$

$$\delta_1 \equiv d_E(1 - \exp(-r_1)) \tag{B.4}$$

In the main text we introduced CTL level $E_{10\to01}$, the level of E_1 where haplotypes 10 and 01 have equal exponential growth rates:

$$E_{1,10=01} = (\frac{\beta T^{ss}}{k})\frac{e^{-s_2} - e^{-s_1}}{e^{-r_2} - e^{-r_1}} \approx (\frac{\beta T^{ss}}{k})\frac{s_1 - s_2}{e^{-r_2} - e^{-r_1}} \tag{B.5}$$

Where $s_1 > s_2$ and $r_1 > r_2$, such that the leapfrog pattern can occur. Therefore, t_{g1} is the time that it takes E to drop from the initial level $\frac{E_{tot}}{n}$ to level $E_{10\to01}$, and is found from Eq. (B.3):

$$t_{g1} = \frac{1}{\delta_1}\log(\frac{E_{tot}}{nE_{1,10\to01}}) \tag{B.6}$$

Substituting for $E_{10\to01}$ from Eq. (B.5) and E_{tot} from Eq. B.1, this becomes:

$$t_{g1} = \frac{1}{\delta_1}\log(\frac{e^{-r_2} - e^{-r_1}}{(s_1 - s_2)\zeta}) \tag{B.7}$$

Where $\zeta = n(1 - \frac{d_I}{\beta T^{ss}})$.

Decay of the first haplotype

The time interval from the moment that the second haplotype, 01, begins to grow until it reaches majority status in the population is found by considering the difference in the exponential growth rates of 01 and 01. The difference between the exponential growth rates of 10 and 01 can be expressed for any level of E_1, using Eq. 3.7 in Chapter 1.

$$\epsilon_{01-vs-10}(t) = \beta T^{ss}(s_1 - s_2) - kE_1(t)(\exp(-r_2) - \exp(-r_1)) \tag{B.8}$$

$$\tag{B.9}$$

At $t = t_{g1}$, $E_1 = E_{1,10\to01}$, and 10 and 01 have equal exponential growth rates. Together with the rate of decay of E_1, (B.3), and the level of E_1 when at t_{g1}, (B.5), this gives:

$$\epsilon_{01-vs-10}(t) = \gamma_1(1 - e^{-\delta_1 t}) \tag{B.10}$$

$$\gamma_1 \equiv \beta T^{ss}(s_1 - s_2) \tag{B.11}$$

Thus, 01 grows with an exponentially changing rate. Where we have again neglected the change in the decay rate of of E_1 while haplotype 01 is in the minority. The frequency of 01 will grow according to the equation (see analogous Eq. 1.10 for two variant competition in Chapter 1):

$$\dot{f}_{01} = \epsilon_{01-vs-10}(t) f_{01}(1 - f_{01}) \tag{B.12}$$

Which has solution:

$$f_{01}(t) = [1 + \frac{1}{f_{01}(0)} \exp[\frac{\gamma_1}{\delta_1} - \gamma_1(t + \frac{1}{\delta_1} \exp(-\delta_1 t)]]^{-1} \tag{B.13}$$

The time interval t_{d1} is found by setting $f_{01} = 0.5$ in Eq. B.13, giving

$$\exp(-\delta_1 t_{d1}) = \frac{\delta_1}{\gamma_1} \log(N) + 1 - \delta_1 t_{d1} \tag{B.14}$$

The lifetime of haplotype 10 is the sum of the two time intervals in Eqs. B.7 and B.14:

$$t_{10,lifetime} = t_{g1} + t_{d1} \tag{B.15}$$

B.2 Lifetime of the second haplotype in the leapfrog pattern

The lifetime of 01 is composed of two time intervals:

1. t_{g2}: The time interval from the moment that the frequency of the second haplotype reaches $f = 0.5$ to the moment when the haplotype 00 begins to grow.

2. t_{d2}: The time for 00 to grow to $f = 0.5$.

Growth of the second haplotype

While 01 is growing but still in the minority, we approximate the decay of E_1 with Eq. B.3. The procedure to calculate the two time intervals that comprise the lifetime of 01 is analogous to that for 10. We reset the clock at $t_{01,lifetime}$ to $t = 0$. E_1 has decayed to level:

$$E_1(0) = E_{10\rightarrow 01} \exp(-\delta_1 t_{d1}) \tag{B.16}$$

At this point, the decay of E_1 slows due to increased recognition ($r_2 < r_1$), and further decay is described by:

$$E_1(t) = E_1(0)e^{-\delta_2 t}, \qquad \frac{d_E}{g}e^{-r_2} \ll 1 \tag{B.17}$$

$$\delta_2 \equiv d_E(1 - \exp(-r_2)) \tag{B.18}$$

The time until the haplotype 00 begins to grow, t_{g2}, is found by setting $E_1(t_{g2}) = E_{01\to00}$ in Eq. B.17.

$$E_{01\to00} = E_1(0)\exp(-\delta_2 t_{g2}) \tag{B.19}$$

Where $E_1(0)$ is given by Eq. B.16 and

$$E_{01\to00} = (\frac{\beta T^{ss}}{k})\frac{1 - \exp(-s_2)}{1 - \exp(-r_2)} \tag{B.20}$$

Solving for t_{g2} in Eq. B.19 gives:

$$t_{g2} = \frac{1}{\delta_2}(\log[\frac{E_{10\to01}}{E_{01\to00}}] - \delta_1 t_{d1}] \tag{B.21}$$

Where t_{d1} is given by Eq. B.14.

Decay of the second haplotype

Using the difference in exponential growth rates between 00 and 01 we can find the time interval from when 00 begins to grow, until is reaches $f = 0.5$. The advantage of 00 for an arbitrary value of E_1 is found using Eq. 3.7 in Chapter 1.

$$\epsilon_{00-vs-01}(t) = \beta T(1 - \exp(-s_2)) - kE(t)(1 - \exp(-r_2)) \tag{B.22}$$

When $E_1(t) = E_{1,01\to00}$, 01 and 00 have equal exponential growth rates. Substituting Eq. B.17 and for rate of decay of E_1 and the initial value, $E_{1,01\to00}$, which is found in analogy to Eq. **??** in Chapter 1, we find that 00 grows with an exponentially changing rate.

$$\epsilon_{00-vs-01}(t) = \beta T s_2 (1 - e^{-\delta_2 t}) \tag{B.23}$$

The frequency of 01 will grow according to:

$$\dot{f}_{00} = \epsilon_{00-vs-01}(t) f_{00}(1 - f_{00}) \tag{B.24}$$

Which has solution:

$$f_{00}(t) = [1 + \frac{1}{f_{00}(0)} \exp[\frac{\gamma_2}{\delta_2} - \gamma_2(t + \frac{1}{\delta_2}\exp(-\delta_2 t)]]^{-1} \tag{B.25}$$

$$\gamma_2 \equiv \beta T^{ss} s_2 \tag{B.26}$$

Setting $f_{00} = 0.5$ in Eq. (B.25), we can solve for t_{d2}, the time when $f_{00} = 0.5$:

$$\exp(-\delta_2 t_{d2}) = \frac{\delta_2}{\gamma_2}\log(N) + 1 - \delta_2 t_{d2} \tag{B.27}$$

The lifetime of haplotype 01 is the sum of the two time intervals in Eqs. B.21 and B.27.

$$t_{01,lifetime} = t_{g2} + t_{d2} \tag{B.28}$$

Appendix C

Supplementary Tables for Model 1 and Model 2 in Chapter 4

Table 1. Model 1 parameter estimates

Para-meter	Description	Units	Estimate
p_R	Efficiency of resting CD4 T cell infection, estimated based on initial virus slope (Sergeev et al., 2010b).	1/(day %CD4)	0.5
p_A	Efficiency of activated CD4 T cell infection, assumed to be much higher efficiency than for resting target cells.	1/(day %CD4)	125
s	Intensity of homeostatic replenishment of CD4 T cells. Only the target population that is destined to become productively infected is explicitly modeled, a subset that at peak viral levels is 7% of the population by measurements of CD4 T cells in gut-associated lymphoid tissue (Li et al., 2005).	%CD4/day	0.07
d_R	Inverse duration of the resting CD4 T cell phase. It is estimated that less than 1% of the entire population of resting memory cells turns over each day.	1/day	0.01
d_I	Inverse duration of the eclipse phase of a short-lived infected CD4 T cell, estimated from virus decay slop under ART (Brandin et al., 2006; Markowitz et al., 2003).	1/day	1
d_P	Death rate of productively infected cells due to viral pathogenicity	1/day	0
k	Efficiency of killing by CTL, estimated from steady state CTL levels in both experiments considered (Barouch et al., 2000; Letvin et al., 2006).	1/(day %CD8)	2
c	Maximum division rate of effector CTLs, estimated from measurements of single specific CD8 T cell responses to acute LCMV infection (De Boer et al., 2003; Homann et al., 2001)	1/day	1
d	Death rate of effector CTLs (De Boer et al., 2003; Homann et al., 2001)	1/day	0.4
c_H	Maximum expansion rate of effector helper cells (De Boer et al., 2003; Homann et al., 2001)	1/day	1
d_H	Death rate of helper cells in the absence of virus, estimated by combining the two decay phases (De Boer et al., 2003; Homann et al., 2001)	1/day	0.04
H_0	Characteristic helper cell number for indirect CTLs determined by observed steady state levels of helper cells and the steady-state equation for helper cells	%CD4	$3 \cdot 10^{-3}$

P_{H0}	Characteristic productive infected cell number for stimulation of helper cells estimated from the steady state levels of viremia in vaccinated, SHIV challenged animals (Barouch et al., 2000), together with the equilibrium condition for infected cells in the low-virus steady state (Sergeev et al., 2010b)	%CD4	$2 \cdot 10^{-3}$
P_0	Characteristic productive cell number for direct effector CTLs, estimated from the steady state levels of viremia in untreated, unvaccinated animals (Barouch et al., 2000), together with the equilibrium condition for infected cells in the high-virus steady state (Sergeev et al., 2010b)	%CD4	0.2

Table 2. Model 2 parameter estimates

Para-meter	Description	Units	Value
x	Ratio of the virus production rate of long-lived infected cells to that of short-lived infected cells. Estimated from two experiments: i) Viremia decay in ART shows that the average contribution of long-lived infected cells to free virus is ~ 1% (Palmer et al., 2008; Perelson et al., 1997). ii) Tissue studies show that infected cells with low production rate appear on day 2 after onset of ART (Cavert et al., 1997; Zhang et al., 1999). In two days number of short-lived cells decay by a factor $\exp(-2d_I) \sim 0.15$, providing an estimate of the fraction of low-producing infected cells in the high-virus steady state.	1	1/15
d_{IL}	Inverse duration of eclipse phase for a long-lived infected CD4 T cell. The rate of decay in the second phase of viremia decay after ART is used to estimate the length of the corresponding eclipse phase (Perelson et al., 1997), $d_{IL}^{-1} \sim$ 10-30 days.	1/day	1/10
d_{PL}	Inverse duration of the productive phase for a long-lived infected cell can be directly estimated from ART in SIV infected macaques including an IN inhibitor (Dinoso et al., 2009).	1/day	1/20
d_P	Death rate of productively infected cells due to viral pathogenicity	1/day	0
k	Efficiency of killing by CTL, as in table S1 above. Since macaques expressing MHC molecule MAMU-A*01 are observed to have up to 10-fold higher epitope specific CTL responses than macaques expressing MAMU-A*02 (Newberg et al., 2006), we take k to be higher for MAMU-A*02 animals (Model 2 applied to SIV infection (Letvin et al., 2006))	1/(day %CD8)	9
k_L	Killing efficiency of long-lived infected cell by CTL. We assume that, due to relatively low expression of virus proteins, long-lived infected cells are weakly recognizable by CTL ($k_L << k$). The nearly constant second phase of viral decay during the first few weeks of ART time (Perelson et al., 1997) despite strong changes in CTL levels (Ogg et al., 1999) confirms that the lifetime of long-lived infected cells is not limited by CTL in the high steady state.	1/(day %CD8)	0.09
γ_0	Fraction of newly infected cells following long-lived pathway at low virus loads, estimated from steady state viremia levels in vaccinated animals challenged with SIV (Letvin et al., 2006).	1	0.8
P_{single}	Virus level at which the fraction of newly infected cells following the long-lived pathway sharply decreases, estimated together with γ_0 from steady state virus levels.	%CD4	$1.4 \cdot 10^{-2}$

References are given in the main text.

Table 3. Steady State Equations for Model 1

Approximate equation	**Steady state expression**	**Value**	**Strong inequalities**
High-virus steady state			
$dE_D/dt = [\beta c - (1-\beta)d]\, E_D$	$P = P_0 \ln[1 + d/c]$	0.07	
$dR/dt = s - p_R PR$	$R = s/p_R P$	2	$d_R << p_R P$
$dI/dt = p_R RP - d_I I$	$I = s/d_I$	0.07	
$dP/dt = d_I I - kE_D P$	$E_D = s/kP$	0.5	$E << E_D$
Low-virus steady state			
$dH/dt = [\alpha c_H - (1-\alpha)d_H]\, H$	$P = P_{H0} \ln[1 + d_H/c_H]$	8e-5	$p_A P << c_H$
$dE/dt = [\sigma c - (1-\sigma)\, d]\, E$	$H = H_0 \ln[1 + d/c]$ $\times (c_H + d_H)/d_H$	0.03	
$dR/dt = s - d_R R$	$R = s/d_R$	7.0	$p_R P << d_R$
$dI/dt = p_R RP - d_I I$	$I = p_R sP/d_I d_R$	3e-4	
$dP/dt = d_1 I - kEP$	$E = p_R s/d_R k$	2	$E_D << E$

Table 4. Steady State Equations for Model 2

Equation	**Steady state expression**	**Value**	**Strong inequalities**
High-virus steady state			
$dE_D/dt = [\beta c - (1-\beta)d]\, E_D$	$P = P_0 \ln[1 + d/c]$	0.07	$(k_L/k)P_L << P \Leftrightarrow$ $\beta \approx 1 - \exp(-P/P_0)$
$dR/dt = s - p_R PR$	$R = s/(p_R P)$	2	$xP_L << P \Leftrightarrow P_V \approx P$ $d_R << p_R P_V$
$dI/dt = p_R RP - d_I I$	$I = s/d_I$	0.07	$P_V \approx P$ $d_R << p_R P_V$
$dI_L/dt = \gamma d_I I - d_{IL} I_L$	$I_L = s\gamma/d_{IL}$	0.04	$P_V \approx P$
$dP/dt = (1-\gamma)d_I I - kE_D P$	$E_D = (1-\gamma)s/(kP)$	0.1	$E << E_D$ $P_V \approx P$
$dP_L/dt = d_{IL} I_L - d_{PL} P_L$	$P_L = s\gamma/d_{PL}$	7e-3	$E << E_D$ $k_L E_D << d_{PL}$ $P_V \approx P$
Low-virus steady state			
$dH/dt = [\alpha c_H - (1-\alpha)d_H]\, H$	$P = P_{H0} \ln[1 + d_H/c_H]$	8e-5	$x^3 P_L << P \Leftrightarrow P_H \approx P$ $p_A P << c_H$
$dE/dt = [\sigma(c-d) - (1-\sigma)\, r]\, E$	$H = H_0 \ln[1 + c/d]$ $\times (c_H + d_H)/d_H$	0.03	
$dR/dt = s - d_R R$	$R = s/d_R$	7	$xP_L >> P \Leftrightarrow P_V \approx xP_L$ $p_R P_V << d_R$
$dI/dt = p_R RP_V - d_I I$	$I = p_R sxP_L/d_I d_R$	0.01	$P_V \approx xP_L$
$dI_L/dt = \gamma d_I I - d_{IL} I_L$	$I_L = p_R sxP_L\gamma_0/d_{IL} d_R$	0.08	$P_V << P_{\text{single}} \Leftrightarrow \gamma \approx \gamma_0$
$dP_L/dt = d_{IL} I_L - k_L EP_L$	$E = p_R sx\gamma_0/d_R k_L$	3	$d_{PL} << k_L E$
$dP/dt = (1-\gamma)d_I I - kEP$	$P_L = \{\gamma_0 k/[(1-\gamma_0)k_L]\}P$	0.03	$\gamma \approx \gamma_0$

Cell compartment sizes predicted by Model 2 (Fig. 4B and the legend, main text) for two steady states. Starting equations are Equations 2-4 and 6 in *Materials and Methods*, main text. Column 1: Approximate equations with small terms neglected. Column 2: Analytic expressions. Column 3: Numeric values for model parameter values (legend to Fig. 5, main text) shown as percentage of the total CD4 or CD8 T cell count in an average uninfected animal. Column 4: Strong inequalities used.

References

Achaz, G. (2004). A Robust Measure of HIV-1 Population Turnover Within Chronically Infected Individuals. Molecular Biology and Evolution *21*, 1902–1912.

Altes, H. K., Ribeiro, R. M. and De Boer, R. J. (2003). The race between initial T-helper expansion and virus growth upon HIV infection influences polyclonality of the response and viral set-point. Proceedings of the Royal Society B: Biological Sciences *270*, 1349–1358.

Althaus, C. L. and Boer, R. J. D. (2008). Dynamics of immune escape during HIV/SIV infection. PLoS Computational Biology *4*, e1000103.

Asquith, B., Edwards, C. T. T., Lipsitch, M. and McLean, A. R. (2006). Inefficient Cytotoxic T Lymphocyte–Mediated Killing of HIV-1–Infected Cells In Vivo. PLoS Biology *4*, e90.

Ayme, V., Petit-Pierre, J., Souche, S., Palloix, A. and Moury, B. (2007). Molecular dissection of the potato virus Y VPg virulence factor reveals complex adaptations to the pvr2 resistance allelic series in pepper. Journal of General Virology *88*, 1594–1601.

Balfe, P., Simmonds, P., Ludlam, C. A., Bishop, J. O. and Brown, A. J. (1990). Concurrent evolution of human immunodeficiency virus type 1 in patients infected from the same source: rate of sequence change and low frequency of inactivating mutations. Journal of Virology *64*, 6221–33.

Barouch, D. H. (2000). Control of Viremia and Prevention of Clinical AIDS in Rhesus Monkeys by Cytokine-Augmented DNA Vaccination. Science *290*, 486–492.

Batorsky, R., Kearney, M., Palmer, S., Maldarelli, F., Rouzine, I. and Coffin, J. (2011a). Estimate of effective recombination rate and average selection coefficient for HIV in chronic infection". Proc. Nat. Acad. Sci. *108*, 5661–5666.

Batorsky, R., Kearney, M. F., Palmer, S. E., Maldarelli, F., Rouzine, I. M. and Coffin, J. M. (2011b). Estimate of effective recombination rate and average selection coefficient for HIV in chronic infection. Proceedings of the National Academy of Sciences *108*, 5661–5666.

Benson, R. E., Sanfridson, A., Ottinger, J. S., Doyle, C. and Cullen, B. R. (1993). Downregulation of cell-surface CD4 expression by simian immunodeficiency virus Nef prevents viral super infection. The Journal of experimental medicine *177*, 1561–1566.

Bonhoeffer, S. (2004). Evidence for Positive Epistasis in HIV-1. Science *306*, 1547–1550.

Brandin, E., Thorstensson, R., Bonhoeffer, S. and Albert, J. (2006). Rapid viral decay in simian immunodeficiency virus-infected macaques receiving quadruple antiretroviral therapy. Journal of Virology *80*, 9861–9864.

Brown, A. J. (1997). Analysis of HIV-1 env gene sequences reveals evidence for a low effective number in the viral population. Proceedings of the National Academy of Sciences of the United States of America *94*, 1862–1865.

Brunet, E., Rouzine, I. M. and Wilke, C. O. (2008). The Stochastic Edge in Adaptive Evolution. Genetics *179*, 603–620.

Burch, C., Turner, P. and Hanley, K. (2003). Patterns of epistasis in RNA viruses: a review of the evidence from vaccine design. Journal of evolutionary biology *16*, 1223–1235.

Cale, E. M., Hraber, P., Giorgi, E. E., Fischer, W., Bhattacharya, T., Leitner, T., Yeh, W. W., Gleasner, C., Green, L. D., Han, C. S., Korber, B. and Letvin, N. L. (2011). Epitope-Specific CD8+ T Lymphocytes Cross-Recognize Mutant Simian Immunodeficiency Virus (SIV) Sequences but Fail To Contain Very Early Evolution and Eventual Fixation of Epitope Escape Mutations during SIV Infection. Journal of Virology *85*, 3746–3757.

Carlson, J. M., Brumme, Z. L., Rousseau, C. M., Brumme, C. J., Matthews, P., Kadie, C., Mullins, J. I., Walker, B. D., Harrigan, P. R., Goulder, P. J. R. and Heckerman, D. (2008). Phylogenetic Dependency Networks: Inferring Patterns of CTL Escape and Codon Covariation in HIV-1 Gag. PLoS Computational Biology *4*, e1000225.

Cavert, W. (1997). Kinetics of Response in Lymphoid Tissues to Antiretroviral Therapy of HIV-1 Infection. Science *276*, 960–964.

Chun, T. W., Carruth, L., Finzi, D., Shen, X., DiGiuseppe, J. A., Taylor, H., Hermankova, M., Chadwick, K., Margolick, J., Quinn, T. C., Kuo, Y. H., Brookmeyer, R., Zeiger, M. A., Barditch-Crovo, P. and Siliciano, R. F. (1997a). Quantification of latent tissue reservoirs and total body viral load in HIV-1 infection. Nature *387*, 183–188.

Chun, T. W., Stuyver, L., Mizell, S. B., Ehler, L. A., Mican, J. A., Baseler, M., Lloyd, A. L., Nowak, M. A. and Fauci, A. S. (1997b). Presence of an inducible HIV-1 latent reservoir during highly active antiretroviral therapy. Proceedings of the National Academy of Sciences of the United States of America *94*, 13193–13197.

Crawford, H., Matthews, P. C., Schaefer, M., Carlson, J. M., Leslie, A., Kilembe, W., Allen, S., Ndung'u, T., Heckerman, D., Hunter, E. and Goulder, P. J. R. (2011). The Hypervariable HIV-1 Capsid Protein Residues Comprise HLA-Driven CD8+ T-Cell Escape Mutations and Covarying HLA-Independent Polymorphisms. Journal of Virology *85*, 1384–1390.

De Boer, R. J. (2007). Understanding the failure of CD8+ T-cell vaccination against simian/human immunodeficiency virus. Journal of Virology *81*, 2838–2848.

Deeks, S. G. and Walker, B. D. (2007). Human immunodeficiency virus controllers: mechanisms of durable virus control in the absence of antiretroviral therapy. Immunity *27*, 406–16.

Desai, M. M. and Fisher, D. S. (2007a). Beneficial Mutation Selection Balance and the Effect of Linkage on Positive Selection. Genetics *176*, 1759–1798.

Desai, M. M. and Fisher, D. S. (2007b). Beneficial mutation selection balance and the effect of linkage on positive selection. Genetics *176*, 1759–98.

Dinoso, J. B., Rabi, S. A., Blankson, J. N., Gama, L., Mankowski, J. L., Siliciano, R. F., Zink, M. C. and Clements, J. E. (2009). A simian immunodeficiency virus-infected macaque model to study viral reservoirs that persist during highly active antiretroviral therapy. Journal of Virology *83*, 9247–9257.

Ewens, W. (2004). Mathematical Population Genetics: Theoretical introduction. Number v. 1 in Interdisciplinary Applied Mathematics, Springer-Verlag.

Ferrantelli, F. and Ruprecht, R. M. (2002). Neutralizing antibodies against HIV – back in the major leagues? Current Opinion in Immunology *14*, 495–502.

Fischer, W., Ganusov, V. V., Giorgi, E. E., Hraber, P. T., Keele, B. F., Leitner, T., Han, C. S., Gleasner, C. D., Green, L., Lo, C.-C., Nag, A., Wallstrom, T. C., Wang, S., Mcmichael, A. J., Haynes, B. F., Hahn, B. H., Perelson, A. S., Borrow, P., Shaw, G. M., Bhattacharya, T. and Korber, B. T. (2010). Transmission of Single HIV-1 Genomes and Dynamics of Early Immune Escape Revealed by Ultra-Deep Sequencing. PLoS ONE *5*, e12303.

Friedrich, T. C., Dodds, E. J., Yant, L. J., Vojnov, L., Rudersdorf, R., Cullen, C., Evans, D. T., Desrosiers, R. C., Mothé, B. R., Sidney, J., Sette, A., Kunstman, K., Wolinsky, S., Piatak, M., Lifson, J., Hughes, A. L., Wilson, N., O'connor, D. H. and Watkins, D. I. (2004). Reversion of CTL escape–variant immunodeficiency viruses in vivo. Nat Med *10*, 275–281.

Frost, S. D., Dumaurier, M. J., Wain-Hobson, S. and Brown, A. J. (2001). Genetic drift and within-host metapopulation dynamics of HIV-1 infection. Proceedings of the National Academy of Sciences of the United States of America *98*, 6975–6980.

Frost, S. D. W., Nijhuis, M., Schuurman, R., Boucher, C. A. B. and Brown, A. J. L. (2000). Evolution of Lamivudine Resistance in Human Immunodeficiency Virus Type 1-Infected Individuals: the Relative Roles of Drift and Selection. Journal of Virology *74*, 6262–6268.

Ganusov, V. V., Goonetilleke, N., Liu, M. K. P., Ferrari, G., Shaw, G. M., Mcmichael, A. J., Borrow, P., Korber, B. T. and Perelson, A. S. (2011). Fitness Costs and Diversity of the Cytotoxic T Lymphocyte (CTL) Response Determine the Rate of CTL Escape during Acute and Chronic Phases of HIV Infection. Journal of Virology *85*, 10518–10528.

Gheorghiu-Svirschevski, S., Rouzine, I. and Coffin, J. (2006). Increasing Sequence Correlation Limits the Efficiency of Recombination in a Multisite Evolution Model. Molecular Biology and Evolution *24*, 574–586.

Good, B. H., Rouzine, I. M., Balick, D. J., Hallatschek, O. and Desai, M. M. (2012). Distribution of fixed beneficial mutations and the rate of adaptation in asexual populations. Proc Natl Acad Sci USA *109*, 4950–5.

Goonetilleke, N., Liu, M. K., Salazar-Gonzalez, J. F., Ferrari, G., Giorgi, E., Ganusov, V. V., Keele, B. F., Learn, G. H., Turnbull, E. L., Salazar, M. G., Weinhold, K. J., Moore, S., Letvin, N., Haynes, B. F., Cohen, M. S., Hraber, P., Bhattacharya, T., Borrow, P., Perelson, A. S., Hahn, B. H., Shaw, G. M., Korber, B. T. and Mcmichael, A. J. (2009a). The first T cell response to transmitted/founder virus contributes to the control of acute viremia in HIV-1 infection. Journal of Experimental Medicine *206*, 1253–1272.

Goonetilleke, N., Liu, M. K., Salazar-Gonzalez, J. F., Ferrari, G., Giorgi, E., Ganusov, V. V., Keele, B. F., Learn, G. H., Turnbull, E. L., Salazar, M. G., Weinhold, K. J., Moore, S., Letvin, N., Haynes, B. F., Cohen, M. S., Hraber, P., Bhattacharya, T., Borrow, P., Perelson, A. S., Hahn, B. H., Shaw, G. M., Korber, B. T. and Mcmichael, A. J. (2009b). The first T cell response to transmitted/founder virus contributes to the control of acute viremia in HIV-1 infection. Journal of Experimental Medicine *206*, 1253–1272.

Haase, A. T. (2011). Early Events in Sexual Transmission of HIV and SIV and Opportunities for Interventions. Annual review of medicine *62*, 127–139.

Hadany, L. and Beker, T. (2003). On the evolutionary advantage of fitness-associated recombination. Genetics *165*, 2167–2179.

Hill, W. G. and Robertson, A. (2009). The effect of linkage on limits to artificial selection. Genetical Research *8*, 269.

Hinkley, T., Martins, J., Chappey, C., Haddad, M., Stawiski, E., Whitcomb, J. M., Petropoulos, C. J. and Bonhoeffer, S. (2011). A systems analysis of mutational effects in HIV-1 protease and reverse transcriptase. Nature Genetics *43*, 487–489.

Iles, M. M., Walters, K. and Cannings, C. (2003). Recombination can evolve in large finite populations given selection on sufficient loci. Genetics *165*, 2249–2258.

Jin, X., Bauer, D., Tuttleton, S., Lewin, S., Gettie, A., Blanchard, J., Irwin, C., Safrit, J., Mittler, J. and Weinberger, L. (1999a). Dramatic rise in plasma viremia after CD8+ T cell depletion in simian immunodeficiency virus–infected macaques. The Journal of experimental medicine *189*, 991.

Jin, X., Bauer, D., Tuttleton, S., Lewin, S., Gettie, A., Blanchard, J., Irwin, C., Safrit, J., Mittler, J. and Weinberger, L. (1999b). Dramatic rise in plasma viremia after CD8+ T cell depletion in simian immunodeficiency virus–infected macaques. The Journal of experimental medicine *189*, 991.

Josefsson, L., King, M. S., Makitalo, B., Brannstrom, J., Shao, W., Maldarelli, F., Kearney, M. F., Hu, W.-S., Chen, J., Gaines, H., Mellors, J. W., Albert, J., Coffin, J. M. and Palmer, S. E. (2011). Majority of CD4+ T cells from peripheral blood of HIV-1-infected individuals contain only one HIV DNA molecule. Proceedings of the National Academy of Sciences *108*, 11199–11204.

Jung, A., Maier, R., Vartanian, J.-P., Bocharov, G., Jung, V., Fischer, U., Meese, E., Wain-Hobson, S. and Meyerhans, A. (2002). Recombination: Multiply infected spleen cells in HIV patients. Nature *418*, 144–144.

Kadolsky, U. D. and Asquith, B. (2010). Quantifying the Impact of Human Immunodeficiency Virus-1 Escape From Cytotoxic T-Lymphocytes. PLoS Computational Biology *6*, e1000981.

Kalams, S. A., Buchbinder, S. P., Rosenberg, E. S., Billingsley, J. M., Colbert, D. S., Jones, N. G., Shea, A. K., Trocha, A. K. and Walker, B. D. (1999). Association between virus-specific cytotoxic T-lymphocyte and helper responses in human immunodeficiency virus type 1 infection. Journal of Virology *73*, 6715–6720.

Kearney, M., Maldarelli, F., Shao, W., Margolick, J. B., Daar, E. S., Mellors, J. W., Rao, V., Coffin, J. M. and Palmer, S. (2009). Human Immunodeficiency Virus Type 1 Population Genetics and Adaptation in Newly Infected Individuals. Journal of Virology *83*, 2715–2727.

Keele, B. F., Giorgi, E. E., Salazar-Gonzalez, J. F., Decker, J. M., Pham, K. T., Salazar, M. G., Sun, C., Grayson, T., Wang, S., Li, H., Wei, X., Jiang, C., Kirchherr, J. L., Gao, F., Anderson, J. A., Ping, L.-H., Swanstrom, R., Tomaras, G. D., Blattner, W. A., Goepfert, P. A., Kilby, J. M., Saag, M. S., Delwart, E. L., Busch, M. P., Cohen, M. S., Montefiori, D. C., Haynes, B. F., Gaschen, B., Athreya, G. S., Lee, H. Y., Wood, N., Seoighe, C., Perelson, A. S., Bhattacharya, T., Korber, B. T., Hahn, B. H. and Shaw, G. M. (2008). Identification and characterization of transmitted and early founder virus envelopes in primary HIV-1 infection. Proceedings of the National Academy of Sciences *105*, 7552–7557.

Kelleher, A. D., Long, C., Holmes, E. C., Allen, R. L., Wilson, J., Conlon, C., Workman, C., Shaunak, S., Olson, K., Goulder, P., Brander, C., Ogg, G., Sullivan, J. S., Dyer, W., Jones, I.,

Mcmichael, A. J., Rowland-Jones, S. and Phillips, R. E. (2001). Clustered mutations in HIV-1 gag are consistently required for escape from HLA-B27-restricted cytotoxic T lymphocyte responses. The Journal of experimental medicine *193*, 375–386.

Kessler, D. A., Levine, H., Ridgway, D. and Tsimring, L. (1997). Evolution on a smooth landscape. Journal of Statistical Physics *87*, 519–544.

Klatt, N. R., Shudo, E., Ortiz, A. M., Engram, J. C., Paiardini, M., Lawson, B., Miller, M. D., Else, J., Pandrea, I., Estes, J. D., Apetrei, C., Schmitz, J. E., Ribeiro, R. M., Perelson, A. S. and Silvestri, G. (2010). CD8+ lymphocytes control viral replication in SIVmac239-infected rhesus macaques without decreasing the lifespan of productively infected cells. PLoS Pathogens *6*, e1000747.

Korber, B., Gaschen, B., Yusim, K., Thakallapally, R., Kesmir, C. and Detours, V. (2001). Evolutionary and immunological implications of contemporary HIV-1 variation. British Medical Bulletin *58*, 19–42.

Kouyos, R. D., Althaus, C. L. and Bonhoeffer, S. (2006). Stochastic or deterministic: what is the effective population size of HIV-1? Trends in microbiology *14*, 507–511.

Kuroda, M. J., Schmitz, J. E., Charini, W., Nickerson, C., Lifton, M., Lord, C., Forman, M. and Letvin, N. L. (1999). Emergence of CTL coincides with clearance of virus during primary simian immunodeficiency virus infection in rhesus monkeys. Journal of immunology (Baltimore, Md. : 1950) *162*, 5127–5133.

Leslie, A. (2005). Transmission and accumulation of CTL escape variants drive negative associations between HIV polymorphisms and HLA. Journal of Experimental Medicine *201*, 891–902.

Letvin, N. L., Mascola, J. R., Sun, Y., Gorgone, D. A., Buzby, A. P., Xu, L., Yang, Z.-Y., Chakrabarti, B., Rao, S. S., Schmitz, J. E., Montefiori, D. C., Barker, B. R., Bookstein, F. L. and Nabel, G. J. (2006a). Preserved CD4+ central memory T cells and survival in vaccinated SIV-challenged monkeys. Science *312*, 1530–1533.

Letvin, N. L., Mascola, J. R., Sun, Y., Gorgone, D. A., Buzby, A. P., Xu, L., Yang, Z.-Y., Chakrabarti, B., Rao, S. S., Schmitz, J. E., Montefiori, D. C., Barker, B. R., Bookstein, F. L. and Nabel, G. J. (2006b). Preserved CD4+ central memory T cells and survival in vaccinated SIV-challenged monkeys. Science *312*, 1530–3.

Liu, J., O'brien, K. L., Lynch, D. M., Simmons, N. L., Porte, A. L., Riggs, A. M., Abbink, P., Coffey, R. T., Grandpre, L. E., Seaman, M. S., Landucci, G., Forthal, D. N., Montefiori, D. C., Carville, A., Mansfield, K. G., Havenga, M. J., Pau, M. G., Goudsmit, J. and Barouch, D. H. (2029). Immune control of an SIV challenge by a T-cell-based vaccine in rhesus monkeys. Nature *457*, 87–91.

Liu, Y., Mcnevin, J. P., Holte, S., Mcelrath, M. J. and Mullins, J. I. (2011). Dynamics of Viral Evolution and CTL Responses in HIV-1 Infection. PLoS ONE *6*, e15639.

Liu, Y., Mullins, J. I. and Mittler, J. E. (2006). Waiting times for the appearance of cytotoxic T-lymphocyte escape mutants in chronic HIV-1 infection. Virology *347*, 140–146.

Markowitz, M., Louie, M., Hurley, A., Sun, E., Di Mascio, M., Perelson, A. S. and Ho, D. (2003). A novel antiviral intervention results in more accurate assessment of human immunodeficiency virus type 1 replication dynamics and T-cell decay in vivo. Journal of Virology *77*, 5037–5038.

Maynard Smith, J. (1971). What use is sex? Journal of Theoretical Biology *30*, 319–335.

McVean, G., Awadalla, P. and Fearnhead, P. (2002). A coalescent-based method for detecting and estimating recombination from gene sequences. Genetics *160*, 1231–1241.

Mostowy, R., Kouyos, R. D., Fouchet, D. and Bonhoeffer, S. (2011). The Role of Recombination for the Coevolutionary Dynamics of HIV and the Immune Response. PLoS ONE *6*, e16052.

Muller, H. (1932). Some Genetic Aspects of Sex. The American Naturalist *66*, 118–138.

Neher, R. A. and Leitner, T. (2010a). Recombination Rate and Selection Strength in HIV Intra-patient Evolution. PLoS Computational Biology *6*, e1000660.

Neher, R. A. and Leitner, T. (2010b). Recombination Rate and Selection Strength in HIV Intra-patient Evolution. PLoS Computational Biology *6*, e1000660.

Neher, R. A., Shraiman, B. I. and Fisher, D. S. (2010). Rate of Adaptation in Large Sexual Populations. Genetics *184*, 467–481.

Newberg, M. H., McEvers, K. J., Gorgone, D. A., Lifton, M. A., Baumeister, S. H. C., Veazey, R. S., Schmitz, J. E. and Letvin, N. L. (2006). Immunodomination in the evolution of dominant epitope-specific CD8+ T lymphocyte responses in simian immunodeficiency virus-infected rhesus monkeys. Journal of immunology (Baltimore, Md. : 1950) *176*, 319–328.

Novella, I. S. (2004). Negative Effect of Genetic Bottlenecks on the Adaptability of Vesicular Stomatitis Virus. Journal of Molecular Biology *336*, 61–67.

Ogg, G. S. (1998). Quantitation of HIV-1-Specific Cytotoxic T Lymphocytes and Plasma Load of Viral RNA. Science *279*, 2103–2106.

Otto, S. P. and Barton, N. H. (1997). The evolution of recombination: removing the limits to natural selection. Genetics *147*, 879–906.

Perelson, A., Neumann, A., Markowitz, M., Leonard, J. and Ho, D. (1996). HIV-1 dynamics in vivo: virion clearance rate, infected cell life-span, and viral generation time. Science *271*, 1582–1586.

Perelson, A. S. (2002). MODELLING VIRAL AND IMMUNE SYSTEM DYNAMICS. Nature Reviews Immunology *2*, 28–36.

Perelson, A. S., Essunger, P., Cao, Y., Vesanen, M., Hurley, A., Saksela, K., Markowitz, M. and Ho, D. (1997). Decay characteristics of HIV-1-infected compartments during combination therapy. Nature *387*, 188–191.

Poon, A. F. Y., Swenson, L. C., Dong, W. W. Y., Deng, W., Kosakovsky Pond, S. L., Brumme, Z. L., Mullins, J. I., Richman, D. D., Harrigan, P. R. and Frost, S. D. W. (2010). Phylogenetic Analysis of Population-Based and Deep Sequencing Data to Identify Coevolving Sites in the nef Gene of HIV-1. Molecular Biology and Evolution *27*, 819–832.

Quiñones-Mateu, M. E. and Arts, E. J. (2002). Fitness of drug resistant HIV-1: methodology and clinical implications. Drug Resistance Updates *5*, 224–233.

Ramratnam, B., Bonhoeffer, S., Binley, J., Hurley, A., Zhang, L., Mittler, J. E., Markowitz, M., Moore, J. P., Perelson, A. S. and Ho, D. (1999). Rapid production and clearance of HIV-1 and hepatitis C virus assessed by large volume plasma apheresis. Lancet *354*, 1782–1785.

Rice, W. R. (2002). EVOLUTION OF SEXEXPERIMENTAL TESTS OF THE ADAPTIVE SIGNIFICANCE OF SEXUAL RECOMBINATION. Nature Reviews Genetics *3*, 241–251.

Richman, D. D., Havlir, D., Corbeil, J., Looney, D., Ignacio, C., Spector, S. A., Sullivan, J., Cheeseman, S., Barringer, K. and Pauletti, D. (1994). Nevirapine resistance mutations of human immunodeficiency virus type 1 selected during therapy. Journal of Virology *68*, 1660–1666.

Rouzine, I. M. (2005a). Evolution of Human Immunodeficiency Virus Under Selection and Weak Recombination. Genetics *170*, 7–18.

Rouzine, I. M. (2005b). Evolution of Human Immunodeficiency Virus Under Selection and Weak Recombination. Genetics *170*, 7–18.

Rouzine, I. M., Brunet, É. and Wilke, C. O. (2008a). The traveling-wave approach to asexual evolution: Muller's ratchet and speed of adaptation. Theoretical population biology *73*, 24–46.

Rouzine, I. M., Brunet, E. and Wilke, C. O. (2008b). The traveling-wave approach to asexual evolution: Muller's ratchet and speed of adaptation. Theor Popul Biol *73*, 24–46.

Rouzine, I. M. and Coffin, J. M. (1999a). Search for the mechanism of genetic variation in the pro gene of human immunodeficiency virus. Journal of Virology *73*, 8167–8178.

Rouzine, I. M. and Coffin, J. M. (1999b). Linkage disequilibrium test implies a large effective population number for HIV in vivo. Proceedings of the National Academy of Sciences of the United States of America *96*, 10758–10763.

Rouzine, I. M. and Coffin, J. M. (2007). Highly fit ancestors of a partly sexual haploid population. Theoretical population biology *71*, 239–250.

Rouzine, I. M. and Coffin, J. M. (2010). Multi-site adaptation in the presence of infrequent recombination. Theoretical population biology *77*, 189–204.

Rouzine, I. M., Murali-Krishna, K. and Ahmed, R. (2005). Generals die in friendly fire, or modeling immune response to HIV. Journal of Computational and Applied Mathematics *184*, 258–274.

Rouzine, I. M., Rodrigo, A. and Coffin, J. M. (2001a). Transition between stochastic evolution and deterministic evolution in the presence of selection: general theory and application to virology. Microbiology and molecular biology reviews : MMBR *65*, 151–185.

Rouzine, I. M., Rodrigo, A. and Coffin, J. M. (2001b). Transition between stochastic evolution and deterministic evolution in the presence of selection: general theory and application to virology. Microbiol Mol Biol Rev *65*, 151–85.

Rouzine, I. M., Sergeev, R. A. and Glushtsov, A. I. (2006). Two types of cytotoxic lymphocyte regulation explain kinetics of immune response to human immunodeficiency virus. Proceedings of the National Academy of Sciences *103*, 666–671.

Rouzine, I. M., Wakeley, J. and Coffin, J. M. (2003a). The solitary wave of asexual evolution. Proceedings of the National Academy of Sciences of the United States of America *100*, 587–592.

Rouzine, I. M., Wakeley, J. and Coffin, J. M. (2003b). The solitary wave of asexual evolution. Proceedings of the National Academy of Sciences of the United States of America *100*, 587–92.

Salazar-Gonzalez, J. F., Salazar, M. G., Keele, B. F., Learn, G. H., Giorgi, E. E., Li, H., Decker, J. M., Wang, S., Baalwa, J., Kraus, M. H., Parrish, N. F., Shaw, K. S., Guffey, M. B., Bar, K. J., Davis, K. L., Ochsenbauer-Jambor, C., Kappes, J. C., Saag, M. S., Cohen, M. S., Mulenga, J., Derdeyn, C. A., Allen, S., Hunter, E., Markowitz, M., Hraber, P., Perelson, A. S., Bhattacharya, T., Haynes, B. F., Korber, B. T., Hahn, B. H. and Shaw, G. M. (2009). Genetic identity, biological phenotype, and evolutionary pathways of transmitted/founder viruses in acute and early HIV-1 infection. Journal of Experimental Medicine *206*, 1273–1289.

Schmid, B. V., Keşmir, C. and Boer, R. J. D. (2009). The distribution of CTL epitopes in HIV-1 appears to be random, and similar to that of other proteomes. BMC Evol Biol *9*, 184.

Schmitz, J. E. (1999). Control of Viremia in Simian Immunodeficiency Virus Infection by CD8+ Lymphocytes. Science *283*, 857–860.

Schmitz, J. E., Johnson, R. P., McClure, H. M., Manson, K. H., Wyand, M. S., Kuroda, M. J., Lifton, M. A., Khunkhun, R. S., McEvers, K. J., Gillis, J., Piatak, M., Lifson, J. D., Grosschupff, G., Racz, P., Tenner-Racz, K., Rieber, E. P., Kuus-Reichel, K., Gelman, R. S., Letvin, N. L., Montefiori, D. C., Ruprecht, R. M., Desrosiers, R. C. and Reimann, K. A. (2005). Effect of CD8+ lymphocyte depletion on virus containment after simian immunodeficiency virus SIVmac251 challenge of live attenuated SIVmac239delta3-vaccinated rhesus macaques. Journal of Virology *79*, 8131–41.

Sergeev, R. A., Batorsky, R. E., Coffin, J. M. and Rouzine, I. M. (2010a). Interpreting the effect of vaccination on steady state infection in animals challenged with Simian immunodeficiency virus. Journal of Theoretical Biology *263*, 385–392.

Sergeev, R. A., Batorsky, R. E. and Rouzine, I. M. (2010b). Model with two types of CTL regulation and experiments on CTL dynamics. Journal of Theoretical Biology *263*, 369–384.

Sergeev, R. A., Batorsky, R. E. and Rouzine, I. M. (2010c). Model with two types of CTL regulation and experiments on CTL dynamics. Journal of Theoretical Biology *263*, 369–384.

Sethupathy, P. and Hannenhalli, S. (2008). A Tutorial of the Poisson Random Field Model in Population Genetics. Advances in Bioinformatics *2008*, 1–9.

Shriner, D. (2004). Pervasive Genomic Recombination of HIV-1 in Vivo. Genetics *167*, 1573–1583.

Stafford, M. A., Corey, L., Cao, Y., Daar, E. S., Ho, D. D. and Perelson, A. S. (2000). Modeling plasma virus concentration during primary HIV infection. J Theor Biol *203*, 285–301.

Sun, Y., Schmitz, J. E., Buzby, A. P., Barker, B. R., Rao, S. S., Xu, L., Yang, Z. y., Mascola, J. R., Nabel, G. J. and Letvin, N. L. (2006). Virus-Specific Cellular Immune Correlates of Survival in Vaccinated Monkeys after Simian Immunodeficiency Virus Challenge. Journal of Virology *80*, 10950–10956.

Troyer, R. M., McNevin, J., Liu, Y., Zhang, S. C., Krizan, R. W., Abraha, A., Tebit, D. M., Zhao, H., Avila, S., Lobritz, M. A., Mcelrath, M. J., Le Gall, S., Mullins, J. I. and Arts, E. J. (2009). Variable Fitness Impact of HIV-1 Escape Mutations to Cytotoxic T Lymphocyte (CTL) Response. PLoS Pathogens *5*, e1000365.

Tsimring, L., Levine, H. and Kessler, D. (1996). RNA Virus Evolution via a Fitness-Space Model. Physical Review Letters *76*, 4440–4443.

Turnbull, E. L., Wong, M., Wang, S., Wei, X., Jones, N. A., Conrod, K. E., Aldam, D., Turner, J., Pellegrino, P., Keele, B. F., Williams, I., Shaw, G. M. and Borrow, P. (2009). Kinetics of Expansion of Epitope-Specific T Cell Responses during Primary HIV-1 Infection. The Journal of Immunology *182*, 7131–7145.

Weinreich, D. M., Watson, R. A. and Chao, L. (2005). PERSPECTIVE: SIGN EPISTASIS AND GENETIC COSTRAINT ON EVOLUTIONARY TRAJECTORIES. Evolution *59*, 1165–1174.

Wildum, S., Schindler, M., Münch, J. and Kirchhoff, F. (2006). Contribution of Vpu, Env, and Nef to CD4 down-modulation and resistance of human immunodeficiency virus type 1-infected T cells to superinfection. Journal of Virology *80*, 8047–8059.

Wodarz, D. (2001). Helper-dependent vs. Helper-independent CTL Responses in HIV Infection: Implications for Drug Therapy and Resistance. Journal of Theoretical Biology *213*, 447–459.

Wodarz, D., Klenerman, P. and Nowak, M. A. (1998). Dynamics of cytotoxic T-lymphocyte exhaustion. Proceedings. Biological sciences / The Royal Society *265*, 191–203.

Wodarz, D. and Nowak, M. A. (2002). Mathematical models of HIV pathogenesis and treatment. Bioessays *24*, 1178–1187.

Wolfs, T. F., de Jong, J. J., den Berg, H. V., Tijnagel, J. M., Krone, W. J. and Goudsmit, J. (1990). Evolution of sequences encoding the principal neutralization epitope of human immunodeficiency virus 1 is host dependent, rapid, and continuous. Proc Natl Acad Sci USA *87*, 9938–42.

Wong, J. K., Strain, M. C., Porrata, R., Reay, E., Sankaran-Walters, S., Ignacio, C. C., Russell, T., Pillai, S. K., Looney, D. J. and Dandekar, S. (2010). In Vivo CD8+ T-Cell Suppression of SIV Viremia Is Not Mediated by CTL Clearance of Productively Infected Cells. PLoS Pathogens *6*, e1000748.

Wright, S. (1932). The roles of mutation, inbreeding, crossbreeding and selection in evolution. Proceedings of the sixth international congress on genetics *1*, 356–366.

Zhang, Z., Schuler, T., Zupancic, M., Wietgrefe, S., Staskus, K. A., Reimann, K. A., Reinhart, T. A., Rogan, M., Cavert, W., Miller, C. J., Veazey, R. S., Notermans, D., Little, S., Danner, S. A., Richman, D. D., Havlir, D., Wong, J., Jordan, H. L., Schacker, T. W., Racz, P., Tenner-Racz, K., Letvin, N. L., Wolinsky, S. and Haase, A. T. (1999). Sexual transmission and propagation of SIV and HIV in resting and activated CD4+ T cells. Science *286*, 1353–1357.